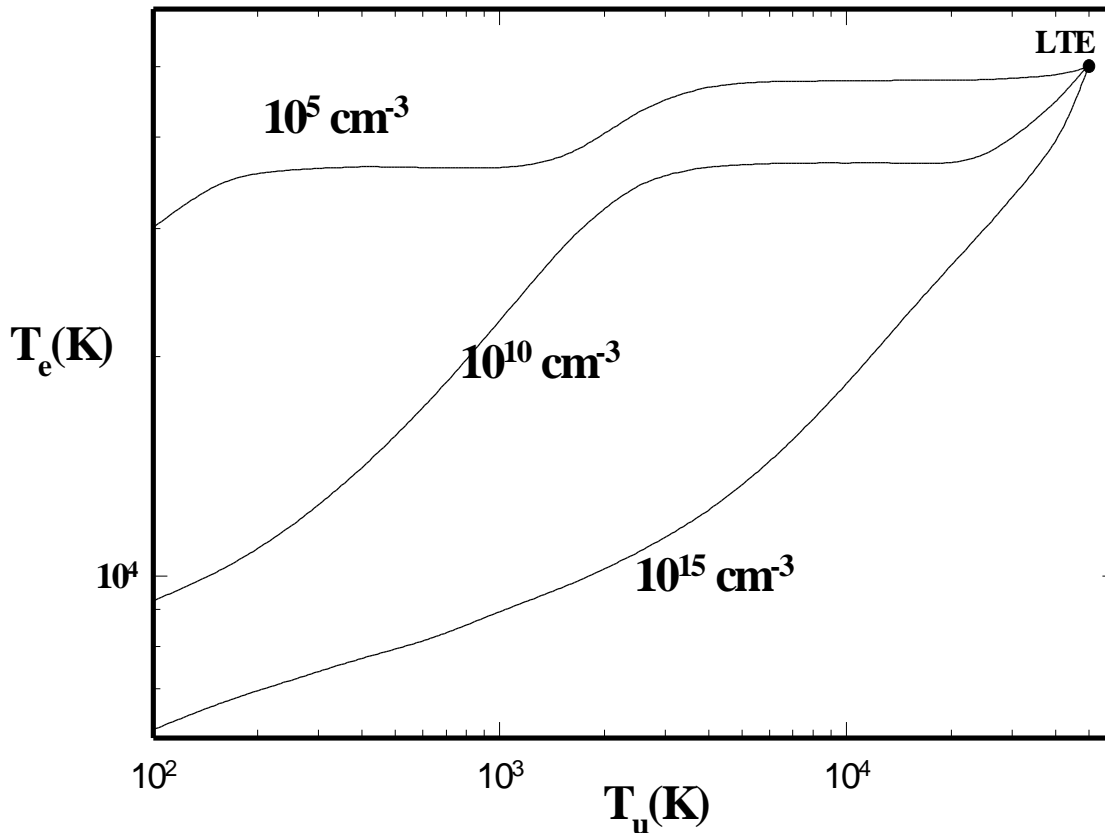


Hazy II

a brief introduction to Cloudy 90
Computational Methods

G.J. Ferland

*Department of Physics and Astronomy
University of Kentucky, Lexington
<http://www.pa.uky.edu/~gary/cloudy>*



Use of this program is not restricted provided each use is acknowledged upon publication. The bibliographic reference to this version of CLOUDY is Ferland, G.J., 1996, *Hazy, a Brief Introduction to Cloudy*, University of Kentucky Department of Physics and Astronomy Internal Report.

Portions of this document have been published, and are copyrighted by, The American Astronomical Society and The Royal Astronomical Society. The remainder of this document, and the code CLOUDY, are copyrighted 1978-1997 by Gary J. Ferland.

CLOUDY is an evolving code. Updates are made on a roughly quarterly basis, while major revisions occur roughly every three years. You should confirm that you have the most recent version of the code by checking the web site <http://www.pa.uky.edu/~gary/cloudy> or asking to be placed on the CLOUDY mailing list.

CLOUDY 90

G. J. Ferland

Department of Physics and Astronomy

University of Kentucky

Lexington

Table of Contents

1. INTRODUCTION.....	201
2. THE CONTINUUM MESH	202
2.1. Overview	202
2.2. Continuum Range.....	202
2.3. The Continuum Mesh.....	202
2.3.1. Defining the continuum energy mesh	202
2.3.2. Changing the energy resolution of the mesh	203
2.3.3. Pointers within the continuum mesh.....	203
2.4. Continuum Arrays.....	203
2.4.1. Continuum definition.....	203
2.4.2. Continuum intensity.....	204
2.4.3. Continuum optical depth arrays	205
2.5. Continuum Generation	205
2.5.1. Blackbody emission.....	206
2.5.2. Continuum Normalization	206
2.6. Energy Units; The Rydberg	206
2.7. Conversion Factors	207
3. CONTINUUM INTERACTIONS	208
3.1. Attenuation of the Incident Continuum.....	208
3.2. Recombination Equilibrium	208
3.2.1. On-the-spot approximation	208
3.2.2. Outward only approximation.....	209
3.3. Continuous Opacities	209
3.3.1. Opacity arrays.....	209
3.3.2. Cross-section array	209
3.3.3. Photoionization rates.....	210
3.3.4. Attenuation within the zone	210
3.3.5. Rayleigh scattering	211
3.3.6. Free-free opacity	212
3.3.7. Bound-free opacity	212
3.3.8. Plasma frequency.....	212
4. LINE DETAILS.....	213
4.1. Overview	213
4.2. Line Boltzmann Factors.....	213
4.3. Optical Depths, Opacities, and Transition Probabilities.....	213

4.3.1. Optical depths	213
4.3.2. Absorption cross section.....	213
4.3.3. Line Widths	214
4.3.4. Oscillator strengths	214
4.3.5. Voigt function.....	214
4.3.6. Mean vs. line center optical depths.....	214
4.4. Optical depths and iterations.....	215
4.4.1. tauout	215
4.4.2. update	215
4.4.3. lgTauOutOn.....	215
4.5. The Einstein Coefficients.....	215
4.6. The Line Source Function.....	216
4.7. The Line Escape Probability Functions.....	216
4.7.1. Escape probability routines.....	216
4.7.2. Incomplete redistribution.....	217
4.7.3. damping constant.....	217
4.7.4. Background opacity and Destruction probability	217
4.7.5. Complete redistribution	217
4.7.6. Masing lines.....	218
4.7.7. Continuum fluorescence.....	218
4.7.8. Stark broadening.....	219
4.7.9. Net escape probability.....	220
4.8. Level populations	220
4.9. Optical Depths and the Geometry.....	221
4.9.1. Open geometry.....	221
4.9.2. Closed geometry overview	221
4.9.3. Wind.....	221
4.10. Collision Strengths.....	221
4.11. Born Approximation.....	222
4.12. The g-bar Approximation	222
4.12.1. The van Regemorter approach.....	222
4.12.2. The g-bar implementation.....	223
4.13. The Critical Density	223
4.14. Thermalization Length.....	223
4.15. Averaging Levels into Terms.....	224
4.15.1. Collision strengths	224
4.15.2. Transition probabilities	224
4.16. The Heavy Element Line Arrays.....	225
4.16.1. Overview	225
4.16.2. Level 1 and Level 2 lines	225
4.16.3. Fine structure lines.....	225
4.16.4. Evaluation of stored quantities.....	225
4.16.5. Contents of the optical depth arrays	226
4.16.6. Dumping the line array.....	228
4.16.7. Generating a line label.....	228
4.16.8. Line excitation temperature	228
4.16.9. A Simple Two Level Atom.....	228
4.16.10. Adding lines to the optical depth arrays	229

5. THE MODEL HYDROGEN ATOM.....	231
5.1. Overview.....	231
5.2. Hydrogen Departure Coefficients.....	231
5.3. Hydrogen Level Energies.....	231
5.4. Effective Hydrogenic Transition Probabilities.....	232
5.4.1. Einstein As.....	232
5.4.2. Hydrogen optical depth arrays.....	232
5.5. Recombination Rates and Cooling.....	233
5.5.1. Formalism.....	233
5.5.2. Results.....	233
5.5.3. Rational approximations.....	235
5.5.4. Recombination coefficients.....	236
5.6. The Collisional Rate Equations.....	236
5.7. The Radiative Rate Equations.....	237
5.7.1. Photoionization - recombination.....	237
5.7.2. Derivation of radiative balance equations.....	238
5.7.3. Final radiative equations.....	238
5.8. Continuous Thermal Emission.....	240
6. H⁻ AND MOLECULES.....	243
6.1. Overview.....	243
6.2. The Saha Equation for Arbitrary Systems.....	243
6.3. The Hydrogen Network.....	245
6.4. LTE Populations of Hydrogen Molecules.....	245
6.5. The H ⁻ Balance; Radiative Processes.....	246
6.5.1. Radiative attachment.....	246
6.5.2. Photodetachment.....	247
6.5.3. Photodetachment by hard photons.....	247
6.5.4. The approach to LTE; high radiation densities.....	248
6.6. The H ⁻ Balance; Collisional Processes.....	248
6.6.1. Associative detachment.....	248
6.6.2. Electron collisional detachment.....	249
6.6.3. Collisional ionization by suprathemal electrons.....	249
6.6.4. Mutual neutralization.....	249
6.6.5. Charge neutralization with heavy elements.....	249
6.6.6. Neglected processes.....	250
6.6.7. The approach to LTE; high hydrogen densities.....	250
6.7. The HeH ⁺ Molecular Ion.....	250
6.8. The H ₂ Molecule.....	250
6.8.1. Associative detachment of H ⁻	251
6.8.2. Catalysis on grain surfaces.....	251
6.8.3. Excited atom radiative association.....	251
6.8.4. Excited molecular dissociation.....	252
6.8.5. Discrete absorption into Lyman and Werner bands.....	252
6.8.6. Photo-ionization to H ₂ ⁺	252
6.8.7. Collisional dissociation by H ⁰ , He ⁰ , and e ⁻	253
6.8.8. H ₂ cooling.....	253
6.8.9. H ₂ heating.....	253

6.9. Heavy Element Molecules	253
6.9.1. Collisional Processes.....	254
6.9.2. Photochemical processes and heating.....	254
6.9.3. Cooling.....	254
7. HELIUM.....	255
7.1. Overview	255
7.2. The Helium Ion.....	255
7.3. The Helium Singlets	255
7.4. The Helium Triplets	255
7.5. Ionization Equilibria.....	255
7.6. Line Emission.....	255
7.7. Helium Line and Continuum Arrays.....	256
7.7.1. Recombination coefficients	256
8. THE HEAVY ELEMENTS	257
8.1. Overview	257
8.2. Solar System Abundances.....	258
8.3. Periodic Table.....	258
8.4. Ionization Balance.....	258
8.4.1. Photoionization cross sections	258
8.4.2. Auger multi-electron ejection	258
8.4.3. Collisional ionization rate coefficients	259
8.4.4. Radiative recombination rate coefficients.....	259
8.4.5. Low temperature dielectronic recombination	259
8.4.6. Charge transfer.....	260
8.5. Ionization Potentials	260
8.5.1. Ionization potential pointers.....	260
8.6. Heavy Element Variables.....	262
8.6.1. Atomic weights	262
8.6.2. Ionic and total abundances	262
8.6.3. Element names	262
8.6.4. Photoionization rates	263
8.6.5. Fluorescence yields.....	263
8.6.6. Ionization potential pointers.....	263
8.7. Isoelectronic Sequences	263
8.8. Carbon.....	263
8.9. Nitrogen.....	265
8.10. Oxygen.....	265
8.10.1. The O I model atom	266
8.11. Neon.....	266
8.12. Magnesium.....	266
8.13. Aluminum	267
8.14. Calcium.....	267
8.14.1. The Ca II model atom	267
8.15. Iron.....	268
8.15.1. The FeII model atom.....	268
8.15.2. The FeIV model atom	268
8.15.3. Fe K α emission	268

8.16. Heavy Element Opacities.....	269
8.17. Overall Reliability.....	269
8.18. The Bi-Diagonal Matrix.....	272
9. THERMAL EQUILIBRIUM.....	273
9.1. Overview.....	273
9.2. Thermal Stability.....	273
9.3. Compton Energy Exchange.....	273
9.4. Bound Compton Ionization, Heating.....	277
9.5. Expansion Cooling.....	277
9.6. Free-free Heating-Cooling.....	277
9.7. Photoelectric Heating, Recombination Cooling.....	278
9.8. Collisional Ionization - Three-Body Recombination.....	278
9.9. H ⁻ Heating and Cooling.....	279
9.9.1. H ⁻ bound-free.....	279
9.9.2. H ⁻ free-free.....	279
9.10. Line Cooling, Hydrogen and Helium.....	279
9.11. Heavy Element Line Heating and Cooling.....	280
9.11.1. Overview.....	280
9.11.2. Array pointers.....	280
9.11.3. Two level atoms.....	281
9.11.4. Three level atoms.....	281
9.11.5. N level atoms.....	282
9.11.6. Li Sequence.....	283
9.11.7. Boron Sequence.....	284
9.11.8. Beryllium sequence atoms.....	284
9.12. Evaluation of the Cooling Function.....	285
9.12.1. Total cooling.....	285
9.12.2. The cooling derivative.....	285
9.13. Evaluation of the Heating Function.....	285
9.14. Equilibrium Calculations.....	286
9.14.1. Hydrogen only.....	286
9.14.2. Metal rich gas.....	287
10. GRAIN PHYSICS.....	289
10.1. Overview.....	289
10.2. Grain Opacity.....	289
10.2.1. ISM grains.....	289
10.2.2. Orion grains.....	289
10.2.3. PN grains.....	289
10.2.4. Extinction.....	290
10.3. Photoelectric Emission.....	290
10.4. Collisional Charging of a Grain.....	292
10.5. Grain Potential.....	292
10.6. Grain Drift Velocity.....	293
10.7. Radiative Heating and Cooling of a Grain.....	293
10.8. Collisional Heating of a Grain.....	293
10.9. Grain Temperature.....	294
10.10. Photoelectric Heating of the Gas.....	294

10.11. Collisional Cooling of the Gas	294
10.12. Grain Sublimation.....	294
10.13. Ionic Recombination on Grain Surfaces	295
10.14. Grain Variables	295
11. OTHER PHYSICAL PROCESSES.....	297
11.1. Overview	297
11.2. Cosmic Ray Interactions.....	297
11.3. Line Radiation Pressure	298
11.3.1. Formalism.....	299
11.3.2. Line width.....	300
11.3.3. Background opacity and thermalization	301
11.4. Radiative Acceleration.....	301
11.5. Pressure Laws	302
11.5.1. Units	302
11.5.2. Ideal gas laws	302
11.5.3. Equation of state.....	302
11.5.4. Turbulent pressure?.....	303
11.5.5. Ram or dynamic pressure	303
11.5.6. Pressure variables and routines.....	303
11.6. Wind Geometry.....	304
11.7. Secondary Ionization	305
11.7.1. Ionization, heating, and cooling	305
11.7.2. Evaluation of rate of hot electron energy input	305
11.7.3. Secondary rates per atom.....	305
11.7.4. Total interaction rates	306
11.7.5. Rates during the hydrogen balance solution.....	306
11.7.6. Molecules and Suprathermal Electrons	306
11.8. Jeans Length and Mass.....	307
11.9. Luminosity Distance.....	307
12. GLOSSARY OF SYMBOLS	308
13. REFERENCES	312
14. INDEX.....	319

List of Figures

Free-free gaunt factors.....	211
Hydrogen recombination cooling.....	235
Hydrogen level populations vs density	237
Hydrogen level populations vs radiation density.....	239
Thermal emission from nebular gas	240
Thermal emission near LTE.....	241
H- departure coefficients vs radiation density	248
H- departure coefficients vs density	250
Solar System Abundances.....	257
Iron photoionization cross sections	259

Density of Ionization Potentials	262
The O I model atom.....	266
The Ca II model atom.....	267
Fe II IR model atom.....	268
Fe IV model atom	268
Fe K α fluorescence yield and energy	269
Opacity of neutral gas at high energies.....	270
Thermal equilibria in the Compton limit.....	275
Thermal equilibria near the Compton limit.....	276
Beryllium sequence model atom.....	284
Boron Sequence.....	284
The approach to thermodynamic equilibrium	287
Thermal equilibrium of metal-rich gas	288
ISM grain opacity functions	291
Wind velocity vs depth.....	304

List of Tables

Conversion Factors.....	207
Line Boltzmann Factors	213
Heavy Element Line Pointers.....	227
Needed Line Parameters	230
Hydrogen recombination coefficients	234
Recombination cooling coefficients	234
Ionization Potentials of the Elements	260
Isoelectronic Sequences.....	264
Ionization Balance Reliability.....	269
Lithium Sequence Lines.....	283
Secondary Ionization Variables.....	306
Secondary Ionization Efficiencies	306

1. INTRODUCTION

This section outlines the computational methods used in version 90 of CLOUDY. Parts are modified from Ferland and Mushotzky (1984), Ferland and Rees (1988), Ferland and Persson (1989), Rees, Netzer, and Ferland (1989), Baldwin et al. (1991), Ferland, Fabian, and Johnstone (1994), Ferland et al. (1992) and Ferland (1992). The code has been designed to be as general as possible (but limited to non-relativistic regimes which are not Compton-thick) while remaining computationally expedient. Similar discussions of hydrogen line formation, focusing on the density range $n \leq 10^{11} \text{ cm}^{-3}$ appropriate to quasar emission-line clouds, can be found, for instance, in Mathews, Blumenthal, and Grandi (1980) and Drake and Ulrich (1980). Discussions of line formation and ionization and thermal equilibria are presented by Osterbrock (1988), Davidson and Netzer (1979), Kwan and Krolik (1981), Halpern and Grindlay (1980), Weisheit, Shields, and Tarter (1981), Kallman and McCray (1982), Hubbard and Puetter (1985), Vernazza, Avrett, and Loeser (1981), Avrett and Loeser (1988), and Netzer (1990).

2. THE CONTINUUM MESH

2.1. Overview

Under most circumstances the continuum produced by the central object is the only source of heat and ionization for the emission-line clouds. This section describes how this continuum is treated.

2.2. Continuum Range

The energy interval 1.001×10^{-5} Ryd – 7.354×10^6 Ryd is divided into ~3000 energy bins with nearly logarithmically increasing widths.

emm This is the low energy limit to the continuum array and is stored as the first variable in the common block **bounds**. It can only be changed by modifying the data statement in block data **scalar**. Its current value is 1.001×10^{-5} Ryd.

egamry This is the high energy limit to the continuum array and is stored as the second variable in the common block **bounds**. The current value is 7.354×10^6 Ryd.

ncell All of the continuum vectors described in the following are dimensioned **ncell** long. **ncell** appears in countless parameter statements throughout the code. **ncell** is always the same, no matter how hard or soft the continuum is, and is currently 3000. It is solely used to define the dimension of the arrays described below.

nupper This is the number of cells needed to define the continuum up to its high energy limit of 7.354×10^6 Ryd. It does not depend on the continuum shape but does depend on how fine the frequency mesh is. Frequency pointers are defined up through **nupper**.

nflux Each of the continuum intensity vectors is defined up to the high-energy limit for the particular continuum generated. The pointer to this higher energy limit is the variable **nflux**. **nflux** is chosen so that, for the highest energy considered, $v_{\text{high}} = \text{anu}(\text{nflux})$, $v_{\text{f}}(v_{\text{high}})/v_{\text{f}}(v_{\text{peak}}) < \text{flxfnt}$, where v_{peak} is the frequency where the continuum reaches its maximum v_{f} . **flxfnt** is normally 10^{-10} and is reset with the `set flxfnt` command.

2.3. The Continuum Mesh

2.3.1. Defining the continuum energy mesh

The continuum energy array **anu** is defined in routine **SetPoint**. The continuum energy mesh is established by successive calls to routine **fill**. Each call defines the continuum mesh over a specific energy range at a specific resolution. The full continuum is set by a series of calls to **fill**, each with its own range and resolution.

fill has five arguments. The first two are the lower and upper bounds to the energy range defined by that call to **fill**. The third argument is the energy resolution desired over that energy range, expressed as a relative resolution, $\delta v/v$. The 4th argument is the frequency grid pointer, and can extend up to **ncell**. The fifth

argument is a pointer indicating which energy band this is – it is incremented for each call to **fill**.

The code will stop if it is not possible to define the entire energy range 1.001×10^{-5} Ryd – 7.354×10^6 Ryd with **ncell** cells. **nupper** is set to the pointer to the highest energy cell, at 7.354×10^6 Ryd, after these calls to **fill**.

2.3.2. Changing the energy resolution of the mesh

Altering the value of the third argument to **fill** can change the resolution of a particular range of the continuum mesh. This number is the fractional resolution $\delta v/v$, where v is the energy.

If the energy resolution is increased then the code will require more mesh points to cover the full continuum, and will run more slowly. It may no longer be possible to define the full continuum with only **ncell** points. If this happens then it will be necessary to increase **ncell** everywhere it appears in the code.

2.3.3. Pointers within the continuum mesh

Most of these are called within routine **SetPoint**.

ipoint This function converts energies (Rydberg) into pointers to the cell in **anu** containing the specified energy. It has a single argument, the energy in Rydberg, and returns the pointer to the appropriate cell. **ipoint** will stop if the energy does not lie within the continuum bounds of the code.

ipLinSafe This routine calls **ipoint** and generates a pointer to the energy of an emission line which is guaranteed to be the only line at that energy in **anu**. Line labels are stored in the four-character array **chLineLabel**. The array **flxsav** is used as a temporary holding area by this routine to count the number of lines stored at a given energy.

ipConSafe This routine calls **ipoint** and generates a pointer to the energy of a continuum edge that is guaranteed to be unique. Line labels are stored in the four-character array **chContLabel**. The array **flux** is used as a temporary holding area by this routine to count the number of lines stored at a given energy.

2.4. Continuum Arrays

Several vectors deal with aspects of the attenuated incident and diffuse continua. All fluxes are stored in units $\text{photons cm}^{-2} \text{ s}^{-1} \text{ cell}^{-1}$ and they all map one-to-one with one another.

2.4.1. Continuum definition

anu The energy (in Rydbergs) of the center of each cell is stored in the vector **anu**. There are **nupper** cells with defined energies. This energy grid *does* have a weak dependence on continuum shape since the center of the cell is defined by a weighted average over the incident continuum.

anuSave This array saves the initial frequency array, so that it may be reset when the code is initialized during computations of many grid models. The initial array of opacities is actually defined using this energy array.

corind Continuum Boltzmann factors, the ratio $\exp(-hv/kT)$, are stored in the vector **corind**, which is evaluated in routine **boltgn**.

widflx The width of each cell (Rydbergs) is stored in the vector **widflx**. There are **nupper** cells with defined widths, and this energy grid does not depend on the continuum shape.

2.4.2. Continuum intensity

condif This is a continuum that is carried outward, but does not interact with the gas. It contains mainly continua whose gas interactions are included by other methods, such as OTS. This does not affect the ionization of the gas directly, but is included in the punched continuum.

diffus The local diffuse continuum (total local emission due to all processes, *per unit volume* with no filling factor) is stored in **diffus**. Continuous diffuse emission is evaluated in routine **diffem**.

flux The attenuated incident continuum is stored in the vector **flux**. The actual contents of **flux** are given by

$$flux(n) = 4\pi J_{inc} \frac{\Delta n}{hn} \text{ photons cm}^{-2} \text{ s}^{-1} \quad (100)$$

where the cell width is Δv .

occnum The photon occupation number associated with the attenuated incident continuum is stored in the vector **occnum**. The continuum occupation number at a frequency ν is given by

$$h_n \equiv J_n / \left(2hn^3 / c^2 \right) = \left(\exp(hn / kT_{ex}) - 1 \right)^{-1} . \quad (100)$$

Here J_ν is the mean intensity of the net continuum at the frequency, and T_{ex} is the excitation temperature of the continuum at the frequency.

outcon stores the continua that are carried outward and treated as sources of ionizing radiation. This continuum is the local outward continuum at the current position within the nebula, with correction for r^2 dilution of radiation. This array is incremented in routine **metdif**.

outlin stores the many lines that are carried outward and treated as sources of ionizing radiation.

otscon and otslin Two vectors, **otscon** and **otslin**, store the local on-the-spot (OTS) photon fluxes for continua and lines. Both are totally local rates, and are reevaluated for every zone.

refcon, reflin The “reflected” continuum and lines (that emergent from the illuminated face of the cloud) are stored in the vectors **reflin** and **refcon**. The reflected continuum and lines are updated for each zone in **metdif**, and the contents of the arrays are the quantity integrated over the computed geometry. Throughout the calculation the reflected continuum and lines are stored relative to the inner radius of the cloud. This is only computed for an open geometry.

SummedDif This is the sum of *otscon*, *otslin*, *outlin*, and *outcon*, and is the summed diffuse continua. They are evaluated in routine **SumContinuum**. This and the following two arrays are used to save time in computing photoionization rate integrals. This is evaluated in routine **SumContinuum**.

SummedOcc This is the continuum occupation number corresponding to **SummedCon**. This is evaluated in routine **SumContinuum**.

SummedCon This is the sum of **SummedDif** and *flux*, the attenuated incident continuum. This is evaluated in routine **SumContinuum**.

2.4.3. Continuum optical depth arrays

depabs, **depact** These are the arrays containing the absorption and scattering optical depths from the current position to the illuminated face of the cloud.

exptau The vector **exptau** contains the term $\exp(-\tau_i)$ for each frequency in *anu*. This is the attenuation from the current position to the illuminated face of the cloud.

e2tau The vector **e2tau** contains the term $E_2(\tau)$ where τ is the absorption optical depth from the current position to the illuminated face of the cloud.

facexp This is the term $\exp(-d\tau)$ for the current zone.

opac This is the array of continuous absorption opacities (units cm^{-1}). It is evaluated in **addopc**.

scatop This is the array of continuous scattering opacities (units cm^{-1}). It is evaluated in **addopc**.

tauabs, **tausct**, **tautot** Total absorption, scattering, and total (absorption plus scattering) optical depths are stored in three arrays, **tauabs(ncell,2)**, and **tausct(ncell,2)**, **tautot(ncell,2)**, respectively. These map one-to-one with *anu*. The first element of the second dimension of the array gives the optical depth from the illuminated face to the current position. The second element gives the total optical depth determined in the previous iteration. For an open geometry this optical depth is only the optical depth of the computed structure. For a closed geometry the optical depth at the illuminated face is set equal to the computed optical depth. During an iteration **tauabs(i,1)** is incremented in routine **radinc**.

At the end of the iteration **tauabs(i,2)** is set to the total optical depth in routine **update**.

2.5. Continuum Generation

The continuum is generated by the function **ffun**. **ffun** has a single argument, the energy in Rydbergs, and it returns the number of photons per unit area, time, and Rydberg, at that energy. **ffun** sums over all the specified continua and applies the appropriate normalization factors. Another function, **ffun1**, evaluates each individual continuum, and is normally called only by **ffun**.

The units, and their conversion to other measures of the continuum, are given below. The photon flux density is:

$$j_n(n) = \text{FFUN}(n) \text{ photons cm}^{-2} \text{ s}^{-1} \text{ Ryd}^{-1} . \quad (101)$$

This is stored in the photon array:

$$\text{FLUX}(\mathbf{n}_i) = \mathbf{j}_n(\mathbf{n}) \mathbf{ch}_i = \text{FFUN}(\mathbf{n}_i) \times \text{WIDFLX}(\mathbf{n}) \text{ photons cm}^{-2} \text{ s}^{-1} . \quad (102)$$

Finally, the energy flux density is given by

$$f_n(\mathbf{n}) = \text{FFUN}(\mathbf{n}) h \left(\frac{\mathbf{n}}{\mathbf{n}_{912}} \right) \text{ erg cm}^{-2} \text{ s}^{-1} \text{ Hz}^{-1} \quad (103)$$

and

$$\mathbf{n}f_n(\mathbf{n}) = \text{FFUN}(\mathbf{n}) h \left(\frac{\mathbf{n}}{\mathbf{n}_{912}} \right) \mathbf{n}_{912} h \mathbf{n}_{Ryd} \text{ erg cm}^{-2} \text{ s}^{-1} \text{ Hz}^{-1} . \quad (104)$$

2.5.1. Blackbody emission

For reference, the Planck function is given by

$$B_n = \frac{F_n}{p} = \frac{2h\mathbf{n}^3}{c^2} \frac{1}{\exp(h\mathbf{n}/kT) - 1} \text{ erg cm}^{-2} \text{ s}^{-1} \text{ sr}^{-1} \text{ Hz}^{-1}. \quad (105)$$

Function **plankf** evaluates the Planck function for the current electron temperature. It has a single argument, a pointer to the desired continuum energy. It returns the photon flux for that cell.

2.5.2. Continuum Normalization

The continuum normalization is performed in routine **conorm**.

2.6. Energy Units; The Rydberg

Continuum energies are usually given in Rydbergs. One Rydberg is approximately equal to the ionization potential of hydrogen, which is

$$R_H \equiv 2.178728 \times 10^{-11} \text{ erg} = 13.59842 \text{ eV} = 91.176340 \text{ nm} = 109677.576 \text{ cm}^{-1} \quad (106)$$

This was the Rydberg unit used by CLOUDY before 1988, and *is not* the more commonly used R_∞ , for infinite mass nuclei.

The energy scale is now in terms of R_∞ , using the 1986 CODATA revision of the fundamental constants (Cohen and Taylor 1987). In these units, the wavenumber corresponding to R_∞ is

$$R_\infty \equiv \frac{2\mathbf{p}^2 m_e q_e^4}{ch^3} = 109737.315 \text{ cm}^{-1} , \quad (107)$$

the wavelength in vacuum is

$$1/R_\infty = 91.126732 \text{ nm}, \quad (108)$$

the frequency is

$$c R_\infty = 3.289842 \times 10^{15} \text{ s}^{-1} , \quad (109)$$

and this corresponds to an energy

$$1\text{Ryd} = chR_\infty = 2.179874 \times 10^{-11} \text{ erg} = 13.605698 \text{ eV} = 1.5788866 \times 10^5 \text{ K} . \quad (110)$$

Thus the ionization potential of hydrogen is actually 0.99946 Ryd, referred to by the variable **HlonPot** in parameter statements within the code. This difference is significant since it enters as the third power in the photon phase-space conversion factor $2h\nu^3/c^2$.

Another commonly used unit is the “atomic unit”, also called the Hartree, which is equal to *two* Rydbergs (i.e., $2R_\infty$).

2.7. Conversion Factors

Table 16 gives conversion factors between various common units. The last column of the table gives the variable names for constants that occur in parameter statements within the code. These should be used instead of entering the constant directly. In the following all Rydbergs are for infinite mass nuclei.

The fundamental constants now used by the code are from a variety of revisions of the basic data, some dating back to the 1970’s. An effort is now underway to convert the constants to the 1986 CODATA recommended values (see <http://physics.nist.gov/PhysRefData/codata86/codata86.html>).

Table 16 Conversion Factors

To convert from	Variable	to	multiply by	Parameter
phot/s/cm ²	flux	f_ν	$\nu_{\text{Ryd}} h\nu_1$ (erg)	
phot/Ryd/s/cm ²	flux/widflx	νf_ν	$\nu_{\text{Ryd}}^2 h\nu_1$ (erg)	
phot/Ryd/s/cm ²	flux/widflx	J_ν	$\nu_{\text{Ryd}} h$	
optical depth	tautot	$A_V(\text{mag})$	1.08574	
energy (eV)		ergs	1.602192(-12)	
energy (eV)		K	1.1604448(4)	eVdegK
energy (Ryd)	anu	Kelvin	1.5788866(5)	te1ryd
energy (Ryd)	anu	ergs	2.179874(-11)	en1ryd
energy (Ryd)	anu	cm ⁻¹	109737.315	1/WavNRyd
energy (Ryd)	anu	eV	13.6056981	evRyd
energy (Ryd)	anu	Å	911.6	rydlam
energy (Ryd), T	anu, Te	hν /kT	1.5788866(5)*anu/Te	te1ryd
temperature (K)	Te	eV	8.617385(-5)	
temperature (K)	Te	ergs	1.38063(-16)	boltzmann
temperature (K)	Te	Rydbergs	1/1.5788866(5)	1/te1ryd
wavelength (cm)		microns	1(+4)	
wavelength (cm)		Å	1(+8)	
wavelength (Å)		degree K	1.43877(+8)/λ(cm)	WavNKelv
wavelength (cm)		degree K	1.43877/λ(cm)	WavNKelv
wavelength (micron)		degree K	1.43877(+4)/λ(cm)	WavNKelv
wavenumbers (cm ⁻¹)		ergs	1.98648(-16)	
wavenumbers (cm ⁻¹)		degree K	1.43877	WavNKelv
wavenumbers (cm ⁻¹)		Rydbergs	9.1126732(-6)	WavNRyd

3. CONTINUUM INTERACTIONS

3.1. Attenuation of the Incident Continuum

In an open geometry scattering is assumed to attenuate the incident continuum as

$$I = I_o (1 + 0.5 dt_{scat})^{-1} . \quad (111)$$

Scattering does not affect the continuum in a closed geometry. Absorption is assumed to attenuate the incident continuum as

$$I = I_o \exp(-dt_{abs}) . \quad (112)$$

for both geometries.

3.2. Recombination Equilibrium

3.2.1. On-the-spot approximation

A modified version of the “on-the-spot” (OTS) approximation is used in the treatment of sources of diffuse ionizing radiation when the `diffuse ots` command is used. Were no other opacity sources present, then, for a closed geometry which is optically thick in the Lyman continuum, all recombinations of hydrogen or helium to the ground state would produce ionizing photons which would be quickly absorbed by other atoms of the recombined species. In this case OTS is an excellent approximation (Van Blerkom and Hummer 1967; Bässgen, Bässgen, and Grewing 1988). However, other opacity sources are present, and these compete in absorbing photons produced by recombinations, making the recombination process more efficient than the OTS approximation would suggest.

The recombination coefficients for all states of hydrogen and helium are modified by the presence of all other opacity sources, such as grains, free-free or H⁻ absorption, and the heavy element opacities, in the following manner. The net effective recombination rate coefficient ($\text{cm}^3 \text{s}^{-1}$) to level n , $\hat{a}(T_e, n)$, is written in terms of the spontaneous radiative recombination rate coefficient $a(T_e, n)$, and the opacities (cm^{-1}) κ_n and κ_o for the level n and other opacity sources respectively, as

$$\hat{a}(T_e, n) = a(T_e, n) \left\{ P_c(n) + [1 - P_c(n)] \left(\frac{\kappa_o}{\kappa_o + \kappa_n} \right) \right\} , \quad (113)$$

where $P_c(n)$ is the continuum escape probability. In general, $P_c(n)$ varies between 0 and 0.5 for an optically thick open geometry (see, for example Davidson 1977), $P_c \sim 1$ if the gas is optically thin, and $P_c \sim 0$ for ground states if the gas is optically thick and the geometry is closed. All computed opacity sources are included in κ_o .

These recombination continua produce a flux of local on-the-spot photons, ϕ_{OTS} ($\text{cm}^{-2} \text{s}^{-1}$). The OTS photoabsorption rate Γ_{OTS} (s^{-1}), used to determine the ionization or heating rate for the gas or grain constituents, is then $\Gamma_{\text{OTS}} = \alpha_\nu \phi_{\text{OTS}}$ where α_ν is the absorption cross section at frequency ν . The OTS flux is related to the spontaneous recombination rate coefficient by

$$j_{OTS} = a(T_e, n) n_e n_{ion} \left[\frac{1 - P_c(t)}{k_o + k_n} \right] \text{ cm}^{-2} \text{ s}^{-1} \quad (114)$$

where n_{ion} is the density of the ion in question. These are stored in the vectors **otscon** and **otslin**, which map one-to-one onto **flux** and **anu**.

3.2.2. Outward only approximation

A composite “outward-only”-“on-the-spot” approximation is used in the treatment of sources of diffuse ionizing radiation when the **diffuse outward** command is used. This is the default assumption. The escaping radiation is then propagated in the outward direction (all for the spherical case, and half for an open geometry).

3.3. Continuous Opacities

The cloud is divided into a large number of concentric shells (zones) and the attenuated and diffuse continua and physical conditions are then determined within each.

The main opacity sources in the ultraviolet continuum are generally photoelectric and free-free (inverse brems) absorption, grain opacity, electron scattering (of both bound and free electrons), and the damping wings of Lyman lines (Rayleigh scattering). The main reemission mechanisms are generally free-free (bremstrahlung), grain emission, free-bound, and two photon emission. Grains are not present by default but can be added as an option. Continuous absorption and reemission by all ground states, and many excited states, of all ionization stages of the 30 elements in the calculation are explicitly included. Great care is taken to ensure that each absorption mechanism is balanced by a reemission process, and vice versa, so that energy balance in the strict thermodynamic equilibrium limit can be achieved.

3.3.1. Opacity arrays

Total absorption opacities (cm^{-1}) are stored in the vector **opac**. Total scattering opacities (cm^{-1}) are stored in **scatop**. The opacities are evaluated in routine **AddOpac**.

3.3.2. Cross-section array

Storage. The cross sections per particle (cm^2) for individual species (atoms, ions, molecules, etc) are stored within the array **opsv**, a stack array with a single dimension. These cross sections are evaluated when the code is initialized in routine **opac0**.

Pointers. Each species has an associated pointer that defines the offset between the origin of **opsv**, the frequency array **anu**, and the opacity at the threshold. If this offset has the name **ioff**, for instance, then the cross section at threshold will be given by array element **opsv(ioff)**. If **ip** is the pointer to the threshold energy, then the pointer to the cross section at an energy **i** will be **i-ip+ioff**.

Individual cross-sections. The function **csphot** returns the cross section at a specific frequency for any species. It has three arguments, 1) the pointer to the

frequency in **anu** where the cross section is to be evaluated, 2) the pointer to the threshold for the species, and 3) the **ioff** offset described above. All are integer variables.

3.3.3. Photoionization rates

Photoionization rates (units s⁻¹) can be computed by several functions. Which is used at a particular time is determined by circumstances.

gamfun The photoionization rate is given by

$$\Gamma_n = 4p \int_{n_o}^{\infty} \frac{J_n}{h\nu} a_n d\nu \quad (115)$$

The routine has three integer arguments, the **anu** pointers to the lower and upper energies, and the offset to the opacity array **ioff** (described above).

gamk This computes the photoionization rate with allowance for an arbitrary fluorescence yield. This routine is a major pace-setter for the code since it is used to evaluate the continuum rates in the majority of the cases.

PrtGamma This is a special version of **gamfun** that punches (on any IO unit) the step by step results of the integration. The output lists the product of the photon flux and the cross section, the photon flux, and the opacity.

bnfun This is a special version of **gamfun** that is used when the correction for stimulated emission or induced recombination is important. The photoionization rate is given by

$$\Gamma_n = 4p \int_{n_o}^{\infty} \frac{J_n}{h\nu} a_n d\nu \quad (116)$$

and the rate for induced recombination and its associated cooling is computed as

$$a(ind) = P^* 4p \int_{n_o}^{\infty} \frac{J_n}{h\nu} a_n \exp(-h\nu/kT) d\nu \quad (117)$$

where P* is the LTE population.

3.3.4. Attenuation within the zone

A correction must be made to account for the attenuation of the continuum across the zone (Netzer and Ferland 1983). Assuming that the continuum varies across the zone as

$$\frac{I(n, \mathbf{d})}{I_o(n)} = \exp(-\mathbf{k}(n) f(r) \mathbf{d}) \quad (118)$$

then the intensity averaged over a zone with thickness δr is

$$\left\langle \frac{I(n, \mathbf{d})}{I_o(n)} \right\rangle = \frac{1 - \exp(-\mathbf{k}(n) f(r) \mathbf{d})}{\mathbf{k}(n) f(r) \mathbf{d}} \quad (119)$$

where $\kappa(\nu)$ is the absorption opacity and $f(r)$ is the filling factor. The coefficients giving this ratio as a function of energy are stored in the vector **tmn**, and are

evaluated in subroutine *radinc*. The continuum stored in *flux* is multiplied by these factors in the same subroutine.

3.3.5. Rayleigh scattering

Clouds with neutral hydrogen column densities greater than $\sim 10^{23} \text{ cm}^{-2}$ are optically thick to Rayleigh scattering at wavelengths near $\text{Ly}\alpha$, and this process is a major scattering opacity source at short wavelengths for grain-free environments.

Rayleigh scattering cross sections given by Gavril (1967) are used, joined with expressions for the radiative damping wings of Lyman lines (Mihalas 1978). For wavelengths longward of 1410\AA a power-law fit to Gavril's quantal calculations is used;

$$S_{\text{Ray}} = 8.41 \times 10^{-25} \epsilon^4 + 3.37 \times 10^{-24} \epsilon^6 + 4.71 \times 10^{-22} \epsilon^{14} \text{ cm}^2 \quad (120)$$

where $\epsilon \equiv \nu/cR_\infty$ is the photon energy in Rydbergs. This fit is accurate to typically a percent, with occasional errors as large as 4 percent.

For wavelengths between 1410\AA and the Lyman limit, radiative broadening of the Lyman lines is assumed (Mihalas 1978);

free free gaunt factors

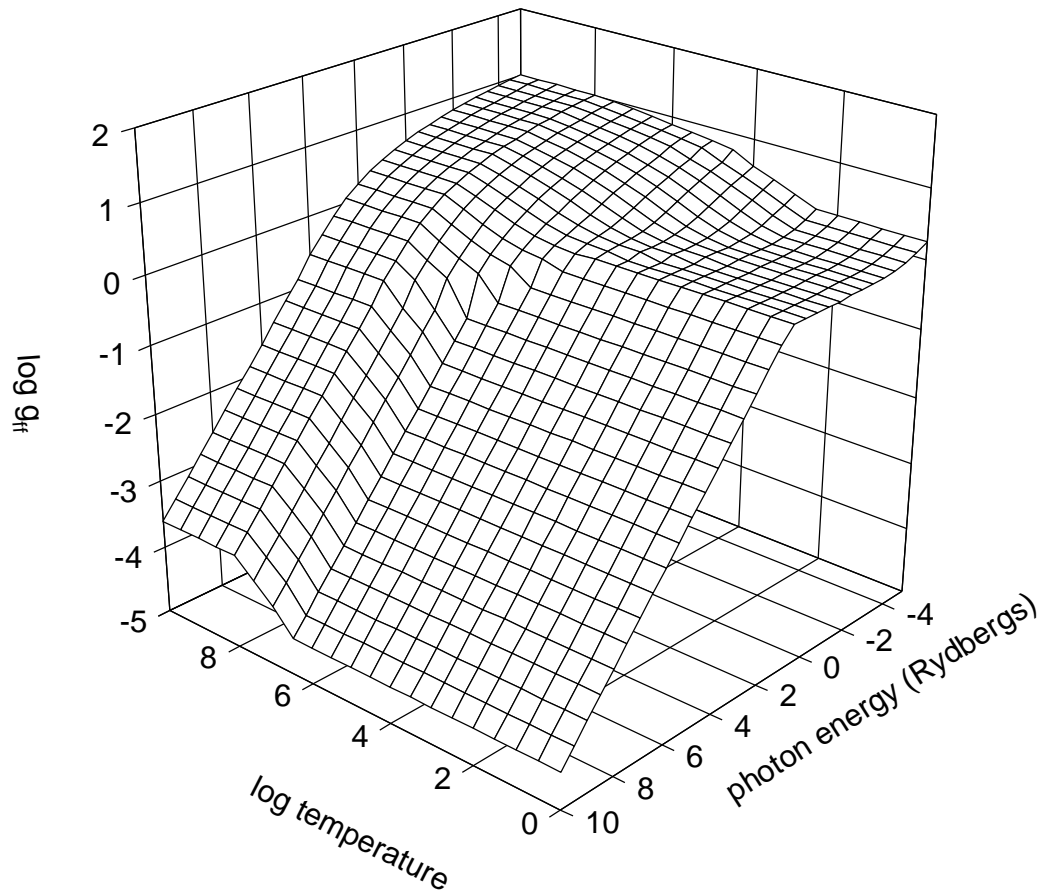


Figure 1 Thermally averaged free-free gaunt factor. The gaunt factor is shown as a function of photon energy and temperature. gaunt

$$\mathbf{s}_{Ray} = \sum_{i=2}^4 \left(\frac{q_e^2 f_{1,i}}{m_e c} \right) \frac{\Gamma / 4\mathbf{p}}{(\mathbf{n} - \mathbf{n}_{1,i})^2} \text{ cm}^2 \quad (121)$$

where Γ is the reciprocal lifetime of the upper level i and the sum is over the first four Lyman lines. This expression gives cross sections in excellent agreement with Gavrilá (1967) for these wavelengths.

3.3.6. Free-free opacity

The main opacity source in the infrared-radio spectral region for many conditions is free-free opacity with a cross section given by

$$\mathbf{a}_n(ff) = 3.69 \times 10^8 \bar{g}_{III}(\mathbf{n}, T) f(r) \mathbf{n}^{-3} T^{-1/2} \{1 - \exp(-h\mathbf{n} / kT)\} \sum_A \sum_z z^2 n_A^{+z} \text{ cm}^2 \quad (122)$$

(see, for example, Mihalas 1978). The sum is over all ions n^{+z} of element A and over all elements. The temperature averaged gaunt factor $\bar{g}_{III}(\mathbf{n}, T)$ is taken from Hummer (1988; see also Karzas and Latter 1961) and are evaluated in routine **gffsub** that was written by D. Hummer.

This routine did not extend to energies that could be treated by asymptotic expansions of the gaunt factor. **gffsub** was modified by J. Ferguson to extend over the full temperature and energy range considered by CLOUDY. Figure 1 shows the gaunt factors as functions of photon energy and temperature.

3.3.7. Bound-free opacity

Continuum optical depths for photoabsorption from level n are given by

$$d\tau_n(\mathbf{n}) = \mathbf{a}_n(n) n_n [1 - \exp(-h\mathbf{n} / kT) / b_n] f(r) d\mathbf{t} \quad (123)$$

where b_n is the departure coefficient for level n and α_v is the absorption cross section.

3.3.8. Plasma frequency

The plasma frequency, the energy where the index of refraction of an ionized medium goes to zero, is given by

$$\mathbf{n}_{pl} = \left(\frac{n_e q_e^2}{\mathbf{p} m_e} \right)^{1/2} = 8.978 \times 10^3 n_e^{1/2} \text{ s}^{-1} = 2.729 \times 10^{-12} n_e^{1/2} \text{ Ryd}. \quad (124)$$

An ionized gas will reflect the incident continuum for energies smaller than this. This shielding becomes important for the energy range considered by CLOUDY for electron densities greater than $\sim 10^{13} \text{ cm}^{-3}$. For higher densities this process is treated by setting the intensity of the incident continuum to zero for energies below the plasma frequency, and adding this portion of the incident continuum to the reflected continuum.

4. LINE DETAILS

4.1. Overview

The effects of optical depths, continuum pumping, collisions, and destruction by background opacity, are computed for *all* permitted and intercombination lines. The cooling is usually distributed among many lines in high-density models, and these lines are usually optically thick.

4.2. Line Boltzmann Factors

The Boltzmann factor $h\nu/kT$ for a line with a known wavelength or energy is given by Table 17. The table lists the ratio $h\nu/k$ for various units of the line energy. Vacuum, not air, wavelengths, must be used for all quantities involving wavelengths.

Line Energy Units	$h\nu/K$ (K)
Angstroms	$1.43877(+8)/\lambda(\text{\AA})$
microns	$1.43877(+4)/\lambda(\mu)$
wavenumbers	$1.43877 \times \sigma$
Rydbergs	$1.5788866(+5) \times E$

4.3. Optical Depths, Opacities, and Transition Probabilities

4.3.1. Optical depths

The line center optical depth for a transition $u-l$, where u and l are the upper and lower levels, is given by

$$d\tau_{l,u} = a_n (n_l - n_u g_l / g_u) f(r) dr . \quad (125)$$

Here $f(r)$ is the filling factor and α_ν the absorption cross section (cm^2).

The term in parenthesis is the population of the lower level, with correction for stimulated emission. This term is the only place where stimulated emission enters in the radiative balance equations (Elitzur et al. 1983) .

4.3.2. Absorption cross section

The line center absorption cross section α_ν (cm^2) is related to the dimensionless absorption oscillator strength f_{lu} or f_{abs} by

$$a_n = \frac{p^{1/2} q_e^2 I f_{abs}}{m_e c v_{Dop}} j_n(x) = 0.014974 f_{abs} \frac{I_{cm}}{v_{Dop}} j_n(x) = 1.4974 \times 10^{-6} f_{abs} \frac{I_{mn}}{v_{Dop}} j_n(x) \quad \text{cm}^2 \quad (126)$$

with the relative line displacement given by

$$x \equiv \frac{n - n_o}{\Delta n_{Dop}} \quad (127)$$

and $j_n(x)$ is the Voigt function. With this definition of the relative line displacement, the line profile due to thermal motions along is $\exp(-x^2)$. Equation 126 is evaluated in routine **abscf**.

4.3.3. Line Widths

In equation 126 the velocity Doppler width (cm s^{-1}), the observed half-width of the line, is given by

$$v_{Dop}^2 = 2kT / m_A + v_{turb}^2 \quad (128)$$

as determined by the local electron temperature. The micro-turbulent velocity v_{turb} is assumed to be zero unless it is reset with the `turbulence` command. The Doppler width (cm s^{-1}) is computed in routine `velset`, and values are stored in the array `doppler`. The element of the array `doppler(n)` is the velocity width of the element with atomic number n , and this extends from hydrogen through the value of `limelm`, currently 30.

In `velset` the Doppler width is evaluated as

$$v_{Dop} = \sqrt{2kT / m_A + v_{turb}^2} = \sqrt{1.651 \times 10^8 T / m_{AMU} + v_{turb}^2} \quad (129)$$

The atomic weight in atomic mass units, m_{AMU} , is stored in the vector `AtomicWeight`, which contains m_{AMU} for the first 30 elements.

4.3.4. Oscillator strengths

The absorption (f_{abs} , $f_{l,u}$) and emission (f_{em} , $f_{u,l}$) oscillator strengths are related by

$$g_l f_{l,u} = -g_u f_{u,l} \quad (130)$$

where the g 's are the statistical weights. This product is symmetric, neglecting sign, and the code tries to use gf 's throughout.

4.3.5. Voigt function

Optical depths a relative displacement x away from line center are related to the line center optical depth by

$$t(x) = t_o j_n(x) \quad (131)$$

The relative displacement is given by

$$x \equiv \frac{n}{n_{Dop}} \quad (132)$$

where v_{Dop} is given by equation 129. The Voigt function is normalized to unity at line center and is approximately given by

$$j_n(x) \approx \exp(-x^2) + a / (p^{1/2} x^2) \quad (133)$$

4.3.6. Mean vs. line center optical depths

CLOUDY tries to work with line center optical depths throughout (see, for example, Mihalas 1978). In many places routines or approximations using *mean* optical depths are encountered (e.g., Hummer and Kunasz 1980). For comparison, the line center optical depth is $\pi^{1/2}$ times *smaller* than the mean optical depth.

4.4. Optical depths and iterations

4.4.1. *tauout*

Routine ***tauout*** is called soon after the initial boundary conditions are established, to estimate the total line and continuum optical depths for hydrogen and helium. It uses various methods to estimate these.

4.4.2. *update*

Routine ***update*** is called at the end of an iteration to use the computed structure, together with results of previous iterations, to estimate total line and continuum optical depths for the next iteration.

4.4.3. *lgTauOutOn*

This logical variable indicates whether or not the outward optical depths have been estimated. It is false on the first iteration and true thereafter.

4.5. The Einstein Coefficients

The oscillator strength is related to the transition probability by

$$g_u f_{em} = \frac{mcI_{cm}^2}{8p^2 q_e^2} g_u A_{u,l} = 1.4992 g_u A_{u,l} I_{cm}^2 = 1.499 \times 10^{-8} g_u A_{u,l} I_{mm}^2 \quad (134)$$

where $\lambda_{\mu m}$ is the wavelength in microns and λ_{cm} the wavelength in centimeters. Neglecting sign the absorption oscillator strength is related to the transition probability by

$$f_{abs} = \frac{mcI_{cm}^2}{8p^2 q_e^2} \frac{g_u}{g_l} A_{u,l} = 1.4992 \times 10^{-8} A_{u,l} I_{mm}^2 \frac{g_u}{g_l} \quad (135)$$

or

$$A_{u,l} = \frac{8p^2 q_e^2}{mcI_{cm}^2} \frac{g_l}{g_u} f_{abs} = \frac{f_{abs}}{1.4992 \times 10^{-8}} I_{mm}^{-2} \frac{g_l}{g_u} \quad (136)$$

Equation 136 is evaluated in routine ***eina***. Combining equations 126 and 135 we obtain an expression relating the transition probability and the absorption cross section;

$$a_n = \frac{c^2 g_u}{8pn^2 g_l} \frac{j_n(x)}{p^{1/2} v_{Dop}} A_{u,l} = \frac{I^2 g_u}{8pg_l} \frac{j_n(x)}{p^{1/2} v_{Dop}} A_{u,l} = 2.24484 \times 10^{-14} A_{u,l} I_{mm}^3 \frac{g_u}{g_l} \frac{j_n(x)}{v_{Dop}} \text{ cm}^2 \quad (137)$$

The coefficient for induced emission, B_{ul} , is related to A_{ul} by the phase space factor $2h\nu^3 / c^2$;

$$A_{u,l} = \frac{2h\nu^3}{c^2} B_{ul} \quad (138)$$

and the induced emission and absorption probabilities are related by

$$g_l B_{l,u} = g_u B_{u,l} \quad (139)$$

so that the rate of induced radiative excitation (continuum pumping) is given by

$$r_{l,u} = n_l B_{l,u} J_{l,u} = n_l A_{u,l} \frac{J}{2h\mathbf{n}^3 / c^2} \frac{g_u}{g_l} = n_l A_{u,l} \mathbf{h}_{l,u} \frac{g_u}{g_l} \quad (140)$$

where η is the continuum occupation number at the line energy. Similarly the rate of induced radiative de-excitation is related by detailed balance,

$$r_{u,l} = r_{l,u} \frac{g_l}{g_u} . \quad (141)$$

The absorption cross section is related to $B_{l,u}$ by

$$\mathbf{a}_n = \frac{h\mathbf{n}}{4\mathbf{p}} B_{l,u} \text{ cm}^2 .$$

In these terms the optical depth increment (equation 125) is given by

$$d\tau_{l,u} = \mathbf{a}_n (n_l - n_u g_l / g_u) f(r) dr = B_{l,u} \frac{h\mathbf{n}}{4\mathbf{p}} (n_l - n_u g_l / g_u) f(r) dr . \quad (142)$$

4.6. The Line Source Function

The source function for a line is defined as

$$S_n(T_{exc}) \equiv B_n(T_{exc}) \equiv \frac{j_n}{\mathbf{k}_n} = \frac{A_{u,l} n_u}{B_{l,u} (n_l - n_u g_l / g_u)} \text{ erg Hz}^{-1} \text{ sr}^{-1} \text{ s}^{-1} \quad (143)$$

where T_{exc} is the line excitation temperature (see equation 185, page 228), and $B_v(T_{exc})$ is the Planck function at the line excitation temperature. Combining the definitions of the Einstein relations we find equation

$$S_n(T_{exc}) = \frac{2h\mathbf{n}^3}{c^2} \frac{n_u / g_u}{(n_l / g_l - n_u / g_u)} . \quad (144)$$

4.7. The Line Escape Probability Functions

At low densities, line scattering for a two level atom is coherent in the atom's reference frame, and the line profile function is described by the incomplete redistribution function. At high densities the Stark effect can broaden the line. When the radiation density is high scattering within excited states can broaden resonance lines such as Ly β (line interlocking), destroying the coherence of the scattering process. In these cases complete redistribution in a Doppler core more closely describes the scattering process. CLOUDY uses two escape probability functions to take these processes into account. Strong resonance lines are treated with partial redistribution with a Voigt profile. Subordinate lines are treated with complete redistribution in a Doppler core.

4.7.1. Escape probability routines

Three routines compute the fundamental escape probabilities. These are **esccom**, **escinc**, and **escla**. They compute escape probabilities for complete redistribution (either with or without the damping wings), incomplete redistribution, and Ly α . A

separate routine, **escmase**, is called by these to compute escape probabilities when the optical depth is less than zero. These routines are called by higher level line transfer routines throughout the code.

4.7.2. Incomplete redistribution

Incomplete redistribution is assumed for resonance transitions such as C IV $\lambda 1549$ and the Ly α transitions of hydrogen and helium. Two studies of line formation using this approximation are those of Bonilha et al. (1979) and Hummer and Kunasz (1980). Both studies suggest escape probabilities of the form

$$P_l(\tau) = \{1 + b(\tau)\tau\}^{-1} \quad (145)$$

but there is substantial disagreement in the form and value of the factor $b(\tau)$, sometimes by more than a factor of 2. (This is after due allowance for the different definitions of line opacities in the two papers.) CLOUDY uses the Hummer and Kunasz (1980) results for HI, He I, and HeII Ly α and strong resonance lines such as CIV $\lambda 1549$. Their tabulated values were fitted by interpolation.

4.7.3. damping constant

The damping constant a is given by

$$a = \frac{\Gamma}{4p\Delta n_D} = \frac{I_{cm} \sum A}{4pv_{Dop}} = \frac{I_{cm} \sum A 7.958 \times 10^{-2}}{v_{Dop}} = \frac{I_{mm} \sum A 7.958 \times 10^{-6}}{v_{Dop}} \quad (146)$$

where Γ is the sum of the A's from the upper level, and Δv_D is the Doppler width in frequency units (Mihalas 1978), λ_{cm} and $\lambda_{\mu m}$ are the wavelengths in cm and microns respectively, and v_{Dop} is the Doppler width in cm s^{-1} . The ratio $\Gamma\lambda/4\pi$ is stored in the vectors **dampln**, **hdamp**, **he1dmp**, and **he2dmp**. The a 's are then evaluated in the routines deriving the escape probabilities.

4.7.4. Background opacity and Destruction probability

The ratio of continuous to total opacity is parameterized as

$$X_c = \frac{\sum \kappa_c n_c}{\kappa_l n_l + \sum \kappa_c n_c} \quad (147)$$

where the κ_l 's are the line center absorption opacities and the n 's the number of absorbers.

Destruction probabilities are computed in routine **eovrlp**.

4.7.5. Complete redistribution

Lines arising from excited states (hydrogen Balmer, Paschen, etc.) and Lyman lines with $n_u > 2$ are treated assuming complete redistribution in a Doppler core (i.e., the damping constant a is assumed to be zero). In this case, if the total optical depth of the slab is T , then the escape probability at a depth τ from the illuminated face is given by;

$$P_{u,l}(\tau, T, X_c) = [1 - X_c F(X_c)] \frac{1}{2} [K_2(\tau, X_c) + K_2(T - \tau, X_c)] \quad , \quad (148)$$

and the destruction probability is

$$D_{u,l}(X_c) = X_c F(X_c). \quad (149)$$

The function is

$$F(X_c) = \int_{-\infty}^{\infty} \frac{j(x)}{X_c + j(x)} dx, \quad (150)$$

where in these expressions (and in this part of the code) the *mean opacity is used*, and $\varphi(x) \approx \pi^{-1/2} \exp(-x^2)$ is the Voigt function. $F(X_c)$ is interpolated from the tables presented by Hummer (1968). The function

$$K_2(t, X_c) \equiv \frac{1}{1 - X_c F(X_c)} \int_{-\infty}^{\infty} \frac{j^2(x)}{X_c + j(x)} E_2[(X_c + j(x))t] dt \quad (151)$$

is evaluated numerically.

4.7.6. Masing lines

A line mases when its optical depth is negative. Routine **escmase** evaluates this escape probability as (Elitzur 1992; p 32)

$$b(t) = \frac{1 - \exp(-t)}{t}. \quad (152)$$

The code will generate a comment if strong maser action occurs for any transition.

4.7.7. Continuum fluorescence

Continuum fluorescence is treated as in Ferland and Rees (1988) and Ferland (1992).

Consider the case of a continuum that has been attenuated by photoelectric (and all other) opacity sources. The transmitted continuum has a flux of photons φ_v (photons $\text{cm}^{-2} \text{s}^{-1} \text{Ryd}^{-1}$). Continuum pumping is included among the general line excitation processes for all lines considered by the code.

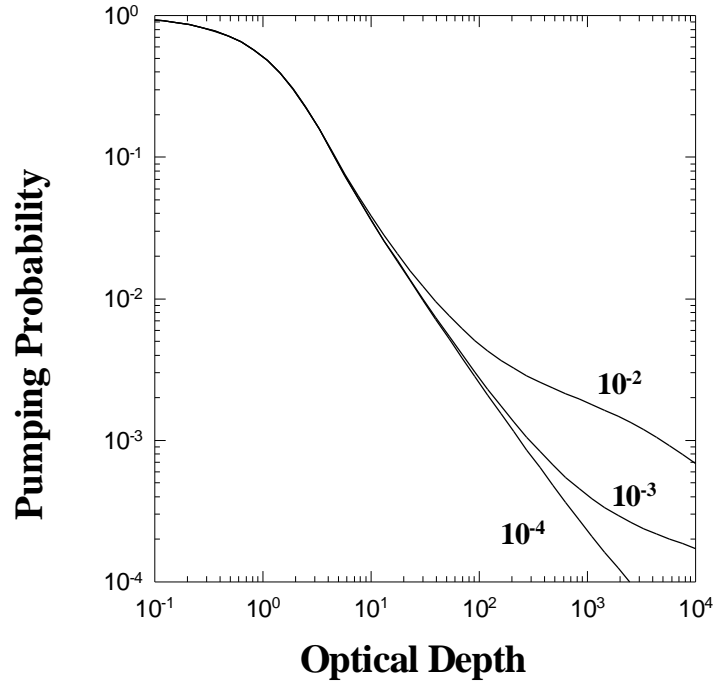


Figure 2 This figure shows the probability that a photon will penetrate to the line center optical depth shown on the x-axis, and then be absorbed by the line. The curves are for various values of the damping constant a (the ratio of damping width to Doppler width), as indicated on the figure. ppump

The photon occupation number of the attenuated continuum is given by

$$h_n = j_n \frac{c^2}{8p n_1^3 n_{\text{Ryd}}^2} \quad (153)$$

where ν_{Ryd} is the frequency in Rydbergs, ν_1 is the frequency of 1 Rydberg, and the other symbols have their usual meaning. The rate ions are excited from a lower level with population n_1 (cm^{-3}) is then given by

$$r_{l,u} = A_{u,l} \frac{g_u}{g_l} h_n g_{u,l} n_l \quad (154)$$

where $A_{u,l}$ is the transition rate and the g 's are the statistical weights. In this expression $\gamma_{l,u}$ is the probability that continuum photons penetrate a line-center distance τ_0 and are then absorbed by an atom:

$$g_{u,l} = \int_0^\infty j_n \exp(-t j_n) dn / \int_0^\infty j_n dn \quad (155)$$

where, in this expression only, ϕ_ν is the Voigt function. Figure 2 shows $\gamma_{l,u}$ for a wide variety of values of the damping constant a .

4.7.8. Stark broadening

Distant collisions with charged particles broaden the upper levels of lines, and in the limit of very high densities this will make the scattering process completely non-coherent even for Ly α (i.e., complete redistribution obtains). CLOUDY closely follows the treatment of Puetter (1981) in treating Stark broadening. For transitions described by incomplete redistribution a total escape probability $P_{l, \text{tot}}$ given by

$$P_{u,l} = \min(P_{inc} + P_{Stark}, P_{com}) \quad (156)$$

is defined, where the escape probabilities are those for incomplete, Stark, and complete redistribution respectively. The total effective escape probability is not allowed to exceed the complete redistribution value for $\tau > a^{-1}$.

4.7.9. Net escape probability

If τ is the optical depth in the direction towards the source of ionizing radiation and T is the total optical depth computed in a previous iteration, then the escape probability entering the balance equations is

$$P_{u,l}(t, T) = \{P_{u,l}(t) + P_{u,l}(T - t)\} / 2 \quad (157)$$

In general the total optical depth T is only known after the first iteration, so more than one iteration must be performed when radiative transfer is important.

4.8. Level populations

Both escape and destruction probabilities enter in the calculation of a level population and line emissivity. The true escape probability (the probability that a line photon will escape in a single scattering, Elitzur et al. 1983; Elitzur 1984) is given by $P_{u,l}$. The destruction probability (the probability that a line photon will be destroyed in a single scattering) is given by $D_{u,l}$.

The radiative line de-excitation rate is given by

$$\left(\frac{dn_u}{dt}\right)_{rad} = n_u A_{u,l} (P_{u,l} + D_{u,l}) - n_l A_{u,l} h g_{u,l} \quad (158)$$

where η is the photon occupation number of the attenuated external radiation field and $\gamma_{u,l}$ is the fluorescence probability.

The net emission from a transition between the level n to a lower level l is then simply

$$4\pi j(n, l) = n_n A_{n,l} h n_{n,l} P_{u,l}(t_{n,l}) f(r) \quad (159)$$

where $f(r)$ is the filling factor. The local cooling rate ($\text{erg cm}^{-3} \text{s}^{-1}$) due to the line is related to the level populations by

$$\Lambda_{u,l} = (n_l C_{l,u} - n_u C_{u,l}) f(r) h n \quad (160)$$

and the local flux ($\text{cm}^{-2} \text{s}^{-1}$) of “on-the-spot” (OTS) photons caused by line loss (used to compute heating or photoionization rates for the sources of the background opacity) is

$$j_{OTS} = \frac{n_u A_{u,l} D_{u,l}(X_c)}{\sum_c k_c n(c)} \quad (161)$$

The ratio of inward to total line intensity is then given by

$$\frac{4p_{j(in)}}{4p_{j(total)}} = \frac{P_{u,l}(t)}{[P_{u,l}(t) + P_{u,l}(T-t)]} \quad (162)$$

4.9. Optical Depths and the Geometry

The terms open and closed geometry are defined in a section in Part I. The treatment of transfer in these two limits is described here.

4.9.1. Open geometry

This is the default. During the first iteration the line escape probability is defined using only optical depths accumulated in the inward direction. This optical depth is initialized to **taumin**, a very small number, at the start of the calculation. At the end of the first iteration the total optical depth is set to the optical depth accumulated in the inward direction in routine **update**. At the end of subsequent iterations the total optical depth is defined as a mean of the new and old inward optical depths.

4.9.2. Closed geometry overview

Continuum photons are assumed to interact with gas fully covering the continuum source. At the end of the first iteration the total continuum optical depths are set equal to twice the computed optical depths, and the inner optical depths reset to the computed optical depths. The same recipe is followed on subsequent iterations, except that means of old and computed optical depths are used.

Closed expanding geometry This is the default if the **sphere** command is entered. In this case it is assumed that line photons do not interact with lines on the “other” side of the expanding spherical nebula. The treatment of the optical depths is entirely analogous to that described for an open geometry, since the presence of the distant material has no effect on line transfer.

Closed static geometry This is assumed if the **sphere static** command is entered. In this case line photons from all parts of the spherical shell do interact. As a result, the optical depth scale is poorly defined on the first iteration, and more than one iteration is required. On second and later iterations the total line optical depth is set to twice the optical depth of the computed structure, and the optical depth at the illuminated face of the shell is set to half of this. The optical depth scale is only reliably defined after at least a second iteration.

4.9.3. Wind

The model is a large velocity gradient ($v \propto R$ Sobolev approximation) wind. This is described further on page 304.

4.10. Collision Strengths

I have tried to follow the Opacity Project notation throughout this document (Lanzafame et al. 1993). The energy specific collision strength Ω_{lu} for a transition between upper and lower levels u and l is related to the excitation cross section Q_{lu} (cm^2) by

$$Q_{lu} = \frac{p\Omega_{lu}}{g_l k_{lu}^2} \quad (163)$$

where k_{lu}^2 is the wavenumber of the collision energy. If the collisions are with thermal electrons having a Maxwellian velocity distribution $f(v)$ and velocity v then the rate coefficient q_{lu} is given by

$$q_{lu} = \int_0^\infty f(v)vQ_{lu} dv = \frac{2p^{1/2}\hbar^2}{g_l m_e} a_o \left(\frac{R_\infty}{kT} \right) Y_{lu} \exp\left(-\frac{E_{lu}}{kT}\right) \sqrt{\frac{2kT}{m_e}} \quad (164)$$

E_{ul} is the transition energy in Rydbergs, a_o is the Bohr radius,

$$a_o = \frac{\hbar^2}{m_e q_e^2} = 0.529177249 \times 10^{-8} \text{ cm} \quad (165)$$

and R_∞ is the Rydberg energy. Then the thermally averaged collision strength is given by

$$Y_{lu} = \int_0^\infty \Omega_{lu} \exp\left(-\frac{e}{kT}\right) d\left(\frac{e}{kT}\right) \quad (166)$$

The rate coefficient for collisional de-excitation is then given by

$$q_{ul} = \frac{Y}{g_u \sqrt{T_e}} \left(\frac{2p}{k} \right)^{1/2} \frac{\hbar^2}{m_e^{3/2}} = \frac{Y 8.6291 \times 10^{-6}}{g_u \sqrt{T_e}} \text{ cm}^3 \text{ s}^{-1} \quad (167)$$

The rate coefficient for excitation follows from detailed balance:

$$q_{lu} = q_{ul} \frac{g_u}{g_l} \exp(-c) = \frac{Y 8.6291 \times 10^{-6}}{g_l \sqrt{T_e}} \exp(-c) \text{ cm}^3 \text{ s}^{-1} \quad (168)$$

4.11. Born Approximation

For energies much larger than the excitation energy of the transition, the Born approximation is valid and the energy specific collision strength is given by Bethe (1930)

$$\Omega_{lu} \approx \frac{4g_l f_{lu}}{E_{lu}} \ln\left(\frac{4e}{E_{lu}}\right) \quad (169)$$

where f_{lu} is the absorption oscillator strength of the permitted transition.

4.12. The g-bar Approximation

4.12.1. The van Regemorter approach

The g-bar or van Regemorter (1962) approximation relates the collision strength to the transition probability A_{ul} and wavelength λ (in microns). Here, the collision strength for the downward transition Y_{ul} is approximately given by

$$\begin{aligned}
Y_{u,l} &= \frac{2\mathbf{p}}{\sqrt{3}} \frac{m^2 e^2}{h^3} I_{mm}^3 10^{-12} g_u A_{u,l} \bar{g} \\
&\approx 2.388 \times 10^{-6} I_{mm}^3 g_u A_{u,l} \bar{g} \\
&\approx 159 I_{mm} g_l f_{abs} \bar{g}
\end{aligned} \tag{170}$$

where g_u and g_l are the statistical weights of the upper and lower levels and f_{abs} is the absorption oscillator strength. For energies of interest in astrophysical plasmas, where $kT < h\nu$, \bar{g} is approximately given by

$$\bar{g} \approx \begin{cases} 0.2; & \text{positive ions} \\ (kT / h\nu) / 10; & \text{neutrals} \end{cases} \tag{171}$$

(van Regemorter 1962). These approximations are generally accurate to better than 1 dex.

4.12.2. The g-bar implementation

Far better collision data are available today. Dima Verner wrote a routine, **ColStrGBar**, which uses the best available data to generate collision strengths for the transferred emission lines, using data stored in the line array. The array element **ipLnCS1** points to stored information identifying the type of transition.

4.13. The Critical Density

The critical density is defined as the density at which the radiative de-excitation rate $A_{ul} P_{ul}$ (A is the transition probability and P is the escape probability) equals the collisional de-excitation rate $q_{ul} n_e$. Setting

$$A_{ul} P_{ul} = C_{ul} = q_{ul} n_e = Y \frac{8.629 \times 10^{-6}}{g_u \sqrt{T_e}} n_e \tag{172}$$

where Y is the thermally averaged collision strength, the critical density is given by

$$n_{crit} = \frac{A_{ul} P_{ul} g_u \sqrt{T_e}}{Y 8.629 \times 10^{-6}} \text{ cm}^{-3}. \tag{173}$$

For an optically allowed transition, in which the g-bar approximation may apply, this density is approximately given by

$$n_{crit} = \frac{4.8 \times 10^{10} \sqrt{T_e}}{I_{mm}^3 \bar{g}} \text{ cm}^{-3}. \tag{174}$$

4.14. Thermalization Length

Radiative transfer will affect the thermal equilibrium of the gas when the collision time scale approaches an effective lifetime $\tau \sim (A_{ul} / N_{scat})^{-1}$, where A_{ul} is the transition probability and N_{scat} is the number of scatterings a line photon undergoes before escape. For permitted metal lines (which often have optical depths $\sim 10^4 - 10^6$) line thermalization becomes important at densities $n_e > 10^{15} / \tau \sim 10^{10} \text{ cm}^{-3}$. These effects are important for hydrogen at considerably lower densities. Additionally,

continuum transfer affects the ionization and thermal equilibrium of the gas at all densities.

4.15. Averaging Levels into Terms

4.15.1. Collision strengths

Often cases are encountered in which a multiplet consisting of many lines can be treated as the equivalent two-level atom with a single transition. In these cases it is necessary to define effective collision strengths and transition probabilities. If the collision strength from an individual level i is Y_i , and the statistical weights of the level and term are g_i and g_{tot} respectively, then the effective collision strength Y_{eff} is related to Y_i by a simple argument. The collision rate q_i is proportional to the ratio

$$n_i q_i \propto n_i \frac{Y_i}{g_i} \quad (175)$$

so that

$$n_{tot} q_{tot} = \sum_i n_i q_i \propto \sum_i n_i \frac{Y_i}{g_i} . \quad (176)$$

In many cases it is valid to assume that the levels within the term are populated according to their statistical weight, viz.,

$$n_i = n_{tot} \frac{g_i}{g_{tot}} . \quad (177)$$

Then, the effective collision strength Y_{tot} is operationally defined by the relations

$$n_{tot} \frac{Y_{tot}}{g_{tot}} = \sum_i n_i \frac{Y_i}{g_i} = n_{tot} \sum_i \frac{g_i}{g_{tot}} \frac{Y_i}{g_i} = n_{tot} \frac{\sum_i Y_i}{g_{tot}} . \quad (178)$$

So, the effective collision strength of the entire multiplet is

$$Y_{tot} = \sum_i Y_i . \quad (179)$$

4.15.2. Transition probabilities

Under similar circumstances an effective transition probability A_{eff} may be defined as

$$n_{tot} A_{tot} = \sum_i n_i A_i = n_{tot} \sum_i \frac{g_i}{g_{tot}} A_i \quad (180)$$

so that the effective transition probability is

$$A_{tot} = \sum_i \frac{g_i}{g_{tot}} A_i . \quad (181)$$

So collision strengths are added, and transition probabilities averaged.

4.16. The Heavy Element Line Arrays

4.16.1. Overview

Each emission line is associated with a vector containing all the details needed to transfer it and predict its intensity. These vectors are variables in common block **TauLines** and **WindData**. Each is dimensioned 37 long, the dimension of the variable *nta* in the file **nta.par**. Although the two groups are considered differently under some circumstances, their internal structure is identical.

4.16.2. Level 1 and Level 2 lines

Level 1 Lines: The **TauLines** common block appears in two forms. The version contained in the file **TLinesEXP.com** explicitly lists all the emission lines so that any individual line can be addressed directly. The version contained in **TLinesARR.com** addresses the line information as a two dimensional vector **TauLines(nta, nTauLines)**. *nta* is described above and *nTauLines* is an integer variable that gives the number of lines. In this second form all lines can be accessed in a simple loop. For most purposes the explicit form of the array is used. All level 1 lines are guaranteed to have a pointer to a unique energy cell, whose line OTS is totally controlled by that line.

Level 2 Lines: The **WindData** array is the large group of lines brought in by Dima Verner. Many of these lines have Opacity Project wavelengths, generally accurate to about 10%. Level 2 lines do not have unique pointers to continuum bins (there are too many of these lines), and so do not control a local OTS flux.

4.16.3. Fine structure lines

In versions 86 and before, the infrared fine structure lines of the heavy elements were stored in a separate line array from the permitted UV and X-Ray lines. There is a single unified treatment of heavy element line transfer in the current version. The infrared fine structure lines were singled out because their absorption of the incident continuum has long been known to be an important heating mechanism in photodissociation regions (Tielens and Hollenbach 1985a) and the lines can mase (Greenhouse et al 1993; Ferland 1993).

The code will still indicate whether the infrared fine structure lines are optically thick, or if *any* of the transferred lines are an important heating source or mase. For this purpose an infrared transition is defined as one with $t(ipLnEnrWN)$ less than 10^4 wavenumbers.

4.16.4. Evaluation of stored quantities

Line arrays store information dealing with the solution of the equations of statistical equilibrium, and rates related to the line transfer. Quantities dealing with the populations are evaluated in the routine that computes the level populations, and this depends on the individual lines. Quantities dealing with the line transfer are evaluated in routine **MakeRT**, which calls either **MakeStatRT** (for static solutions) or **MakeWindRT** (for a large velocity gradient model).

4.16.5. Contents of the optical depth arrays

Nearly all interactions between a line and the physical environment are computed using quantities stored with the line optical depth arrays. Quantities within the line vector should be addressed using the pointers stored in the parameter statements in the **ipLnArray** parameter statements. The names of these pointers and the physical meaning of the quantity are indicated in the following table.

ipLnTauIn The optical depth in the inward direction (i.e., towards the illuminated face of the cloud). This is incremented in subroutine **tauinc**.

ipLnTauTot The total optical depth through the cloud, computed in the previous iteration. This is not defined on the first iteration.

ipLnTauCon The optical depth to the continuum source.

ipLnEscP The escape probability for the line. The escape probabilities are evaluated in **MakeRT**.

ipLnDesP The destruction probability for the line. This includes only line destruction by background opacity sources, generally photoelectric, bremsstrahlung, or grains.

ipLnInwd The fraction of the line escaping in the inward direction. This is between 0 and 1.

ipLnPump This is the local rate of continuum pumping for the transition. It is the product of the local continuum and the pumping probability, given by

$$\text{TauArray}(\text{ipLnPump}) = A_{u,l} \left(\frac{g_u}{g_l} \right) P h \quad (182)$$

where η is the occupation number of the attenuated continuum, and P the line pumping probability.

ipLnWlAng The wavelength (\AA) of the line as used in the print out of the line optical. This number is only a label and can be an air wavelength.

ipLnDampRel The ratio $\Gamma\lambda/4\pi$, used to derive the damping constant. For a two level system this is just $A_{ul}\lambda/4\pi$. This is given by

$$\text{TauArray}(\text{ipLnDampRel}) = 531 f_{abs} \mathbf{I}_{mm} \frac{g_l}{g_u} . \quad (183)$$

ipLnPopl, **ipLnPopu**, These are the lower and upper level populations (cm^{-3}) for the transition.

ipLnPopOpc The correction for stimulated emission is included in the optical depth scale for all lines of the heavy elements. The effective population determining the optical depth scale is given by the population stored here, computed as

$$n_l^{\text{eff}} = n_l - n_u \frac{g_l}{g_u} . \quad (184)$$

ipLnCS1, **ipLnCS2** These indicates the type of transition, and is used when the Mewe or Verner g-bar routines are used as the source of the collision strengths. If

ipLnCS1 is zero then the line is a “high quality” or “level 1” transition, and has its own pointer to the OTS line array. If ***ipLnCS1*** is not zero, (a “level 2” transition) then the collision strength is generated from the contents of ***ipLnCS1*** and ***ipLnCS2***.

ipLnIpCont This is the pointer to the line in the continuum array.

ipLnRedis This indicates the type of line redistribution function to be used, for level 1 lines only. Valid values are -1 and +1. If the value is positive then incomplete redistribution is used. If it is negative then complete redistribution in a Doppler core (Hummer’s ‘K2’ function) is used.

ipLnGl*, *ipLnGu These are the statistical weights of the lower and upper levels.

Table 18 Pointers within heavy element line arrays

Variable	quantity	where computed	
1	<i>ipLnTauIn</i>	inward optical depth	tauinc
2	<i>ipLnTauTot</i>	total optical depth	tauinc
3	<i>ipLnEscP</i>	escape probability	MakeRT
4	<i>ipLnInwd</i>	fractional inward part of the line	MakeRT
5	<i>ipLnWlAng</i>	line WL	block data
6	<i>ipLnDampRel</i>	related to the damping constant	block data
7	<i>ipLnIpCont</i>	pointer to line in continuum array	routine ipline
8	<i>ipLnGl</i>	lower stat. weight	block data
9	<i>ipLnGu</i>	upper stat. weight	block data
10	<i>ipLnGF</i>	gf value	block data
11	<i>ipLnAul</i>	A_ul	from gf
12	<i>ipLnBolt</i>	trans energy degrees kelvin	from <i>ipLnEnrWN</i>
13	<i>ipLnDesP</i>	destruction probability by background opacities	MakeRT
14	<i>ipLnOpac</i>	line opacity	from gf
15	<i>ipLnEnrWN</i>	excitat energy-wavenumbers	block data
16	<i>ipLnIonStg</i>	stage of ionization	block data
17	<i>ipLnPump</i>	continuum pumping rate	MakeRT
18	<i>ipLnPopl</i>	lower level population	line cooling function
19	<i>ipLnEnrErg</i>	trans energy ergs	derived from <i>ipLnEnrWN</i>
20	<i>ipLnNPhots</i>	num of phot EMIT per s in line	line cooling function
21	<i>ipLnAovTOT</i>	ratio A21/(A21+C21)	line cooling function
22	<i>ipLnNelem</i>	atomic number of the atom	block data
23	<i>ipLnDamp</i>	damping constant for line	routines
24	<i>ipLnColovTOT</i>	ratio of collisional to total excitation	cooling routine
25	<i>ipLnInten</i>	intensity of line	cooling routine
26	<i>ipLnRedis</i>	redistribution function	block data
27	<i>ipLnCS</i>	line collision strength	it depends
28	<i>IpLnRyd</i>	line excitation energy in Rydbergs	routine ipline
29	<i>ipLnOTS</i>	local OTS line destruction, photons/sec	cooling routine
30	<i>ipLnDTau</i>	total opacity (cm ⁻¹) in line	tauchn
31	<i>ipLnCool</i>	heat exchange, collisional excitation	cooling routine
32	<i>ipLnHeat</i>	heat exchange, collisional de-excitation	cooling routine
33	<i>IpLnCS1</i>	type of transition, for Mewe g-bar	block data
34	<i>ipLnCS2</i>	second part of CS expansion for above	block data
35	<i>ipLnPopu</i>	upper level population	cooling routine
36	<i>ipLnPopOpc</i>	pop of low level - corrected for stim em	cooling routine
37	<i>ipLnTauCon</i>	optical depth to the continuum source	tauinc

4.16.6. Dumping the line array.

The contents of the line array can be printed by calling routine **DumpLine**, with the single argument being the line optical depth array.

4.16.7. Generating a line label

Two functions can be used to generate a designation for an emission line using the information stored in the line arrays. A 10-character function, **chLineLbl**, will generate a label for an emission line. This label is the spectroscopic designation for a line, such as C 4 1549Å. It is called with a single argument, the line array.

The spectroscopic designation of the ion by itself (“C 4”, “O 6”, etc) can be obtained from the 4 character function **chIonLbl**. It is called with a single argument, the line array.

Two cautions about routine **chLineLbl**. It cannot be used in a Fortran write statement since it uses a write statement to generate the label. Also, this routine is surprisingly slow and should be used as sparingly as possible.

4.16.8. Line excitation temperature

Routine **TexcLine** will use the contents of the line array to generate the line excitation temperature. The line excitation temperature T_{exc} is operationally defined from the relative level populations n_u and n_l and the line energy $h\nu$ as

$$\frac{n_u / g_u}{n_l / g_l} = \exp(-h\nu / kT_{exc}) \quad . \quad (185)$$

Routine **TexcLine** uses the contents of the line arrays to evaluate T_{exc} as follows:

$$T_{exc} = -t(ipLnBolt) / \log\left(\frac{t(ipLnPopu) / t(ipLnGu)}{t(ipLnPopl) / t(ipLnGl)}\right) \quad (186)$$

if both populations are positive. The routine returns an excitation temperature of zero if either population is non-positive.

4.16.9. A Simple Two Level Atom

The following code fragment uses the information in the line optical depth arrays to compute the population of a two level atom. The treatment includes pumping by the attenuated external radiation field, collisional excitation and deexcitation, and photon escape and destruction by background opacity. To see more examine routine *level2* within the code.

```
* following is explicit form of line arrays
  include "TLinesEXP.com"
* following is set of pointers to line arrays
  include "ipLnArray.par"
* following includes variables te and eden, the electron
* temperature and electron density
  include "phycon.com"
* following contains abundances of all ions
  include "IonFrac.com"
* following includes sqrte, the square root of te
  include "sqrte.com"
*
* radiative de-excitation by line escape and destruction
  Aul = t(ipLnAul)* ( t(ipLnEscP) + t(ipLnDesP) )
* upward pumping by external continuum
```

```

PumpLU = t(ipLnPump)
* downward pumping by external continuum
PumpUL = PumpLU * t(ipLnGl) / t(ipLnGu)
*
* collisions from lower to upper, and upper to lower
* Boltzmann factor
Boltz = t(ipLnBolt) / te
* collisions from upper to lower
Cul = 8.629E-6/sqrte * t(ipLnCS)* eden / t(ipLnGu)
* collisional excitation
* sexp is special form of exp that sets zero if very small
Clu = Cul * t(ipLnGu)/t(ipLnGl) * sexp(-Boltz)
*
* xIonFrac(nelem,i) density of ith ion stage (cm^-3)
Abun = xIonFrac( int(t(ipLnNelem)) ,int(t(ipLnIonStg)) )
* this is ratio of upper to lower level population
ratio = (Clu+PumpLU) / ( Cul+PumpUL+Aul )
* upper level population
upper = Abun / (1. + 1./ratio)
*

```

4.16.10. Adding lines to the optical depth arrays

The two versions of the line common block (*TLineARR* and *TLineEXP*) are generated automatically by the program `makelist.f` that lives in the *TauLines* sub-directory off the main CLOUDY directory. The program `makelist.f` and the file `lines.dat` within this sub-directory should be used to add or remove lines from CLOUDY – this must not be done by hand.

Follow these steps:

- **Assign a unique label to the emission line, and add this to the list of lines in the file `lines.dat`, located in the `cloudy/TauLines` subdirectory.** All level 1 lines are contained in the file `lines.dat`. The line label should begin in the first column and the label ends with the first space. The label can be any valid Fortran 90 variable name. A field containing a description of the line can follow the label. This field can contain anything since it is ignored. For simplicity, the lines are sorted within the `lines.dat` list to be in order of increasing atomic number and level of ionization.
- **Run the `makelist.f` program.** It is called `a.out`. This program will read in the contents of the `lines.dat` file and generate the common block files `TLineARR.com` and `TLineEXP.com`. A parameter statement for the number of lines *nTauLines* will appear in the `TLineARR.com` file.
- **Copy the `TLineARR.com` and `TLineEXP.com` files up into the CLOUDY directory. The script `cpup` will do this for you.**
- **Enter the atomic data.** Edit the file `blkline.for` (this lives in the CLOUDY sub-directory), which is a block data file containing all atomic data for the lines. The existing data statements should provide an outline of what the data statements should look like, and Table 19 provides a worksheet. Each line should have all the associated data statements clustered together. Data that must be entered are the following. The line wavelength (used only as a label when printing the line). The statistical weights of the lower and upper levels of the transition. The gf value or the transition probability for the transition (either can be entered, but the other must be set to zero). The excitation energy of the transition in wavenumbers (this is used to get the line photon energy

and Boltzmann factors). The ionization stage of the ion (1 for atom, 2 for first ion, etc.). The atomic number for the element (6 for carbon, etc.). Finally, the form of the redistribution function (-1 for complete redistribution, +1 for incomplete redistribution). The reference for the source of the gf or A should be given as a comment.

- **Compute the line intensity and cooling.** This is done by calling one of the line cooling routines, *level2*, *level3*, etc. It will be necessary to assign a collision strength to the transition. This can be done by calling *PutCS*, a routine with two arguments, the collision strength and the line vector.
- **Add the line to the line output routine.** This is done in one of the members of the *lines* Family of routines. A call to routine *PutLine*, which has as a single argument the line vector, will enter all of the needed information about the line production in the current zone.
- **Update CLOUDY** Go to the CLOUDY directory and “touch” all files which contain the line arrays. This can be done with the *update* script that also lives in the main directory. Type

```
update TLineARR.com
update TLineEXP.com
```

then “make” the code.

Table 19 Needed Line Parameters

Label	λ	g_l	g_u	gf	E(σ)	Ion	Nelem	Redis	A _{ul}
	ipLnWIAng	ipLnGl	ipLnGu	ipLnGF	ipLnEnrWN	ipLnIonStg	ipLnNelem	ipLnRedis	ipLnAul

label Fortran variable name. This must also be entered in the *lines.dat* file in the *TauLines* sub-directory.

l This is the line wavelength in Ångstroms or microns, and is only used as a line label. It can be an air wavelength.

g_l, g_u Lower and upper statistical weights.

gf, A It is only necessary to specify either the gf or A. If the transition probability is to be entered instead of the gf, the gf must be assigned a value of zero. If gf is specified then A does not need to be set.

E(s) This is the line energy in wavenumbers, and is used to generate Boltzmann factors.

Redis This must be non-zero. Negative values indicate complete redistribution with a Doppler core, and positive values incomplete redistribution.

5. THE MODEL HYDROGEN ATOM

5.1. Overview

CLOUDY is designed to model environments that range from the low density limit to LTE. Hydrogen is treated as a multi-level atom plus continuum. Tests in the low-density, or nebular, limit show that the model atom predicts level populations and emissivities that are in much better than 1% agreement with Seaton (1959), and with the Storey and Hummer (1995) results. The atom goes to LTE in the high radiation or matter density limits.

5.2. Hydrogen Departure Coefficients

Departure coefficients, rather than actual level populations, are used in the solution of the hydrogen level populations. The LTE relative population density for level n is stored in the vector **hlte** and is given by

$$P_n^* = \frac{n_n^*}{n_e n_p} = \frac{g_n}{g_e g_p} \left(\frac{h^2}{2\pi m k T} \right)^{3/2} \exp(+c_n) \quad (187)$$

$$= \frac{g_n}{g_e g_p} 4.14158 \times 10^{-16} T^{-3/2} \exp(+c_n) \text{ cm}^3$$

where the electron statistical weight is $g_e = 2$, all nuclear statistical weights are ignored, and $g_n = 2n^2$ is the statistical weight of hydrogen level n . These are stored in the vector **hstat(n)**. n_n^* is the LTE population of level n (cm^{-3}), and the other symbols have their usual meaning. Here

$$c_n = \frac{I_n}{kT} = \frac{15.7807 \times 10^4 Z^2}{n^2 T} \quad (188)$$

where I_n is the ionization threshold for level n and Z is the nuclear charge, and the exponent in equation 187 is greater than one. The departure coefficients are stored in the vector **hbn** and are related to the LTE relative population density by

$$b_n = \frac{n_n}{P_n^* n_e n_p} \quad (189)$$

where n_n is the actual population of the level.

5.3. Hydrogen Level Energies

Boltzmann factors for transitions between levels are stored in the array **hbold**, defined as

$$\text{HLBOLT}(l, u) \equiv \exp(c_u - c_l), \quad (190)$$

and evaluated in subroutine **hcolst**. The sign convention is such that **hbold** is less than unity, decreasing with increasing temperature. Boltzmann factors for levels relative to the continuum are stored in the vector

$$\text{HCBOLT}(n) \equiv \exp(-c_n). \quad (191)$$

Line temperatures in degrees Kelvin are stored in the array **HdetlaT**(u,l). Energies in Rydbergs are stored in **HEnrRyd**(u,l). Ionization threshold energies relative to the continuum are stored in **HNIonRyd**(n) and **HCionT**(n), in Rydbergs and Kelvin respectively.

5.4. Effective Hydrogenic Transition Probabilities

5.4.1. Einstein As

Two routines are used to compute hydrogenic transition probabilities, in the limit of a completely l-mixed atom. The routine **fosc**(u, l) returns the absorption oscillator strength of the transition. Routine **EinstA**(u, l) drives **fosc** to actually obtain the transition probability. These routines were coded by Jason Ferguson, using algorithms given by Johnson (1972).

Note that the code considers the 2s and 2p as two separate levels. These routines return transition probabilities for a well l-mixed atom, and cannot be applied directly to the separate 2s and 2p levels.

5.4.2. Hydrogen optical depth arrays

Several arrays are defined to store information related to the hydrogen optical depth scale and escape probabilities.

hbul(n) The term $\sum_u A_{u,n} (g_u / g_n) h_{u,n} g_{u,n}$ is stored here.

hesc The escape probability for the transition u-l is stored as the element **hesc**(u,l), while the effective transition rate (the spontaneous rate multiplied by the escape probability) is stored in **hesc**(l,u). Escape and destruction probabilities are evaluated in routine **HydroPesc**, which is called by routine **htrans**.

htau The optical depth for the center of the zone is stored in **htau**(u,l); this includes corrections for stimulated emission so it may be negative. (A comment is printed if a level inversion occurs.)

htnext The optical depth for the center of the next zone is stored in **htnext**(u,l).

hfrcin The fraction of the escapes that occur in the inward direction is stored in **hfrcin**(u,l).

htlim The limiting outward optical depth deduced from previous iterations is stored here.

pestrk The Stark contribution to the total escape probability is stored in **pestrk**(u,l); **pestrk**(l,u) contains this escape probability multiplied by the spontaneous transition rate for the u-l transition.

hdest The array **hdest** contains the corresponding arrays of destruction rates.

iphl These are the hydrogen line pointers **iphl**(u, l).

nh These are the hydrogen continuum pointers **nh**(n).

hemis(u,l) This stores the product $A_{u,l} P_{u,l}$.

hjbar(u,l) This function returns the continuum occupation number.

hcont(u,l) The term $\eta A \gamma$ is stored here.

5.5. Recombination Rates and Cooling

State-specific rates for radiative recombination and radiative recombination cooling are needed for the temperature range $2.8 \text{ K} \leq T_e \leq 10^{10} \text{ K}$. The methods and assumptions used to derive these for hydrogenic ions are described here.

5.5.1. Formalism

The Milne relation for the state-specific radiative recombination rate coefficient ($\text{cm}^3 \text{ s}^{-1}$) to a level n can be expressed as (Brown and Mathews 1974; Gould 1978; Mihalas 1978);

$$\begin{aligned} a_n(T) &= \left(\frac{2p m_e k}{h^2} \right)^{-3/2} \frac{8p}{c^2} \frac{g_n}{g_e g_{ion}} T^{-3/2} \int_{hn_o}^{\infty} n^2 a_n(n) \exp(-h(n - n_o) / kT) dn \\ &= 4.12373 \times 10^{11} \frac{g_n}{g_e g_{ion}} T^{-3/2} \int_{hn_o}^{\infty} n_{\text{Ryd}}^2 a_n(n) \exp(-h(n - n_o) / kT) dn_{\text{Ryd}} \end{aligned} \quad (192)$$

where the g 's are the statistical weights of the constituents, $h\nu_{\text{Ryd}}$ is the photon energy in Rydbergs, $h\nu_o \sim z^2/n^2$ is the ionization potential in Rydbergs, $\alpha_\nu(n)$ is the photoionization cross section, and the other symbols have their usual meanings.

In implementing this formalism the fact that, for hydrogen, the energy scale is shifted by the ratio of the reduced mass of the nucleus to an infinite mass was explicitly taken into account. If the energy of level n of hydrogen is $n^{-2} R_H$, then the temperature corresponding to 1 Rydberg, appearing in the exponential, is 157807 K, not the commonly quoted 157890 K. This does affect the results slightly since the energy scale enters as an exponential in equation 192.

Hydrogenic photoionization cross sections are required over a very wide range of energy since recombination coefficients over a wide range of temperature are needed. Cross sections $\alpha_\nu(n)$ were calculated using a program based on routines developed by Hummer (1988) and Storey and Hummer (1991, and private communication). The program generates the cross section values at arbitrary photon energies for all hydrogenic (n,l) states, as well as for the total n , employing analytic expressions and some very accurate expansions and numerical procedures. The calculations were carried out at a number of different mesh sizes to check for convergence. The results are typically accurate to better than 0.1 percent.

The recombination cooling rate coefficient ($\text{erg cm}^3 \text{ s}^{-3}$) is given by

$$kTb(t, n) = \left(\frac{2p m_e k}{h^2} \right)^{-3/2} \frac{8p}{c^2} \frac{g_n}{g_e g_{ion}} T^{-3/2} \int_{hn_o}^{\infty} n^2 a_n(n) h(n - n_o) \exp(-h(n - n_o) / kT) dn \quad (193)$$

5.5.2. Results

Table 20 State Specific and Case B Recombination Coefficients

$\log(T_e)$	1	2	3	4	5	6	case B
0.5	9.258-12	5.087-12	3.512-12	2.684-12	2.172-12	1.825-12	5.758-11
1.0	5.206-12	2.860-12	1.974-12	1.508-12	1.220-12	1.025-12	2.909-11
1.5	2.927-12	1.608-12	1.109-12	8.465-13	6.842-13	5.737-13	1.440-11
2.0	1.646-12	9.028-13	6.216-13	4.732-13	3.811-13	3.183-13	6.971-12
2.5	9.246-13	5.055-13	3.460-13	2.613-13	2.084-13	1.720-13	3.282-12
3.0	5.184-13	2.805-13	1.888-13	1.395-13	1.085-13	8.717-14	1.489-12
3.5	2.890-13	1.517-13	9.779-14	6.884-14	5.099-14	3.912-14	6.430-13
4.0	1.582-13	7.699-14	4.555-14	2.965-14	2.053-14	1.487-14	2.588-13
4.5	8.255-14	3.461-14	1.812-14	1.076-14	6.953-15	4.775-15	9.456-14
5.0	3.882-14	1.316-14	6.059-15	3.314-15	2.022-15	1.331-15	3.069-14
5.5	1.545-14	4.196-15	1.736-15	8.918-16	5.219-16	3.335-16	8.793-15
6.0	5.058-15	1.146-15	4.392-16	2.160-16	1.229-16	7.694-17	2.245-15
6.5	1.383-15	2.760-16	1.005-16	4.807-17	2.685-17	1.660-17	5.190-16
7.0	3.276-16	6.031-17	2.129-17	1.000-17	5.523-18	3.385-18	1.107-16
7.5	7.006-17	1.227-17	4.251-18	1.976-18	1.083-18	6.606-19	2.221-17
8.0	1.398-17	2.377-18	8.139-19	3.759-19	2.052-19	1.248-19	4.267-18
8.5	2.665-18	4.455-19	1.515-19	6.970-20	3.796-20	2.303-20	7.960-19
9.0	4.940-19	8.175-20	2.769-20	1.271-20	6.913-21	4.190-21	1.457-19
9.5	9.001-20	1.481-20	5.005-21	2.294-21	1.247-21	7.552-22	2.636-20
10.0	1.623-20	2.662-21	8.985-22	4.116-22	2.235-22	1.354-22	4.737-21

The numerical results are presented in Tables 20 and 21. The first column of the table gives the log of the temperature. Columns 2 through 7 give the total recombination coefficient for $1 \leq n \leq 6$ summed over l states. The last column gives the case B sum, $2 \leq n \leq 1000$. A very large temperature range is considered for completeness; actually, at very low temperatures three-body recombination predominates for most densities (Bates et al. 1963), while at very high temperatures other processes (i.e., Compton scattering, collisions) dominate the balance and the neutral fraction is vanishingly small.

As tests, these predictions of the recombination rate coefficients are compared with those of Seaton (1959), Ferland (1980), Hummer and Storey (1987), and Martin (1988). (Note that the total recombination rate given by Hummer and Storey is the sum of radiative and net three-body recombination. For this comparison their results for a density of 10^2 cm^{-3} were used to minimize the contribution of the second process.) The agreement with all of these results is good, usually much better than 1

Table 21 State Specific and Case B Recombination Cooling Coefficients

$\log(T_e)$	1	2	3	4	5	6	case B
0.5	4.025-27	2.211-27	1.527-27	1.167-27	9.441-28	7.929-28	2.295-26
1.0	7.158-27	3.932-27	2.713-27	2.072-27	1.676-27	1.406-27	3.595-26
1.5	1.273-26	6.985-27	4.815-27	3.671-27	2.962-27	2.479-27	5.514-26
2.0	2.262-26	1.239-26	8.507-27	6.451-27	5.171-27	4.293-27	8.236-26
2.5	4.015-26	2.184-26	1.483-26	1.107-26	8.708-27	7.074-27	1.187-25
3.0	7.099-26	3.785-26	2.488-26	1.784-26	1.341-26	1.039-26	1.629-25
3.5	1.241-25	6.245-26	3.796-26	2.505-26	1.740-26	1.255-26	2.082-25
4.0	2.094-25	9.195-26	4.856-26	2.845-26	1.795-26	1.198-26	2.395-25
4.5	3.234-25	1.112-25	4.923-26	2.557-26	1.483-26	9.305-27	2.376-25
5.0	4.173-25	1.056-25	3.990-26	1.891-26	1.034-26	6.240-27	1.981-25
5.5	4.149-25	7.981-26	2.698-26	1.208-26	6.389-27	3.771-27	1.390-25
6.0	3.121-25	4.961-26	1.572-26	6.827-27	3.549-27	2.073-27	8.316-26
6.5	1.843-25	2.616-26	8.015-27	3.429-27	1.768-27	1.028-27	4.307-26
7.0	9.016-26	1.204-26	3.628-27	1.541-27	7.917-28	4.591-28	1.967-26
7.5	3.847-26	4.978-27	1.487-27	6.296-28	3.229-28	1.870-28	8.109-27
8.0	1.490-26	1.897-27	5.644-28	2.385-28	1.222-28	7.077-29	3.092-27
8.5	5.397-27	6.811-28	2.023-28	8.541-29	4.375-29	2.533-29	1.115-27
9.0	1.867-27	2.346-28	6.959-29	2.937-29	1.504-29	8.706-30	3.872-28
9.5	6.261-28	7.849-29	2.327-29	9.820-30	5.028-30	2.910-30	1.316-28
10.0	2.057-28	2.575-29	7.633-30	3.220-30	1.649-30	9.543-31	4.436-29

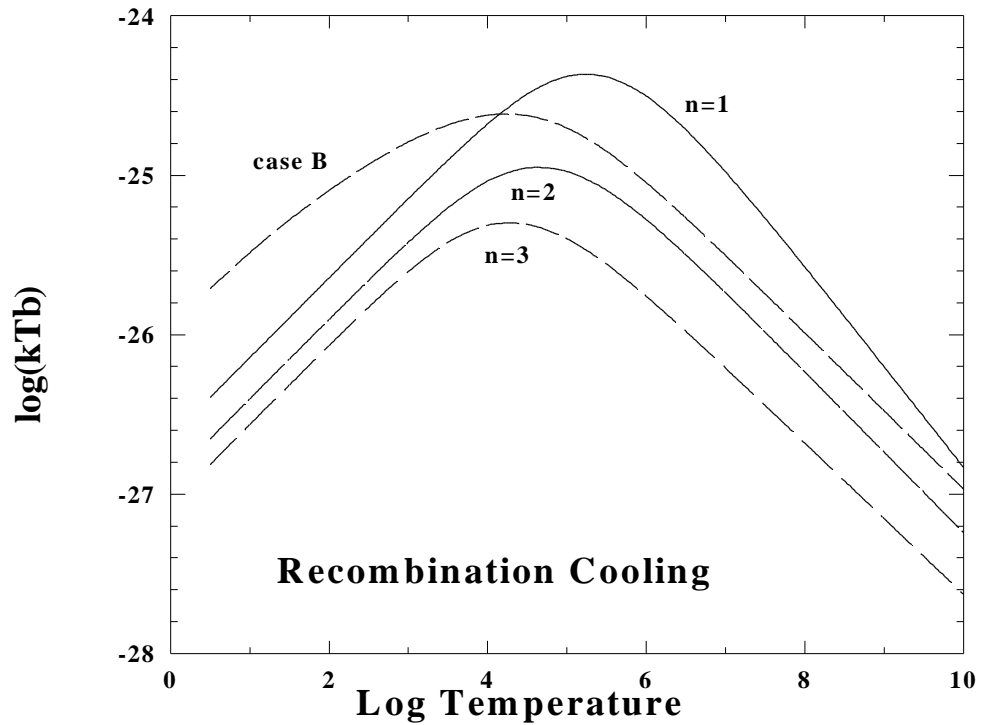


Figure 3 The recombination cooling for several states is shown as a function of temperature.

percent. Seaton (1959) calculates the recombination cooling coefficients. The present results agree with his to better than 5 percent. Figure 3 shows the recombination cooling coefficient for several states.

5.5.3. Rational approximations

It is not numerically expedient to compute these rate coefficients on-the-fly in large scale ionization/thermal structure calculations. The rate coefficients were fitted with a high-order rational approximation. The recombination rate coefficient is expressed as

$$a(n, T) = 10^{F(n, T)} T^{-1} \quad (194)$$

with

$$F(n, T) = \frac{a_n + c_n x + e_n x^2 + g_n x^3 + i_n x^4}{1 + b_n x + d_n x^2 + f_n x^3 + h_n x^4} \quad (195)$$

and $x \equiv \log(T)$. The coefficients for the expansion are given in routine **hrctf**, which evaluates the rate. These approximations reproduce the numerical results with a mean error well below 0.1 percent. For levels below $n=20$ the largest error is also under 0.1 percent, although errors as large as 1.4 percent occur for the highest sum at temperatures below 100 K.

Recombination cooling coefficients were fitted to equations of the form

$$kTb(n, T) = 10^{F(n, T)} \quad (196)$$

where $F(T,n)$ is given above, and the fitting coefficients are given in the code. The errors in fitting these coefficients are larger, typically 0.5 percent, but sometimes as large as several percent.

5.5.4. Recombination coefficients

Hydrogen and helium recombination coefficients are stored in the two dimensional vectors **hrec**, **he1rec**, and **he2rec**. The first dimension of the vector indicates the level of the model atom - **hrec**(1,x) would refer to the ground level. The second dimension points to several quantities related to computation of the effective recombination coefficient.

hrec(n,1) This is the radiative recombination rate coefficient to level n ($\text{cm}^3 \text{s}^{-1}$), the term $\alpha(T,n)$ in equation 113.

hrec(n,2) This is the dimensionless OTS effective recombination efficiency, given by the term

$$\left\{ P_c(n) + [1 - P_c(n)] \left(\frac{\mathbf{k}_o}{\mathbf{k}_o + \mathbf{k}_n} \right) \right\} \quad (197)$$

This term is zero deep in the cloud, and unity for an optically thin region.

hrec(n,3) This is the continuum escape probability $P_c(n)$.

ophf These are the vectors containing the ratio of “other” to “total” opacities, which appears as the term $\kappa_o / (\kappa_o + \kappa_n)$ in equation 197.

5.6. The Collisional Rate Equations

The collision rates between two terms in strict TE are related by detailed balance. Then

$$n_l^* C_{l,u} = n_u^* C_{u,l} \quad (198)$$

and we get the usual relation between collisional excitation and de-excitation rates,

$$C_{l,u} = \left(\frac{n_u^*}{n_l^*} \right) C_{u,l} = \left(\frac{g_u}{g_l} \right) \exp(-c/kT) C_{u,l} \quad (199)$$

Considering only collisional terms, the departure coefficient for level n is given by

$$\frac{db_n}{dt} = \sum_l b_l C_{n,l} + \sum_u \frac{P_u^*}{P_n^*} b_u C_{u,n} - b_n \left\{ \sum_l C_{n,l} + \sum_u \frac{P_u^*}{P_n^*} C_{u,n} + C_{n,k} (1 - b_n^{-1}) \right\} \quad (200)$$

where the sums are over upper and lower levels. The collision rates (s^{-1}) from level i to level j are denoted by C_{ij} . The first term on the RHS represents collisional excitation to n from lower levels, the second is collisional deexcitation to n from higher levels, and the last term accounts for destruction processes. These include collisions to lower levels, upper levels, and the continuum. The factor multiplying the collisional ionization rate $C_{n\kappa}$ accounts for collisional ionization less three-body recombination. Note that this is often a net recombination process for the atom since, under many circumstances, $b_n < 1$.

Figure 4 shows a test case where collisional processes are dominant. All of the radiative processes discussed below are actually included, but the intensity of the external continuum is set to a very low (and hence negligible) value. As a result collisional and spontaneous radiative processes are dominant. The electrons are given a temperature of 50,000 K, and the level populations and ionization of the gas are determined by solving the full set of equations of statistical equilibrium. The model is of a very thin cell of gas that is optically thin in the lines and continuum. Departure coefficients for the ground state, 2s, 2p, and 4 are shown.

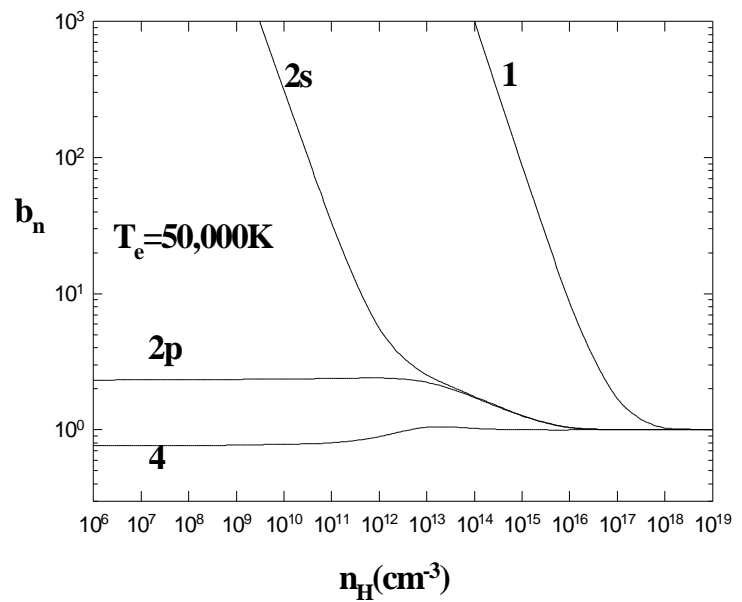


Figure 4 The equilibrium populations of the ground state and levels 2s, 2p, and 4 of the model hydrogen atom are shown as a function of the total hydrogen density n_{H} . hbnvsn

The radiation field is set to a very low intensity, and the column density is kept small enough for optical depth effects to be negligible. A constant electron temperature of 5×10^4 K is assumed, so the gas is primarily collisionally ionized and excited. Levels 2s and 2p do not mix until a density of nearly 10^{14} cm^{-3} is reached, and do not come into LTE until the density is nearly 100 times higher. The entire atom is nearly in LTE at densities greater than 10^{18} cm^{-3} .

The ground state is overpopulated relative to its LTE value when upward collisional processes are much slower than downward radiative processes. It is only when the collisional rates approach the radiative rates that b_1 approaches unity. The 2s level also has a large overpopulation for much the same reason. It is highly metastable and accumulates a large overpopulation until 2s - 2p collisions become fast enough to mix the two l levels. The more highly excited levels ($n \geq 3$) have a behavior very similar to that of $n=4$, which is shown in the figure. They are underpopulated relative to their LTE value when radiative decays to lower levels are competitive with collisional processes. It is only at a density of $n_{\text{H}} > 10^{18}$ cm^{-3} that collisional processes completely dominate the rate equations and the atom reaches LTE. The mean departure coefficient at a density of 10^{19} cm^{-3} is $\bar{b}_i = 1.0007 \pm 0.0022$ for the entire atom, and the largest single deviation from unity is 0.7% (for the ground term).

5.7. The Radiative Rate Equations

5.7.1. Photoionization - recombination

The photoionization rate (s^{-1}) from level n , stored in the vector $\mathbf{hgamnc}(n)$, is given by

$$\Gamma_n = 4p \int_{n_0}^{\infty} \frac{J_n}{hn} \mathbf{a}_n dn \quad (201)$$

and the induced recombination rate coefficient ($\text{cm}^3 \text{s}^{-1}$) by

$$\mathbf{a}(\text{ind}) = P_n^* 4p \int_{n_0}^{\infty} \frac{J_n}{hn} \mathbf{a}_n \exp(-hn/kT) dn . \quad (202)$$

This is evaluated at each zone by direct integration.

The ground level of the model hydrogen atom also includes destruction due to bound Compton scattering.

Spontaneous radiative recombination rate coefficients are computed as described above. The rate coefficients are evaluated in subroutine **htrans**, are stored in **hrec(n,1)**, and have units $\text{cm}^3 \text{s}^{-1}$. These recombinations produce ionizing radiation, and a recombination efficiency is defined to take this into account. These efficiencies are stored in the array **hrec(n,i)**. Elements **hrec(n,3)** are the escape probabilities, computed including only the single-flight absorption due to the geometry, while the escape probabilities stored in **hrec(n,2)** include both this as well as destruction by the background absorbing continuum.

5.7.2. Derivation of radiative balance equations

Consider the balance for a level n of a three level system, with upper and lower levels u and l .

$$n_n (B_{n,u} + B_{n,l} + A_{n,l}) = n_u (B_{u,n} + A_{u,n}) + n_l B_{l,n} . \quad (203)$$

Converting densities n_i into departure coefficients, $n_i = b_i P_i^*$, we obtain

$$P_n^* b_n (B_{n,u} + B_{n,l} + A_{n,l}) = P_u^* b_u (B_{u,n} + A_{u,n}) + P_l^* b_l B_{l,n} . \quad (204)$$

Gathering LTE densities we find

$$b_n (B_{n,u} + B_{n,l} + A_{n,l}) = \frac{P_u^*}{P_n^*} b_u (B_{u,n} + A_{u,n}) + \frac{P_l^*}{P_n^*} b_l B_{l,n} . \quad (205)$$

Writing $B_{ln} = B_{nl} g_n / g_l$, we obtain the final form

$$b_n \left(\frac{g_u}{g_n} B_{u,n} + B_{n,l} + A_{n,l} \right) = \frac{P_u^*}{P_n^*} b_u (B_{u,n} + A_{u,n}) + \frac{P_l^*}{P_n^*} b_l \frac{g_n}{g_l} B_{n,l} . \quad (206)$$

5.7.3. Final radiative equations

The full set of radiative balance equations can be written as

$$\begin{aligned} \frac{db_n}{dt} = & \sum_l \frac{P_l^*}{P_n^*} b_l A_{n,l} \frac{g_n}{g_l} \mathbf{h}_{n,l} \mathbf{g}_{n,l} + \sum_u \frac{P_u^*}{P_n^*} b_u (A_{u,n} P_{u,n} + A_{u,n} \mathbf{h}_{u,n} \mathbf{g}_{u,n}) + \\ & [\mathbf{a}(\text{rad}) + \mathbf{a}(\text{ind})] / P_n^* - \\ & b_n \left(\sum_l (A_{n,l} P_{n,l} + A_{n,l} \mathbf{h}_{n,l} \mathbf{g}_{n,l}) + \sum_u A_{u,n} \frac{g_u}{g_n} \mathbf{h}_{u,n} \mathbf{g}_{u,n} + \Gamma_n \right) \end{aligned} \quad (207)$$

where the continuum occupation number in the transition ij is given by

$$h_{i,j} \equiv J_n(i, j) / (2hn_{ij}^3 / c^2) = (\exp(hn / kT_{ex}) - 1)^{-1} \quad (208)$$

Here $J_v(ij)$ is the mean intensity of the net continuum at the line frequency, and T_{ex} is the excitation temperature of the continuum at the level frequency.

Figure 5 shows a test case that, in contrast to that shown in Figure 4, is dominated by radiative transitions.

Again, the full set of equations coupling the levels are solved, but spontaneous and induced processes are more important than collisions for many values of the radiation density.

The model is of a very thin cell of gas, so that all lines and continua are

optically thin, has a density of $n(\text{H}) = 10^{10} \text{ cm}^{-3}$, and an electron temperature of $5 \times 10^4 \text{ K}$. The gas is exposed to a black body continuum with a color temperature of $T_{\text{color}} = 5 \times 10^4 \text{ K}$, but the intensity of this continuum is varied. This intensity is parameterized by an energy density temperature defined by $T_u \equiv (u/a)^{1/4}$ where u and a are, respectively, the actual radiation energy density and Stefan's radiation density constant.

A radiation field given by Planck's law (i.e., $T_u \equiv T_{\text{color}}$) forces the ionization and level population of an atom or ion to LTE in much the same way that high electron densities do. As Figure 5 shows, at very low values of T_u (low photon densities) the ground and $n = 2$ states are overpopulated for much the same reason that this occurs at low electron densities; the downward spontaneous radiative rates are fast relative to the induced (upward and downward) rates. At very low T_u ($< 500 \text{ K}$), $n \geq 3$ levels are under populated since they decay at a rate much faster than the induced rates (for $T_e = 5 \times 10^4 \text{ K}$ these levels have $h\nu \ll kT$, so induced processes will be fast relative to spontaneous rates when $T_u = T_{\text{color}}$ and the atom is in LTE). As T_u increases, fluorescence from the ground state over-populates excited states (because the ground state is itself overpopulated) and b_4 exceeds unity. Finally, in the limit where $T_u = T_{\text{color}}$, the departure coefficients reach unity and the atom goes to LTE. (The actual mean departure coefficient for the entire atom is $\bar{b}_i = 1.013 \pm 0.029$). Note that the

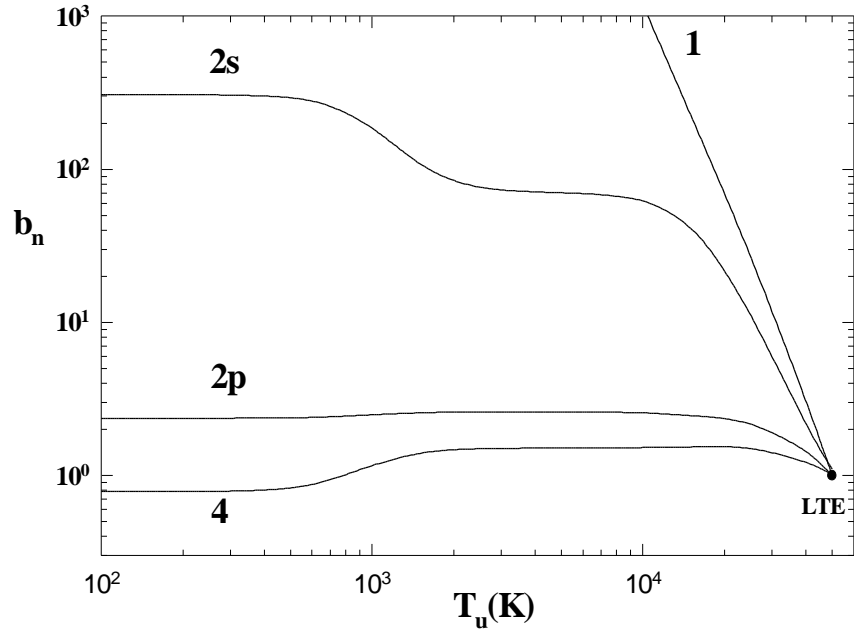


Figure 5 The calculations are for a constant temperature ($T_e = 5 \times 10^4 \text{ K}$) optically thin gas exposed to black body radiation with a color temperature of $T_{\text{color}} = 5 \times 10^4 \text{ K}$, but with various values of the energy density, parameterized as $T_u = (u/a)^{1/4}$, where u is the actual radiation density. $h\nu \ll kT$

vast majority of the neutral hydrogen population is in excited states when the atom approaches LTE at these temperatures.

The hydrogen density ($n(\text{H}) = 10^{10} \text{ cm}^{-3}$) is low enough for radiation to be the main agent affecting level populations for most values of T_u . Fluorescence from the ground state drives the population of $n=4$ above its LTE value for many radiation densities. Induced processes, mainly transitions between adjacent levels, drive the atom to LTE when T_u reaches $5 \times 10^4 \text{ K}$.

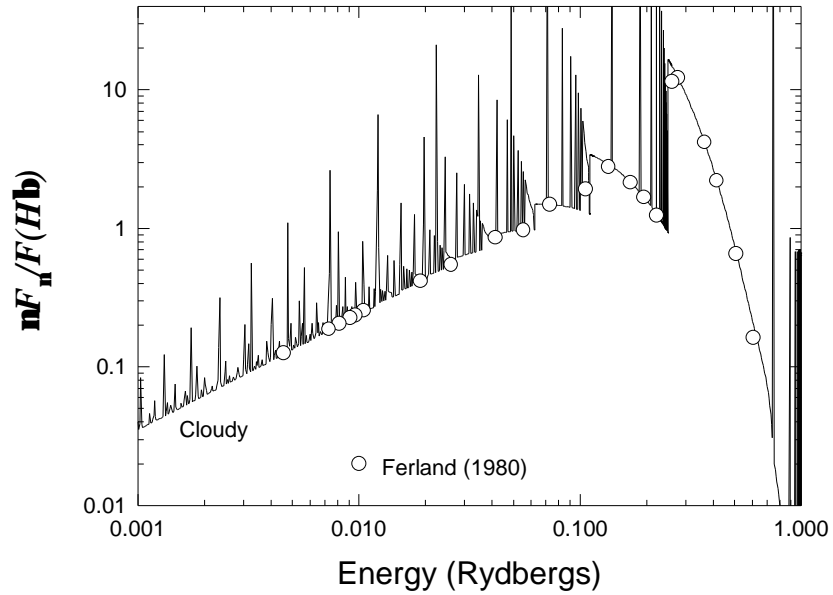


Figure 6 The emission from a slab of gas is compared with the predictions of Ferland (1980). hemis

5.8. Continuous Thermal Emission

Diffuse emission (free-free and free-bound) by the model hydrogen atom is computed using the stored photoabsorption cross sections and detailed balance (i.e., the Milne relation; see Mihalas 1978).

Free-bound continua of all levels of hydrogen and helium are treated as follows. The Milne relation for the emissivity $4\pi j$ ($\text{erg cm}^3 \text{ Hz}^{-1} \text{ s}^{-1}$) can be expressed as (Brown and Mathews 1970)

$$4\pi j_n = h\nu \left(\frac{2\pi m_e k}{h^2} \right)^{-3/2} \frac{8\pi}{c^2} \frac{g_n}{g_e g_{ion}} T^{-3/2} n^2 a_n(n) \exp(-h(n - n_o) / kT) \quad (209)$$

where the statistical weight of level n is $g_n = 2n^2$ for H^0 and He^+ , and $g_n = n^2$ for helium singlets. Statistical weights for hydrogen are stored in the vector **hstat**, while statistical weights for singlet and ionized helium are stored in **hel1stat** and **he2stat**.

The code actually works with units similar to photons $\text{Ryd}^{-1} \text{ s}^{-1} \text{ cm}^{-2}$. The photon emissivity (photons $\text{cm}^3 \text{ s}^{-1} \text{ Ryd}^{-1}$) is then

$$\begin{aligned} j_n(T, n) &= \left(\frac{2\pi m_e k}{h^2} \right)^{-3/2} \frac{8\pi}{c^2} \frac{g_n}{g_e g_{ion}} T^{-3/2} n^2 a_n(n) \exp(-h(n - n_o) / kT) \\ &= 4.12373 \times 10^{11} \frac{g_n}{g_e g_{ion}} T^{-3/2} n_{\text{Ryd}}^2 a_n(n) \exp(-h(n - n_o) / kT) \end{aligned} \quad (210)$$

where the g 's are the statistical weights of the constituents, ν_{Ryd} is the photon energy in Rydbergs, $h\nu_o \sim z^2/n^2$ is the ionization potential in Rydbergs, $\alpha_\nu(n)$ is the

photoionization cross section, and the other symbols have their usual meanings. Equation 210 is evaluated directly using the stored photoionization cross sections. A similar approach is used for other absorption opacities, such as brems and H-. Detailed balancing between absorption and emission mechanisms is necessary if LTE is to be achieved.

A test case with an ionized hydrogen plasma at a temperature of 10^4 K and a density of 10^7 cm^{-3} (to suppress two photon emission) was computed, and is shown in Figure 6.

The input stream used to derive the figure is given as `hemis.in` in Part III of this document. As can be seen from the figure, the predicted diffuse continuum is generally within 10 percent of the exact value (Ferland 1980).

Figure 7 shows another series of test cases in which a very high density gas with cosmic abundances is irradiated with a 50,000 K blackbody radiation field in strict

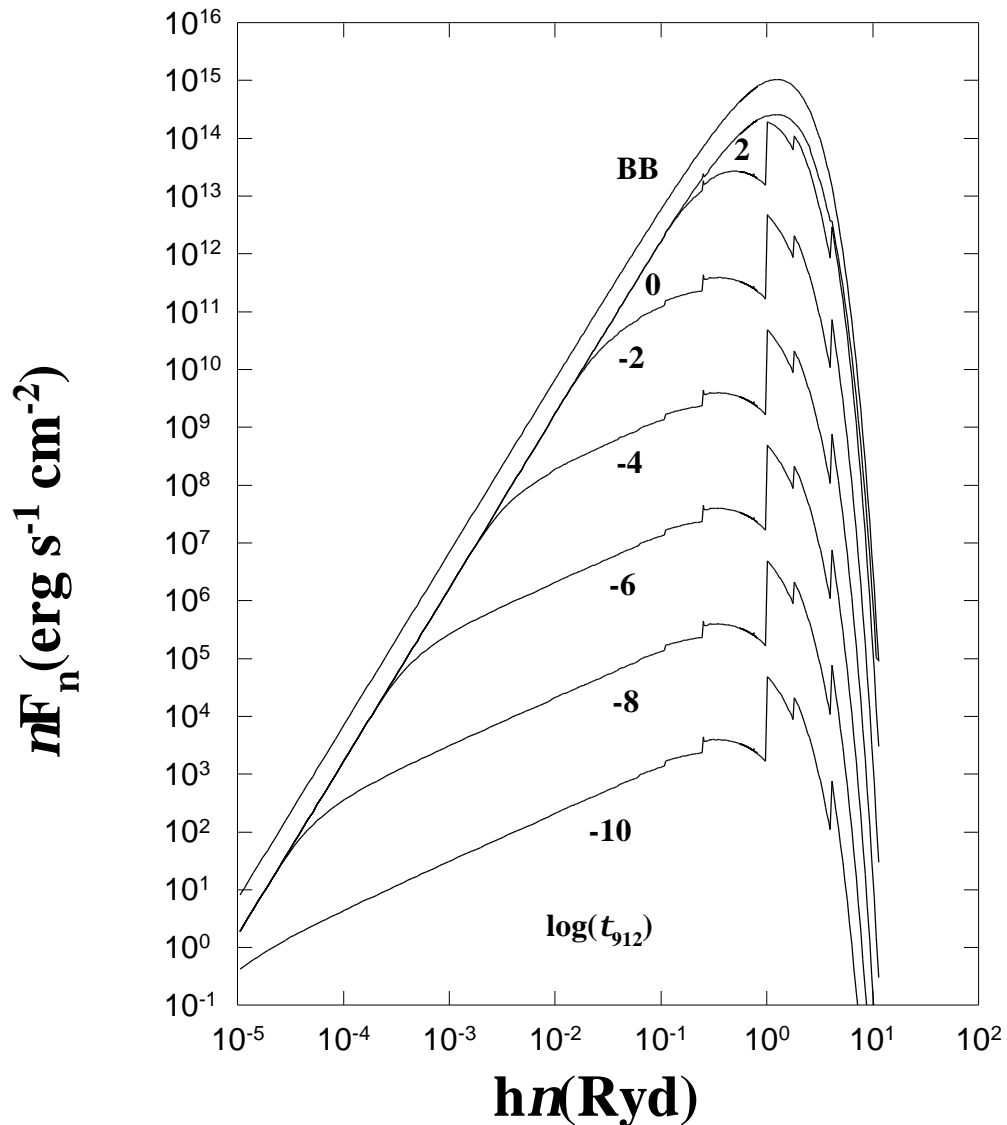


Figure 7 The emission from a dense slab of gas with cosmic abundances is shown as a function of the optical depth at the Lyman limit. The log of this optical depth is indicated on the figure. The top curve is for emission given by Planck's law. The continuous emission goes to the blackbody limit in the case of large continuum optical depths. conlte

thermodynamic equilibrium. As can be seen from the figure, the predicted continuum goes to the blackbody limit.

6. H⁻ AND MOLECULES

6.1. Overview

An ion-molecule network, initially based on Black (1978) but heavily revised to include the network described by Hollenbach and McKee (1979; 1989), is included in CLOUDY. The network presently includes H⁻, H₂, H₂⁺, H₃⁺, HeH⁺, OH, OH⁺, CH, CH⁺, O₂, O₂⁺, CO, CO⁺, H₂O, H₂O⁺, H₃O⁺, and CH₂⁺.

The treatment of the major hydrogen molecules (i.e., H₂, H₂⁺, H₃⁺ and H⁻) is discussed in the first subsection, and is based on Lambert and Pagel (1968); Black (1978); Lites and Mihalas (1984); Hollenbach and McKee (1979; 1989; hereafter HM79 and HM89); Tielens and Hollenbach (1985a, b; hereafter TH85), Lenzuni, Chernoff, and Salpeter (1991; hereafter LCS91), and Wolfire, Tielens, and Hollenbach (1990); Crosas and Weisheit (1993); and Puy et al (1993). This section is adapted from Ferland and Persson (1989) and Ferland, Fabian, and Johnstone (1994).

6.2. The Saha Equation for Arbitrary Systems

The Boltzmann equation relates the densities of related species by the expression

$$\frac{n_{final}}{n_{initial}} = \frac{\mathbf{r}_{final}}{\mathbf{r}_{initial}} \exp(-\Delta E / kT) \quad (211)$$

where $n_{initial}$ and n_{final} indicate the densities of the initial and final states, and the ρ 's are the densities of available states at a given energy. Consider the process $i \Rightarrow j+k$. The energy change during this process is

$$\Delta E = c_i + \frac{1}{2}mv^2 \quad (212)$$

where the first term is the ionization or dissociation potential of the initial system, and the second term represents the kinetic energy of the system in the final state. The sign of ΔE is related to the energies of the initial and final systems by

$$E_{final} = E_{initial} + \Delta E \quad (213)$$

The ρ 's entering equation 211 are the total densities of states accessible at an energy E . Since the initial state is a bound particle we can take it as at rest in the lab frame, and consider the final state consisting of two constituent particles moving with kinetic energy ΔE . The density of states of the final particles can be written as the product of densities of states due to electron spin and to motion of the particle. Nuclear spins are assumed to be uncorrelated, so nuclear statistical weights cancel out and are not carried through.

Considering only spin and motion (momentum) the total density of states is the spin statistical weight of the particle g_{spin} multiplied by the density of states due to momentum g_p (Mihalas 1978, p 112; Elitzur 1992, p 14):

$$\mathbf{r}_{total} = g_{spin} g_p \quad (214)$$

where g_p is

$$g_p = \frac{dx dy dz dp_x dp_y dp_z}{h^3} . \quad (215)$$

The volume element can be removed from the problem by defining it as the volume containing one particle,

$$dx dy dz = (n_k / g_k)^{-1} \quad (216)$$

while the momentum volume element is given in terms of the particle's speed v by

$$dp_x dp_y dp_z = 4\mathbf{p}^2 dp = 4\mathbf{p} m^3 v^2 dv . \quad (217)$$

Combining these with equation 211 we find

$$\frac{n_{final} n_k}{n_{initial} n_i} = \frac{n_j n_k}{n_i} = \left(\frac{g_{spin,j} g_{spin,k}}{g_{spin,i}} \right) \left(\frac{g_{p,j} g_{p,k}}{g_{p,i}} \right) \exp(-\Delta E / kT). \quad (218)$$

Shortening $g_{spin,x}$ to simply g_x , and using equation 217, we find

$$\frac{n_j n_k}{n_i} = \left(\frac{g_j g_k}{g_i} \right) \left(\frac{4\mathbf{p}^3 m_j^3 v_j^2 \exp(-\frac{1}{2} m_j v_j^2 / kT) dv_j m_k^3 v_k^2 \exp(-\frac{1}{2} m_k v_k^2 / kT) dv_k}{h^3 m_i^3 v_i^2 \exp(-\frac{1}{2} m_i v_i^2 / kT) dv_i} \right) \exp(-c / kT) \quad (219)$$

Integrating each energy term over velocity, making the substitution

$$x \equiv \left(\frac{m}{2kT} \right)^{1/2} v , \quad (220)$$

we find

$$\int_0^\infty v_j^2 \exp(-\frac{1}{2} m_j v_j^2 / kT) dv_j = \left(\frac{2kT}{m_j} \right)^{3/2} \int_0^\infty \exp(-x^2) x^2 dx = \left(\frac{2kT}{m_j} \right)^{3/2} \frac{\mathbf{p}^{1/2}}{4} \quad (221)$$

where the root π over 4 is the value of the integral. The final form of the Saha equation, for an arbitrary system, is:

$$\begin{aligned} \frac{n_j n_k}{n_i} &= \left(\frac{g_j g_k}{g_i} \right) \left(\frac{2\mathbf{p} kT}{h^2} \frac{m_j m_k}{m_i} \right)^{3/2} \exp(-c / kT) \\ &= 8.7819 \times 10^{55} \left(\frac{g_j g_k}{g_i} \right) \left(\frac{T m_j m_k}{m_i} \right)^{3/2} \exp(-c / kT) \end{aligned} \quad (222)$$

For the case of ionization producing an electron, the mass of the electron is neglected relative to the mass of the atom. If the atom and ion are i and j , then the assumption is that m_i and m_k are identical, and cancel out. In this case we obtain the form of the Saha equation most often encountered, with the 2 being the spin statistical weight of the electron:

$$\frac{n_{ion} n_e}{n_{atom}} = \left(\frac{2g_j}{g_i} \right) \left(\frac{2\mathbf{p} m_e kT}{h^2} \right)^{3/2} \exp(-c / kT). \quad (223)$$

In the case of molecular hydrogen

$$\frac{n_H n_H}{n_{H_2}} = 4 \left(\frac{\mathbf{p} k T m_p}{h^2} \right)^{3/2} \exp(-\mathbf{c} / kT). \quad (224)$$

6.3. The Hydrogen Network

The main hydrogen network includes H^- , H_2 , H_2^+ , H_3^+ , and HeH^+ , and its solution is performed in subroutine **hmole**.

The statistical weight of H_2^+ is 4 while that of H_2 is 1 and the dissociation energies are 2.647 eV and 4.477 eV respectively.

The set of balance equations for the first three species is solved simultaneously, using the matrix:

$$\begin{pmatrix} H \text{ conservation} \\ H^- \text{ balance} \\ H_2 \text{ balance} \\ H_2^+ \text{ balance} \\ H_3^+ \text{ balance} \end{pmatrix} \begin{pmatrix} n(H^o) \\ n(H^-) \\ n(H_2) \\ n(H_2^+) \\ n(H_3^+) \end{pmatrix} = \begin{pmatrix} n(H^o) \\ 0 \\ 0 \\ 0 \\ 0 \end{pmatrix}. \quad (225)$$

In the balance equations the process that destroy species x are entered as $c(x, x)$, (these are negative), while those which create x from y are entered as $c(x, y)$.

6.4. LTE Populations of Hydrogen Molecules

In much of the following discussion comparison and relationships will be made between the predicted hydrogen species populations and their LTE values.

The LTE relative population density of H^- is

$$P^*(H^-) = \frac{n^*(H^-)}{n_e n(H^o)} = \frac{g_{H^-}}{g_{H^o} g_e} \left(\frac{h^2}{2\mathbf{p} m_e kT} \right)^{3/2} \exp(I(H^-) / kT) \quad (\text{cm}^3) \quad (226)$$

where g_i is the statistical weight of the constituents, ($g_{H^-} = 1$; $g_{H^o} = 2$; and $g_e = 2$), $I(H^-) = 0.055502$ Ryd is the binding energy of the negative hydrogen ion, and other constants have their usual meaning. This population ratio is computed in routine **hmole** and assigned the variable name **phmlte**.

The LTE relative population density of H_2 is

$$P^*(H_2) = \frac{n^*(H_2)}{n(H^o)n(H^o)} = \frac{g_{H_2}}{g_{H^o} g_{H^o}} \left(\frac{h^2}{\mathbf{p} m_p kT} \right)^{3/2} \exp(I(H^-) / kT) \quad (\text{cm}^3) \quad (227)$$

This is referred to as **ph2lte**. The LTE population of H_2^+ is computed similarly, and referred to as **phplte**.

6.5. The H⁻ Balance; Radiative Processes

Although only a trace amount of hydrogen is in the form of H⁻, the opacity provided by this ion is often dominant in the optical and near infrared, and helps couple energy in the near infrared continuum to moderately ionized gas. The methods and approximations employed to include heating and cooling by H⁻ are described here. Other discussions can be found in Lambert and Pagel (1968), Vernazza, Avrett, and Loeser (1981), and Lites and Mihalas (1984). This section is based on Ferland and Persson (1989).

The equilibrium density of H⁻ is determined by assuming statistical equilibrium, and balancing production and destruction mechanisms. Great care is taken in including both forward and back reactions, to ensure that the present treatment of H⁻ is capable of going to LTE in the limit of high radiation or particle densities.

6.5.1. Radiative attachment

This is the most important creation mechanism for H⁻ at low densities, when three-body processes are negligible;



For temperatures greater than 10⁴ K the rate coefficient is evaluated by numerically integrating the photodetachment cross section over frequency;

$$a_{rad}(T) = P^*(H^-) \int_{n_0}^{\infty} a_n \frac{8\pi n^2}{c^2} \exp(-hn/kT) dn \quad (\text{cm}^3 \text{ s}^{-1}) \quad (229)$$

where cross sections computed by Wishart (1979) and spline interpolation are used. These cross sections are in excellent agreement with the velocity operator bound-free cross sections tabulated by Doughty et al. (1966). The energy interval between the photodetachment threshold at 0.055502 Ryd and ~1.8 Ryd is divided into roughly 100 cells with logarithmically increasing width, and the integration is carried out as a straight forward sum.

This method is not numerically expedient for very low temperatures, where the energy bandwidth of the integral is small, and a much finer frequency grid would be required. Rather, the integration was carried out using spline interpolation and 32 point gaussian quadrature, integrating over factors of two in $h\nu/kT$. The results were then fitted with a set of power-laws. The rate coefficients ($\text{cm}^3 \text{ s}^{-1}$) can be approximated by:

$$a(T_e) = \begin{cases} 8.934 \times 10^{-18} T^{0.505} & 1K \leq T < 31.62 \text{ }^\circ\text{K} \\ 5.159 \times 10^{-18} T^{0.664} & 31.62K \leq T < 90 \text{ }^\circ\text{K} \\ 2.042 \times 10^{-18} T^{0.870} & 90K \leq T < 1200 \text{ }^\circ\text{K} \\ 8.861 \times 10^{-18} T^{0.663} & 1200K \leq T < 3800 \text{ }^\circ\text{K} \\ 8.204 \times 10^{-17} T^{0.393} & 3800K \leq T \leq 10^4 \text{ }^\circ\text{K} \end{cases} \quad (230)$$

These approximations fit the exact numerical results with a mean deviation of 0.7 percent, and the largest error of 2.05 percent, over the indicated temperature range.

Tests show that the numerical radiative attachment rates computed here are in very good agreement with the approximation given by Hutchings (1976), who used the cross sections computed by Doughty et al. (1966), for temperatures $500 \text{ K} \leq T \leq 2500 \text{ K}$. (Notice that there is a typographical error in the approximation for the radiative attachment rate given by Palla, Salpeter, and Stahler 1983.) It is also within 10% of the value given by Dalgarno and Kingston (1963), which was based on earlier calculations of the photodetachment cross section.

Continuum occupation numbers can be large in the infrared. The induced radiative attachment rate coefficient is

$$a_{ind}(T) = P^*(H^-) \int_{n_0}^{\infty} a_n \frac{4p J_n(t)}{hn} \exp(-hn/kT) dn \quad (\text{cm}^3 \text{ s}^{-1}) \quad (231)$$

where the mean intensity of the depth-dependent continuum is $J_\nu(\tau)$. This expression is used for all temperatures.

6.5.2. Photodetachment

Photodetachment,



is the dominant H⁻ destruction mechanism for many conditions. The rate is evaluated in the standard manner;

$$\Gamma(H^-) = \int_{n_0}^{\infty} a_n(bf) \frac{4p J_n(t)}{hn} dn \quad (\text{s}^{-1}) \quad (233)$$

The integral is evaluated as a sum over the numerically binned continuum. The incident continuum is then attenuated by optical depth increments

$$dt(H^-) = a_n(bf) n(H^-) \left\{ 1 - \exp(-hn/kT) / b_{H^-} \right\} f(r) dr \quad (234)$$

where b_{H^-} is the departure coefficient for H⁻, $b_{H^-} \equiv n(H^-) / n^*(H^-)$, $f(r)$ is the filling factor, and $n^*(H^-)$ is the LTE H⁻ density.

6.5.3. Photodetachment by hard photons

The H⁻ photoabsorption cross section increases above $\sim 3/4$ Ryd, energies where excitation of $n \geq 2$ levels is possible. Cross sections that include this process are taken from Broad and Reinhardt (1976). These calculations do not extend to high energies, so I scaled high-energy hydrogen cross sections by the ratio of H⁻ to H⁰ cross sections at 18\AA in order to take absorption of x- and γ - rays into account.

The cross section for $(\gamma, 2e^-)$ absorption is much smaller than (γ, e^-) (Broad and Reinhardt 1976), and this latter process is neglected.

6.5.4. The approach to LTE; high radiation densities

As a test of the assumptions and methods, the approach to LTE under conditions determined by radiative attachment (spontaneous and induced) and photodetachment are first considered. Tests in which gas with temperature T_e is exposed to black body radiation fields with color temperature T_{color} are computed. The color and gas temperatures are set equal, $T_e = T_{\text{color}}$, and the intensity of the radiation field is varied up to the black body limit. The intensity of the radiation field is parameterized by the equivalent energy density temperature $T_u = (u/a)^{1/4}$, where u is the energy density (erg cm^{-3} ; see above) and a is the Stefan's radiation density constant. The equilibrium population of H^- was computed, including all process mentioned below, but with the hydrogen density small enough (typically $\sim 10^5 \text{ cm}^{-3}$) for radiative processes to be most important. The H^- population is expressed as a departure coefficient, and the results are shown in Figure 8, for tests in which $T_{\text{color}} = 0.5, 1, \text{ and } 2 \times 10^4 \text{ K}$.

When $T_u = T_{\text{color}}$, and the radiation field is in strict thermodynamic equilibrium, radiative processes must hold H^- in LTE and departure coefficients of unity are expected. The computed departure coefficients for the three temperatures are 0.9998, 0.9996, and 1.0030, respectively. As the Figure shows, when T_u is lowered below T_{color} , the intensity of the radiation field falls below its thermodynamic equilibrium value, and the population of H^- increases. This is because the photodetachment rate (which is proportional to the intensity of the radiation field) is no longer in balance with the radiative attachment rate (which is proportional only to the electron density).

6.6. The H^- Balance; Collisional Processes

6.6.1. Associative detachment

The most important H_2 formation mechanism in grain-free environments, and a significant H^- destruction mechanism, is associative detachment,

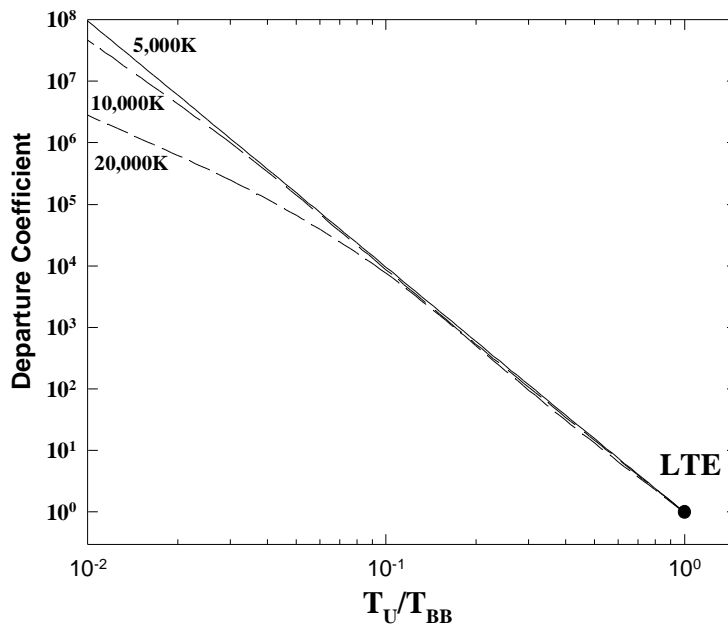


Figure 8 Departure coefficients for H^- . The figure shows tests in which the hydrogen density was held fixed at a low and the gas irradiated by black bodies with color temperatures of 5, 10, and $20 \times 10^3 \text{ K}$. Gas temperature and color temperatures were equal. The energy density temperature T_u was varied up to its LTE limit. The H^- departure coefficient is within 0.2% of unity when $T_u = T_{\text{color}}$.

where rate coefficients from Bieniek and Dalgarno (1979) are used. The reverse reaction rate coefficient C_R , for electron collisional dissociation of H_2^- , is related to the forward rate coefficient C_F by detailed balance;

$$C_R = C_F \frac{P^*(H^-)}{P^*(H_2^-)} . \quad (236)$$

6.6.2. Electron collisional detachment

For nebular temperatures ($\sim 10^4$ K) and moderate levels of ionization, the process



is a competitive H^- destruction mechanism. Rates taken from the compendium of Janev et al. (1987) are used. The reverse process, electron three-body recombination with neutral hydrogen, is included via detailed balance;

$$C_R = C_F P^*(H^-) . \quad (238)$$

6.6.3. Collisional ionization by suprathermal electrons

The total suprathermal collisional ionization rate is computed using approximations from Shull and Van Steenberg (1985). Ionization of H^- by suprathermal electrons is scaled from the H^0 rates using cross sections at 20 eV given by Janev et al. (1987). This energy was chosen as representative of the mean energy of the secondary electron shower. The majority of these collisions are of the form $e^- + H^- \rightarrow H(1s) + 2e^-$, although $e^- + H^- \rightarrow H^+ + 3e^-$ collisions occur roughly 1% of the time.

6.6.4. Mutual neutralization

Neutral hydrogen can charge transfer with the negative ion through



The rate coefficients given in Janev et al. (1987) are used. By far the largest rate coefficients are for collisions that populate hydrogen in the $n=3$ level. These rates are based on both experimental and theoretical data (see, for example, Peart et al. 1985).

The reverse reaction is included using detailed balance. If the rate coefficient for the forward reaction is C_F then the reverse reaction rate, and its rate coefficient C_R , are given by

$$H_{1s} n_i C_R = b_i P^*(H^-) n_e n_p C_F \quad (240)$$

where n_i and b_i are the population and departure coefficient of hydrogen in the i^{th} level.

6.6.5. Charge neutralization with heavy elements

The process



is considered by Dalgarno and McCray (1973), who give rate coefficients for very low temperatures and ionization levels. Judging from the curves given by Peterson et al. (1971), upon which the Dalgarno and McCray rates are based, the

approximation they give should still be valid (although very uncertain) at temperatures of general interest ($\sim 0.5 - 1.0 \times 10^4$ K). Here A^+ is all singly ionized species, which are assumed to be neutralized at the same rate.

6.6.6. Neglected processes

Collisional detachment by protons ($p^+ + H^- \rightarrow H + p^+ + e^-$), which has a negligible rate coefficient according to Janev et al. (1987), is neglected, as is collisional detachment by atomic hydrogen ($H^- + H \rightarrow 2H + e^-$), which has no reliable rate coefficient according to Lites and Mihalas (1984).

6.6.7. The approach to LTE; high hydrogen densities

A series of models in collisional equilibrium was computed. Radiative processes were also included, but the incident radiation field, a 10^4 K blackbody, was given a negligible intensity (an ionization parameter of 10^{-12}). Three temperatures, 0.5, 1, and 2×10^4 K, were considered to span the temperature range typical of regions with significant H^- population. The hydrogen density was varied between 10^8 and 10^{18} cm^{-3} to confirm the approach to LTE at high densities. The results of these calculations are shown in Figure 9.

For the majority of the calculations hydrogen is largely neutral, and for the smaller temperatures a significant fraction of the hydrogen was in the molecular form (H_2 and H_2^+). The calculation confirms that the departure coefficients are within 2% of unity at the highest densities computed.

6.7. The HeH^+ Molecular Ion

Rates for radiative association of He and H^+ to form HeH^+ are taken from Zygelman and Dalgarno (1990).

6.8. The H_2 Molecule

The hydrogen chemistry network includes the ion-molecules H_2 , H^- , H_2^+ , and H_3^+ . All of the chemical reactions involving H_2 described by HM79, TH85, HM89, and LCS91 have been

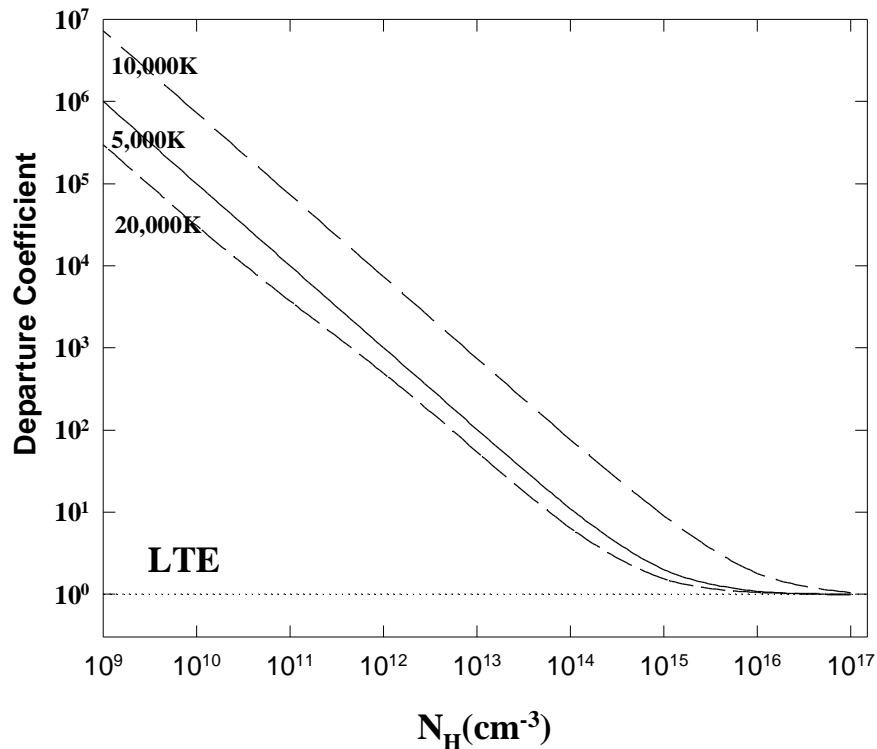


Figure 9 Departure coefficients for H^- are shown. The radiation density was low and the total hydrogen density varied. Three gas temperatures are shown. Collisions bring H^- to LTE at high densities. hmivsn

incorporated in the present treatment. Rather than go into these details, which are well presented in these papers, we only outline details of how some of the processes have been implemented.

6.8.1. Associative detachment of H⁻

The process



is the main H₂ formation mechanism in low-density grain-free regions, and is treated as described above. At temperatures of interest here (~10³ K) the rate for H₂ formation by this process is set by the rate for radiative association to form H⁻, and is of order 10⁻¹⁵ cm³ s⁻¹ (see above).

6.8.2. Catalysis on grain surfaces

The process



is a competitive H₂ formation process when grains are present. The rate coefficient is taken from Hollenbach and McKee (1979). Defining the fraction of atoms which form molecules as

$$f_a = \left(1 + 10^4 \exp(-600 / T_{gr})\right)^{-1} \quad (244)$$

then the rate coefficient is given by

$$a_{gr}(H_2) = 3 \times 10^{-18} \frac{\sqrt{T_e} A_{gr} f_a}{1 + 0.04 \sqrt{T_{gr} + T_e} + 0.002 T_e + 8 \times 10^{-6} T_e^2} \quad (245)$$

where A_{gr} is the grain abundance relative to the ISM value, and T_e and T_{gr} are the electron and grain temperatures respectively. The grain temperature is determined self-consistently, including radiative and collisional heating and cooling, as described in the section “Grain Physics” beginning on page 289.

At T_e=10³ K and T_{gr}=100 K (representative values of the gas and grain temperature in regions near a H⁰-H₂ interface) the rate coefficient for grain catalysis is ~4×10⁻¹⁸ cm³ s⁻¹. For most conditions of interest here radiative association is at least a competitive H₂ formation mechanism. The ratio of the two processes (referred to as the H⁻ and grain H₂ formation routes) is then

$$\frac{r(H^-)}{r(\text{grain})} = \frac{n_e a(H^-)}{n_H a(\text{grain})} \approx \frac{n_e}{n_H} 250 \quad (246)$$

i.e., the H⁻ route is faster for conditions of moderate ionization (n_e/n_H>4×10⁻³) even when grains are present. When grains are absent (or deficient) the H⁻ route dominates.

6.8.3. Excited atom radiative association

Rates for the process



are taken from Latter and Black (1991).

6.8.4. Excited molecular dissociation

Rates for the process



are given in Janev et al. (1987; their process 2.2.17), and these have been adopted by Lenzuni et al. (1991) and Crosas and Weisheit (1993) in their work on high density gas. Tests show that this process, if taken at face value, is by far the fastest destruction mechanism for molecular hydrogen under ISM conditions.

The process outlined by Janev et al. (1987) involves an electron capture by H_2 into vibrationally excited levels ($4 \leq v \leq 9$). The process is fast at low temperatures because the energy barrier is small, and the excited levels have large populations at laboratory densities. The process proceeds much more slowly at ISM densities, however, because excited levels have populations below their LTE value. This situation is thus similar to that described by Dalgarno and Roberge (1979). We have modified the Janev et al. (1987) rates using the physics outlined by Dalgarno and Roberge.

6.8.5. Discrete absorption into Lyman and Werner bands

Line absorption and excitation leading to dissociation through the vibrational continuum,



is the dominant H_2 destruction mechanism in regions where photodissociation (by photons with $h\nu > 14.7$ eV) and photo-ionization (with $h\nu > 15.4$ eV) do not occur (Stecker and Williams 1967).

Photodissociation through the Lyman-Werner bands occurs through a large number of transitions between 1109\AA and the Lyman edge for a region shielded by atomic hydrogen (i.e., no radiation shortward of 912\AA). Individual H_2 electronic transitions become optically thick for sufficient column densities, and eventually the H_2 becomes self-shielding. H_2 then becomes the dominant hydrogen species.

Photodissociation through the Lyman-Werner bands is included using the approximations outlined by TH85. The incident radiation field is taken as the mean over the energy interval $1109\text{\AA} - 912\text{\AA}$, (appropriate for photo-excitation into the $B^1 \Sigma_u^+$ electronic state). This quantity is then reposed in terms of the Habing (1968) radiation field, which is the quantity used by TH85. H_2 self-shielding is included using escape probabilities and the deduced optical depth, again using the approximations described by TH85.

6.8.6. Photo-ionization to H_2^+

Photons with energies greater than 15.4 eV produce H_2^+ via



This process both creates H_2^+ and heats the gas. Photo-absorption cross sections are taken from the compendium of Janev et al. (1987).

6.8.7. Collisional dissociation by H^0 , He^0 , and e

The rate coefficient for the forward process, collisional dissociation by the species S (one of H^0 , He^0 , or e^-),



is taken from Dove and Mandy (1986; dissociation by H^0), Dove et al. (1987; dissociation by He^0) and Janev et al. (1987; dissociation by electrons). These can be important destruction mechanisms only for warm regions of the ISM because of the large binding energy of H_2 ($\sim 50,000$ K).

The reverse reactions are included via detailed balance. Three-body formation of H_2 is important only for very high densities ($n \gg 10^{10} \text{ cm}^{-3}$).

6.8.8. H_2 cooling

Cooling due to collisional excitation of vibration-rotation levels of H_2 is treated using the analytic fits given in Lepp and Shull (1983). Both H_2 -H and H_2 - H_2 collisions are included.

6.8.9. H_2 heating

Many electronic excitations eventually decay to excited vibration-rotation levels within the ground electronic state, and these can then heat by gas following collisionally de-excitation. The scheme outlined by TH85 is again used.

6.9. Heavy Element Molecules

The heavy element molecule network described by Hollenbach and McKee (1989) has been incorporated into CLOUDY.

The system of equations which are solved are as follows:

$$\begin{pmatrix} C \text{ conservation} \\ O \text{ conservation} \\ CH \text{ balance} \\ CH^+ \text{ balance} \\ OH \text{ balance} \\ OH^+ \text{ balance} \\ CH_2^+ \text{ balance} \\ C^+ \text{ balance} \\ CO \text{ balance} \\ CO^+ \text{ balance} \\ H_2O \text{ balance} \\ H_2O^+ \text{ balance} \\ H_3O^+ \text{ balance} \\ O_2 \text{ balance} \\ O_2^+ \text{ balance} \end{pmatrix} \begin{pmatrix} C \\ O \\ CH \\ CH^+ \\ OH \\ OH^+ \\ CH_2^+ \\ C^+ \\ CO \\ CO^+ \\ H_2O \\ H_2O^+ \\ H_3O^+ \\ O_2 \\ O_2^+ \end{pmatrix} = \begin{pmatrix} C_{total} \\ O_{total} \\ 0 \\ 0 \\ 0 \\ 0 \\ 0 \\ 0 \\ 0 \\ 0 \\ 0 \\ 0 \\ 0 \\ 0 \\ 0 \\ 0 \end{pmatrix} \quad (252)$$

The heavy element chemistry network includes the molecules CH, CH⁺, OH, OH⁺, CH₂⁺, CO, CO⁺, H₂O, H₂O⁺, H₃O⁺, O₂, and O₂⁺. The heavy element network, the hydrogen network described above, and the hydrogen-helium ionization balance network, are solved self-consistently. Of the 12 molecules in the heavy element network only CO develops a significant population under most circumstances.

6.9.1. Collisional Processes

The collision network described by Hollenbach and McKee (1989) is included (the original implementation of the network was based entirely on this work). Their approximations for the temperature dependence of the rate coefficients are used.

6.9.2. Photochemical processes and heating

Rates for photochemical reactions of the form $h\nu + XY \Rightarrow X + Y$ are largely taken from the compendium of Roberge et al. (1991). These are posed in terms of the average interstellar radiation field. They have been incorporated by taking the depth-dependent continuum, renormalizing this to the average interstellar radiation field, and then using the coefficients given by Roberge et al.

An exception to this prescription is CO, which can become a major opacity source. Photodissociation is treated by numerically integrating over the continuum (with a threshold of 12.8 eV) using the photodissociation cross section given by HM79.

Photodissociation heats the gas if the internal energy of the daughters is small. The kinetic energy is taken to be $\langle h\nu - DE \rangle$ where DE is the dissociation energy and the mean is over the portion of the Balmer continuum that is active. Again, an exception is CO (the most important since it is the only heavy molecule that becomes optically thick), where the heating is evaluated by numerically integrating over the attenuated incident continuum.

6.9.3. Cooling

Cooling due to collisional excitation of vibration-rotation levels of CO, CH, OH, and H₂O is treated using the scheme outlined by HM79. Of these CO is the most important.

7. HELIUM

7.1. Overview

Work on the helium atom is still underway, and this is a portion of the code that is most likely to change over the next few years. The following outlines the treatments of the various ions. The present situation is that the ionization of helium should be exact for all matter and photon densities. Problems arise for predicted HeII line emissivities at low densities, in which case the listed case B predictions should be used instead.

7.2. The Helium Ion

He⁺ is treated as a ten level atom, entirely analogous to the hydrogen atom. Full l-mixing is assumed, and 2s and 2p are treated independently.

7.3. The Helium Singlets

The He singlets are treated as a ten level atom, entirely analogous to the hydrogen atom. Full l-mixing is assumed, and 2s and 2p are treated independently.

7.4. The Helium Triplets

The helium triplets are presently treated as a five level atom. The number of levels is stored as *nhe3lvl*. Populations are stored in the vector *he3n*, which contains the population ratio n_i/He^+ .

The population of the metastable 2³S level is determined including all processes that create and destroy the level. Processes that destroy 2³S include photoionization and collisional ionization, radiative decays to ground, and collisional transitions to the singlets. Processes that create populations include three-body and radiative recombination and collisions to the triplets from the singlets. Including only radiative recombination, exchange collisions to the singlets, and radiative decays to ground, the relative population of 2³S can be written as

$$\frac{He(2^3S)}{He^+} = \frac{5.79 \times 10^{-6} t_4^{-1.18}}{1 + 3110 t_4^{-0.51} n_e^{-1}} \quad (253)$$

where t_4 is the electron temperature in units of 10⁴ K. This actual computed value of this ratio (all processes included) is *hn3n(1)*.

7.5. Ionization Equilibria

The ionization equilibria of the various ions/atoms is accurate for all photon and electron densities. Tests presented in Part III of this document show that the balance goes to LTE in the high photon and electron density limits.

7.6. Line Emission

Emission from the triplets should be nearly exact. The model helium ion and singlets assumes full l-mixing of levels higher than 2, and so the line calculations are

only correct at high densities. At low densities the case B predictions (printed with the label “Ca B”) should be used instead.

The model atoms assume complete l-mixing for the singlets and helium ion, and they give exact results in the context of this assumption. Line intensities predicted by the 10-level atoms are indicated by the label “TOTL”. These include all optical depth and collisional effects.

Although the predictions are exact in the context of the well l-mixed approximation, this approximation is not valid at low densities, and the model atoms do not give accurate emissivities. The greatest problem is HeII $\lambda 4686$, for which the complete l-mixing assumption results in an intensity much smaller than the low density limit approximation. For these situations the simple case B predictions are preferred. Model atom predictions have labels such as “TOTL 4686” while the case B predictions have labels like “Ca B 4686”.

To summarize: For low density conditions, such as galactic nebulae, case B predictions should be used. At intermediate densities ($10^6 \leq n_e \leq 10^9 \text{ cm}^{-3}$) the predictions of the 10-level atom are probably better than case B predictions. At high densities ($n_e > 10^9 \text{ cm}^{-3}$), where collisional and radiative transfer effects are important, predictions of the 10-level atoms are better.

7.7. Helium Line and Continuum Arrays

The treatment of singlet and ionized helium is entirely analogous to that of hydrogen. Escape and destruction probabilities are evaluated in routine **HeTran**.

he1tau and **he1lim** These are the optical depths to the illuminated face, and the total optical depths from the previous iteration, for the HeI singlets.

he2tau and **he2lim** These are the optical depths to the illuminated face, and the total optical depths from the previous iteration, for the HeI singlets.

iphe1l, **iphe2l** Pointers to helium singlet and ion lines are called **iphe1l(u, l)**, and **iphe2l(u, l)**.

nhe1, **nhe2** Pointers to helium singlet and ion level ionization thresholds are called **nhe1(n)**, and **nhe2(n)**.

7.7.1. Recombination coefficients

Hydrogen and helium recombination coefficients are stored in the two dimensional vectors **hrec**, **he1rec**, and **he2rec**. The first dimension of the vector indicates the level of the model atom - **he1rec(1,x)** would refer to the ground level. The second dimension points to several quantities related to computation of the effective recombination coefficient.

he1rec, **he2rec** These mirror the **hrec** terms described on page 236, but for the helium atom and ion.

ophe1f, **ophe2f** These are the vectors containing the ratio of “other” to “total” opacities, which mirror the **ophf** term, described on page 236.

8. THE HEAVY ELEMENTS

8.1. Overview

The treatment of the ionization equilibrium of the elements heavier than helium is fairly conventional (see, for instance, Halpern and Grindlay 1980; Kallman and McCray 1982). This treatment is more approximate than that of hydrogen and helium at high densities ($n_{\text{H}} \gg 10^{10} \text{ cm}^{-3}$) because the majority of ions are treated considering only the ground term and continuum for each ionization stage. In all cases, collisional ionization from ground (using data from Voronov 1997; and Xu and McCray 1991) and a net three-body recombination coefficient (see, for example, Burgess and Summers 1976; the actual code is taken from Cota 1987) are included. Photoionization rates are modified for induced recombination as described by equation 202. All published charge transfer rate coefficients are also included (Kingdon and Ferland 1996). Inner shell photoionization is treated using Auger yields given by Kaastra and Mewe (1993). Photoionization cross sections are from Verner et al. (1996).

This treatment is approximate at high densities for two reasons. First, net radiative recombination coefficients, which have been summed over all levels (Aldrovandi and Pequignot 1972; Aldrovandi and Pequignot 1974; Gould 1978; Verner and Ferland 1996), are used. These sums are correct only in the low-density limit. At high densities levels can undergo collisional ionization before radiative decays to the ground state occur. A second problem is that substantial populations can build up in highly excited states when the density and temperature are high.

When this occurs the partition function of the atom or ion is no longer equal to the statistical weight of the ground state. As a result the ionization equilibrium of the heavy elements is approximate for very high densities ($n \gg 10^{10} \text{ cm}^{-3}$), with uncertainties increasing for higher densities. The statistical and thermal equilibrium of high-density gas is an area of on-going research.

Many exotic line transfer effects can influence certain lines due to coincidental line overlap. A good general reference to a number of these processes is the paper

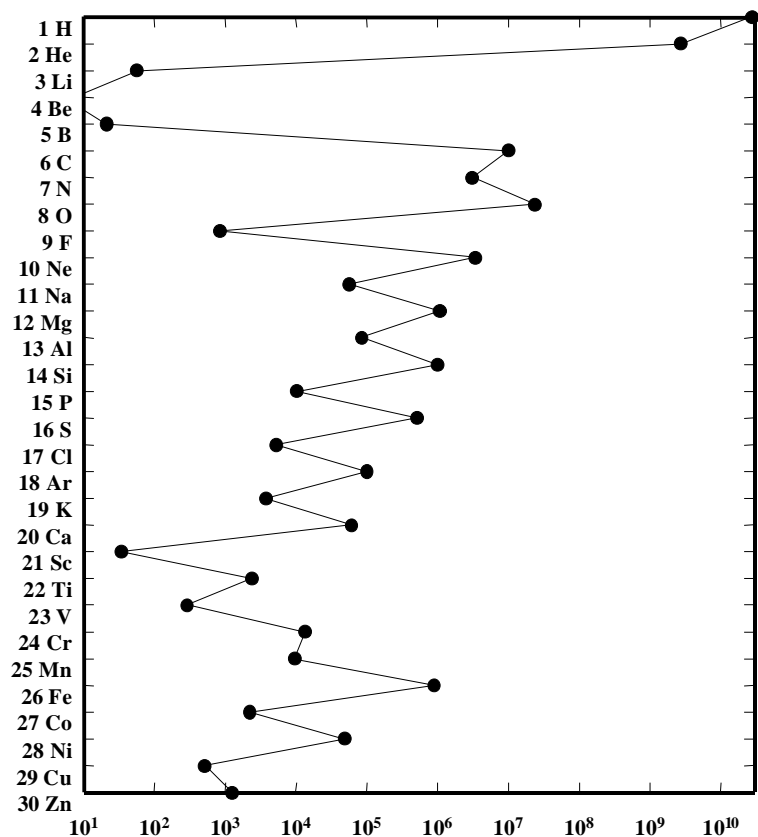


Figure 10 Solar system abundances are shown. ssystem

by Swings and Struve (1940). All of these processes are included in the line formation processes for those lines that are predicted by the code. Morton, York, and Jenkins (1988) and Verner, Verner, and Ferland (1996) provide a line lists for UV resonance lines, and Bowen's 1960 paper on forbidden lines remains a classic.

The effects of resonant structures often dominate collision strengths for infrared transitions. Oliva, Pasquali and Reconditi (1996) stress the uncertainties these may introduce.

8.2. Solar System Abundances

Figure 10 plots the solar system abundances of the elements, as tabulated by Anders and Grevesse (1989) and Grevesse and Noels (1993). These abundances vs atomic number. The x-axis is the abundance by number relative to a scale where the abundance of silicon is 10^6 . The y-axis lists the atomic number and the chemical symbol for the element.

8.3. Periodic Table

A periodic table of the first 36 elements follows.

1 H																2 He	
3 Li	4 Be											5 B	6 C	7 N	8 O	9 F	10 Ne
11 Na	12 Mg											13 Al	14 Si	15 P	16 S	17 Cl	18 Ar
19 K	20 Ca	21 Sc	22 Ti	23 V	24 Cr	25 Mn	26 Fe	27 Co	28 Ni	29 Cu	30 Zn	31 Ga	32 Ge	33 As	34 Se	35 Br	36 Kr

8.4. Ionization Balance

8.4.1. Photoionization cross sections

Photoionization cross sections for all elements are evaluated using Dima Verner's routine *phfit*, which fits Opacity Project data where possible, and the best theoretical or experimental data for other cases. The fitting procedure is described in Verner Yakovlev, Band, and Trzhaskovshaya (1993), Verner and Yakovlev (1995), and Verner, Ferland, Korista, and Yakovlev (1996).

8.4.2. Auger multi-electron ejection

Many electrons may be ejected following removal of an inner electron. This is fully treated using electron yields taken from Kaastra and Mewe (1993), see page 263 for more details. This process couples non-adjacent stages of ionization. The code iterates on the ionization solution to keep the system of equations a bi-diagonal matrix (see page 272).

Figure 11 shows photoionization cross sections for each shell of atomic iron, along with plots of the electron yield, taken from Kaastra and Mewe (1993). A single photoionization of the 1s shell can remove as many as 8 electrons.

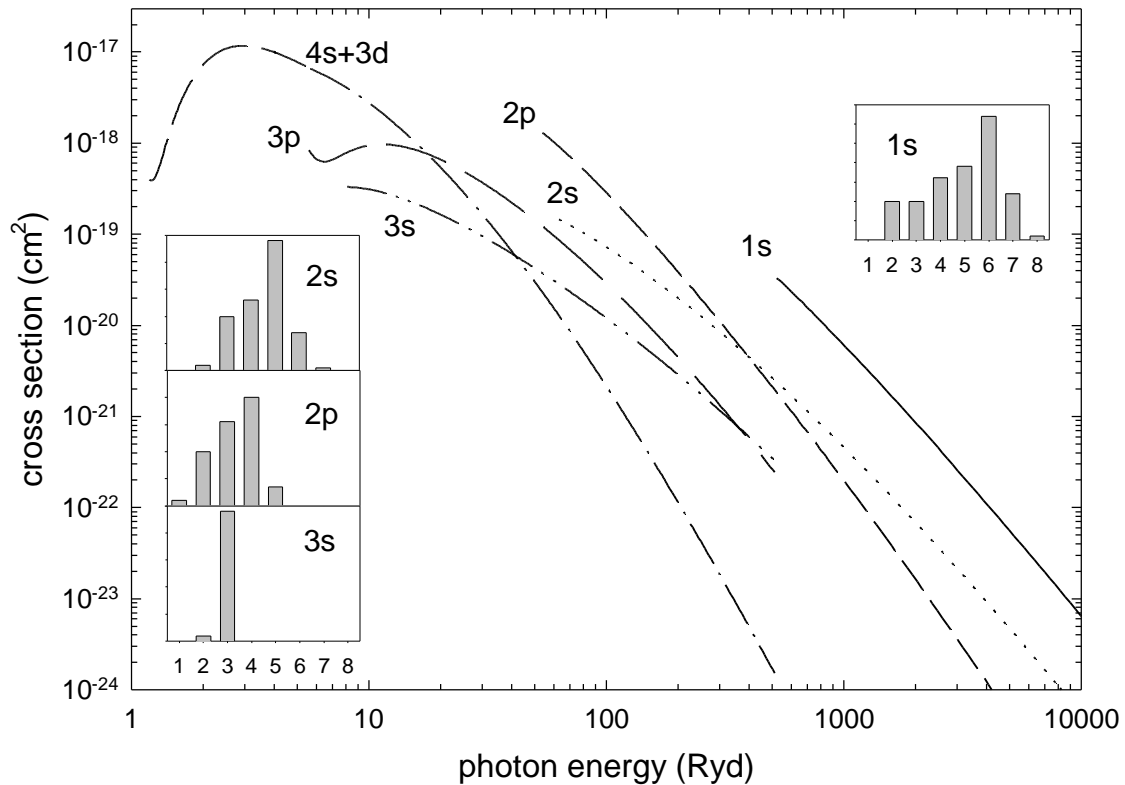


Figure 11 Photoionization cross sections and electron yields for neutral iron. Each of the subshell is shown along with the electron yield. IronPhoto

8.4.3. Collisional ionization rate coefficients

Fits to collisional ionization rate coefficients are evaluated in Dima Verner's routine *cf*it. These rates come mainly from Arnaud and Raymond (1992) and Arnaud and Rothenflug (1985), and by interpolation where rates are not given.

8.4.4. Radiative recombination rate coefficients

Radiative recombination rate coefficients are evaluated by Dima Verner's routine *rf*it, which uses fits by Arnaud and Raymond (1992), Verner and Ferland (1996), Shull and van Steenberg (1982), and by Landini and Monsignori Fossi (1990, 1991). Electron recombination rates are stored in *RecomRate(ion)* and are evaluated in the routine that drives the ionization balance.

8.4.5. Low temperature dielectronic recombination

Dielectronic recombination through low-lying autoionizing states is known to be the dominant recombination mechanism for many ions of second-row elements (i.e., Nussbaumer and Storey 1983). Unfortunately, these have not been computed for most third row or higher elements. This constitutes a major uncertainty in understanding the ionization balance of these elements, and has been described, for instance, by Ali et al. (1991). For those elements where a dielectronic recombination rate coefficient has not been computed and the parent ion is not a closed shell, the mean of the rate coefficient for C, N, O, and Ne is used instead. This assumption can be modified with the *dielectronic recombination* command described in part I.

8.4.6. Charge transfer

Rates for charge transfer between hydrogen and the heavy elements are evaluated using Jim Kingdon's routines **HCTIon** and **HCTRecom**. These rates are evaluated in routine **MakeCharTran**, which is called by routine **ionize**, and stored into master arrays, **HCharExclon** and **HCharExcRec**. The rate coefficient for the process $A_{\text{nelem}}^{i+1} + H^0 \Rightarrow A_{\text{nelem}}^i + H^+$ is stored as **HCharExcRec(i, nelem)**. The rate coefficient for the process $A_{\text{nelem}}^i + H^+ \Rightarrow A_{\text{nelem}}^{i+1} + H^0$ is stored as **HCharExclon(i, nelem)**.

For species more than 4 times ionized, a statistical estimate made by Alex Dalgarno (Ferland et al. 1997) is used. The rate coefficient for transfer between atomic hydrogen and a highly ionized species is given by $1.92 \times 10^{-9} \zeta \text{ cm}^3 \text{ s}^{-1}$, where ζ is the charge of the ion. Other atoms are treated analogously.

Charge transfer rates for elements other than hydrogen are evaluated within each routine responsible for determining the ionization balance of an element. These are accumulated as two sums, **CTHrec(1)** and **CTHion(1)**. Damped values are stored as array elements **CTHrec(2)** and **CTHion(2)**, which are entered within the hydrogen matrix loop. The arrays **HCharExcRec(I,nelem)** and **HCharExclon(I,nelem)** are the hydrogen recombination and ionization charge transfer rates. These were evaluated in routine **MakeCharTran**. The array **chargt(ion,1)** is the ionization, and **chargt(ion,2)** the recombination, charge transfer for species other than hydrogen, and was set in the routine that determines the ionization balance of the element..

8.5. Ionization Potentials

Table 22 lists ionization potentials for photoionization of the outer shell of the first thirty elements. These are given in Rydbergs for infinite mass nuclei.

Figure 12 shows the number of ions with valence shell ionization potentials within logarithmically increasing energy widths, as a function of the log of the ionization potentials in Rydbergs. Two large peaks occur, one near ~ 25 Ryd (~ 350 eV) and a second near ~ 160 Ryd (~ 2 keV). The continuum binning used in the code is designed to resolve these as separate features.

8.5.1. Ionization potential pointers

The vector **ipElement** contains pointers to thresholds of all valence and inner shell ionization edges of the elements. It has four dimensions. The first dimension is atomic weight of the element, and the second is the ionization stage, 1 for the atom, ranging up to the atomic number of the element. The third dimension is the shell number, 1 for the K-shell, ranging up to 7. The fourth dimension is a set of pointers. One is the lower energy limit or threshold for the shell, 2 is the upper limit as set in

Table 22 Ionization Potentials of the Elements (Rydbergs)

	1 H	2 He	3 Li	4 Be	5 B	6 C	7 N	8 O	9 F	10 Ne
1	9.996(-1)	1.807	3.963(-1)	6.852(-1)	6.099(-1)	8.276(-1)	1.068	1.001	1.280	1.585
2		4.000	5.559	1.338	1.849	1.792	2.176	2.581	2.570	3.010
3			9.003	1.131(+1)	2.788	3.520	3.487	4.038	4.609	4.664
4				1.600(+1)	1.907(+1)	4.740	5.694	5.689	6.405	7.138
5					2.500(+1)	2.882(+1)	7.195	8.371	8.393	9.275
6						3.601(+1)	4.058(+1)	1.015(+1)	1.155(+1)	1.161(+1)
7							4.903(+1)	5.434(+1)	1.361(+1)	1.524(+1)
8								6.405(+1)	7.011(+1)	1.757(+1)
9									8.107(+1)	8.790(+1)
10										1.001(+2)

routine **LimitSh**, and element three is the offset pointer to the opacity array.

A parallel two dimensional array, **nsShells(nelem, ion)**, contains the number of shells for the ionization stage *i* of the element with a given atomic weight. With this nomenclature, the pointer to the valence shell threshold of ionization stage *i* of an element *n* would be **ipElement(n,i, nsShells(n,i))**. These valence pointers are also stored in the array **ipHeavy(nelem, nstage)** in the common block of the same name. The array **ipLyHeavy** contains parallel pointers for the Ly α transitions of the elements.

Table 22b Ionization Potentials of the Elements (Rydbergs)

	11 Na	12 Mg	13 Al	14 Si	15 P	16 S	17 Cl	18 Ar	19 K	20 Ca
1	3.777(-1)	5.620(-1)	4.400(-1)	5.991(-1)	7.710(-1)	7.614(-1)	9.533(-1)	1.158	3.191(-1)	4.493(-1)
2	3.476	1.105	1.384	1.202	1.450	1.715	1.750	2.031	2.325	8.724(-1)
3	5.264	5.890	2.091	2.461	2.220	2.560	2.911	2.994	3.367	3.742
4	7.270	8.033	8.820	3.318	3.781	3.477	3.930	4.396	4.477	4.944
5	1.017(+1)	1.039(+1)	1.130(+1)	1.226(+1)	4.780	5.342	4.985	5.514	6.075	6.211
6	1.266(+1)	1.371(+1)	1.400(+1)	1.507(+1)	1.620(+1)	6.471	7.131	6.689	7.309	7.996
7	1.532(+1)	1.653(+1)	1.774(+1)	1.812(+1)	1.934(+1)	2.065(+1)	8.393	9.136	8.643	9.349
8	1.942(+1)	1.955(+1)	2.092(+1)	2.228(+1)	2.274(+1)	2.412(+1)	2.560(+1)	1.055(+1)	1.137(+1)	1.082(+1)
9	2.204(+1)	2.412(+1)	2.426(+1)	2.580(+1)	2.732(+1)	2.786(+1)	2.941(+1)	3.105(+1)	1.292(+1)	1.384(+1)
10	1.077(+2)	2.701(+1)	2.935(+1)	2.950(+1)	3.120(+1)	3.286(+1)	3.349(+1)	3.518(+1)	3.703(+1)	1.553(+1)
11	1.212(+2)	1.295(+2)	3.249(+1)	3.499(+1)	3.525(+1)	3.710(+1)	3.890(+1)	3.961(+1)	4.150(+1)	4.350(+1)
12		1.443(+2)	1.533(+2)	3.848(+1)	4.119(+1)	4.150(+1)	4.351(+1)	4.544(+1)	4.627(+1)	4.830(+1)
13			1.693(+2)	1.792(+2)	4.497(+1)	4.790(+1)	4.827(+1)	5.043(+1)	5.253(+1)	5.341(+1)
14				1.965(+2)	2.070(+2)	5.198(+1)	5.511(+1)	5.555(+1)	5.782(+1)	6.010(+1)
15					2.256(+2)	2.370(+2)	5.949(+1)	6.283(+1)	6.329(+1)	6.575(+1)
16						2.568(+2)	2.689(+2)	6.747(+1)	7.115(+1)	7.162(+1)
17							2.900(+2)	3.029(+2)	7.607(+1)	7.989(+1)
18								3.253(+2)	3.389(+2)	8.504(+1)
19									3.626(+2)	3.770(+2)
20										4.020(+2)

Table 22c Ionization Potentials of the Elements (Rydbergs)

	21 Sc	22 Ti	23 V	24 Cr	25 Mn	26 Fe	27 Co	28 Ni	29 Cu	30 Zn
1	5.396(-1)	5.012(-1)	4.954(-1)	4.974(-1)	5.464(-1)	5.808(-1)	5.780(-1)	5.613(-1)	5.678(-1)	6.904(-1)
2	9.408(-1)	9.981(-1)	1.077	1.213	1.149	1.190	1.255	1.335	1.491	1.320
3	1.820	2.020	2.154	2.275	2.475	2.253	2.462	2.596	2.708	2.919
4	5.401	3.180	3.433	3.613	3.763	4.028	3.768	4.035	4.217	4.366
5	6.752	7.298	4.798	5.105	5.321	5.513	5.843	5.593	5.872	6.071
6	8.136	8.783	9.415	6.662	7.037	7.281	7.497	7.938	7.570	7.938
7	1.014(+1)	1.035(+1)	1.107(+1)	1.177(+1)	8.768	9.187	9.481	9.775	1.022(+1)	9.996
8	1.162(+1)	1.252(+1)	1.275(+1)	1.357(+1)	1.430(+1)	1.111(+1)	1.160(+1)	1.191(+1)	1.227(+1)	1.286(+1)
9	1.323(+1)	1.412(+1)	1.513(+1)	1.538(+1)	1.630(+1)	1.717(+1)	1.368(+1)	1.418(+1)	1.463(+1)	1.492(+1)
10	1.654(+1)	1.587(+1)	1.694(+1)	1.796(+1)	1.825(+1)	1.926(+1)	2.024(+1)	1.651(+1)	1.705(+1)	1.749(+1)
11	1.836(+1)	1.948(+1)	1.879(+1)	1.990(+1)	2.102(+1)	2.133(+1)	2.244(+1)	2.359(+1)	1.956(+1)	2.014(+1)
12	5.052(+1)	2.142(+1)	2.264(+1)	2.191(+1)	2.311(+1)	2.431(+1)	2.469(+1)	2.588(+1)	2.711(+1)	2.284(+1)
13	5.562(+1)	5.790(+1)	2.472(+1)	2.608(+1)	2.525(+1)	2.653(+1)	2.786(+1)	2.822(+1)	2.947(+1)	3.085(+1)
14	6.106(+1)	6.344(+1)	6.585(+1)	2.824(+1)	2.962(+1)	2.883(+1)	3.021(+1)	3.162(+1)	3.197(+1)	3.337(+1)
15	6.817(+1)	6.923(+1)	7.172(+1)	7.431(+1)	3.199(+1)	3.359(+1)	3.263(+1)	3.408(+1)	3.557(+1)	3.601(+1)
16	7.416(+1)	7.673(+1)	7.791(+1)	8.063(+1)	8.327(+1)	3.596(+1)	3.763(+1)	3.663(+1)	3.822(+1)	3.984(+1)
17	8.041(+1)	8.313(+1)	8.584(+1)	8.709(+1)	8.996(+1)	9.275(+1)	4.017(+1)	4.199(+1)	4.094(+1)	4.255(+1)
18	8.915(+1)	8.974(+1)	9.261(+1)	9.547(+1)	9.680(+1)	9.981(+1)	1.027(+2)	4.462(+1)	4.652(+1)	4.549(+1)
19	9.466(+1)	9.893(+1)	9.959(+1)	1.026(+2)	1.056(+2)	1.070(+2)	1.106(+2)	1.133(+2)	4.929(+2)	5.130(+1)
20	4.171(+2)	1.047(+2)	1.093(+2)	1.100(+2)	1.131(+2)	1.163(+2)	1.178(+2)	1.211(+2)	1.242(+2)	5.420(+1)
21	4.435(+2)	4.593(+2)	1.154(+2)	1.201(+2)	1.208(+2)	1.241(+2)	1.275(+2)	1.291(+2)	1.318(+2)	1.357(+2)
22		4.870(+2)	5.036(+2)	1.265(+2)	1.314(+2)	1.322(+2)	1.357(+2)	1.392(+2)	1.400(+2)	1.435(+2)
23			5.326(+2)	5.499(+2)	1.382(+2)	1.382(+2)	1.433(+2)	1.441(+2)	1.478(+2)	1.503(+2)
24				5.803(+2)	5.983(+2)	1.504(+2)	1.557(+2)	1.566(+2)	1.597(+2)	1.629(+2)
25					6.300(+2)	6.489(+2)	1.631(+2)	1.687(+2)	1.689(+2)	1.737(+2)
26						6.819(+2)	7.015(+2)	1.763(+2)	1.807(+2)	1.822(+2)
27							7.357(+2)	7.563(+2)	1.900(+2)	1.945(+2)
28								7.923(+2)	8.129(+2)	2.043(+2)
29									8.504(+2)	8.724(+2)
30										9.106(+2)

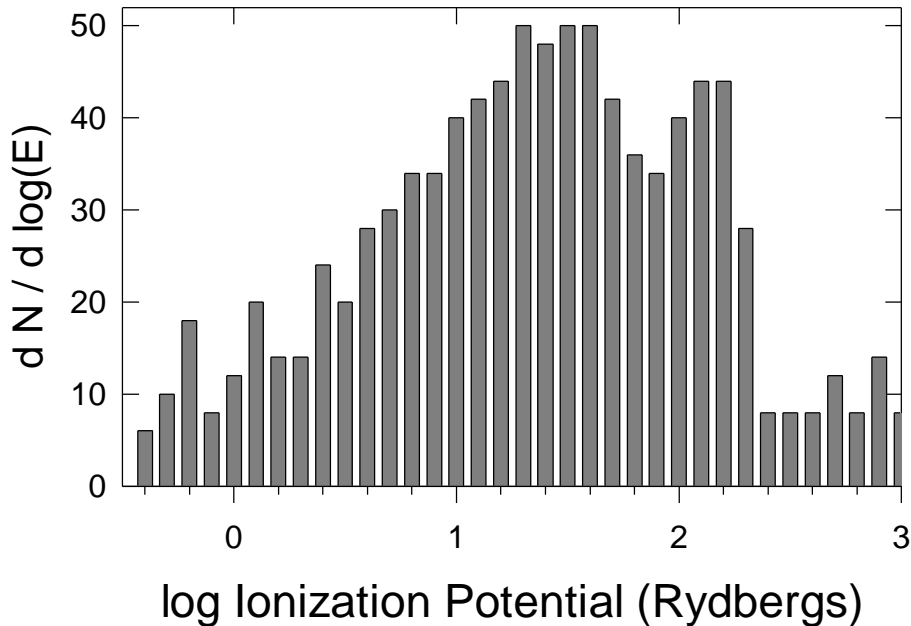


Figure 12 The number of elements with valence shell ionization potentials within logarithmically increasing energy widths is shown as a function of the log off the ionization potential. ipDen

8.6. Heavy Element Variables

8.6.1. Atomic weights

These are stored in atomic mass units, within the vector **AtomicWeight**. The mass (gm) of unit atomic weight m_{AMU} is stored as the included parameter file **amu**.

8.6.2. Ionic and total abundances

Information concerning the abundance of an element and the distribution of this abundance over the various stages of ionization is stored in the two dimensional real array **xIonFracs**(atomic number, ionization stage). This array is the sole member of the common block of the same name. The first dimension is the atomic number of the element, ranging from 1 (hydrogen) through the value of **limelm**, currently 30. The second dimension of the array ranges from 0 through **limelm+1**. Element 0 is the total abundance of that element in all gas phase forms, including molecules (but not grains). Elements 1 and higher are the abundances of that element in these stages of ionization (1 is the atom, 2 the first ion, etc). All abundances have units particles cm^{-3} .

8.6.3. Element names

chElementSym Standard chemical symbols for all elements now in the code are stored within this 2-character variable. This vector is the sole member of common block **ElmntSym**.

chIonStage This is a two character vector **limelm+1** long, containing the numbers from 1 through **limelm+1**. It is used for the spectroscopic designation of the

spectrum produced by a level of ionization. C IV would be represented as C 4. This vector is the sole member of common block **IonStage**.

chElNames This is a four character vector **limelm** long with the first four letters of the names of the first **limelm** elements. This vector is the sole member of common block **ElNames**.

8.6.4. Photoionization rates

These are stored in the multidimensional vector **PhotoRate**. This vector is the sole content of the common block of the same name. The first dimension is the atomic number of the element, and the second is the ionization stage, with the atom being one. The third dimension is a pointer to the shell. These range from 1 to 7, and are 1s, 2s, 2p, 3s, 3p, 3d, 4s. Note that, for neutrals and ions of third row and heavier elements, some of the inner shells may be only partially filled. The 4th dimension contains the photoionization rate (1) and the heating rate (2).

8.6.5. Fluorescence yields

These are taken from the compilation by Kaastra and Mewe (1993), and are stored in common block **yield**. The real variable **yield** has 4 dimensions. These are the atomic number (6 for carbon, etc), the stage of ionization (1 for the atom), the shell number in Dima's notation (1 for the 1s shell), and the fraction of ejected electrons corresponding to that index. For the latter, the index 1 will return the fraction of ionizations of that shell that eject only 1 electron. The second part of the common block is an integer array that indicates the most number of electrons that can be ejected.

8.6.6. Ionization potential pointers

These are set within routine **SetPoint**, which calls routine **ipShells** to actually set the pointers.

8.7. Isoelectronic Sequences

Table 23 lists all isoelectronic sequences for the first thirty elements. For sequences of elements heavier than K the ground configuration is correct for ions twice or more times ionized. For these heavier elements the atom and first ion may have non-standard configurations for the outer shell. The bottom row on the table indicates the shell number, in the nomenclature used for the photoionization shell layering.

8.8. Carbon

Low temperature dielectronic recombination rate coefficients are taken from Nussbaumer and Storey (1983).

Table 23 Isoelectronic Sequences

<i>1 H</i>	<i>2 He</i>	<i>3 Li</i>	<i>4 Be</i>	<i>5 B</i>	<i>6 C</i>	<i>7 N</i>	<i>8 O</i>	<i>9 F</i>	<i>10 Ne</i>
1s ² S	1s ² 1S	2s ² S	2s ² 1S	2p ² P	2p ² 3P	2p ³ 4S	2p ⁴ 3P	2p ⁵ 2P	2p ⁶ 1S
H 1	He 1	Li 1	Be 1	Bo 1	C 1	N 1	O 1	F 1	Ne 1
He 2	Li 2	Be 2	Bo 2	C 2	N 2	O 2	F 2	Ne 2	Na 2
Li 3	Be 3	Bo 3	C 3	N 3	O 3	F 3	Ne 3	Na 3	Mg 3
Be 4	Bo 4	C 4	N 4	O 4	F 4	Ne 4	Na 4	Mg 4	Al 4
Bo 5	C 5	N 5	O 5	F 5	Ne 5	Na 5	Mg 5	Al 5	Si 5
C 6	N 6	O 6	F 6	Ne 6	Na 6	Mg 6	Al 6	Si 6	P 6
N 7	O 7	F 7	Ne 7	Na 7	Mg 7	Al 7	Si 7	P 7	S 7
O 8	F 8	Ne 8	Na 8	Mg 8	Al 8	Si 8	P 8	S 8	Cl 8
F 9	Ne 9	Na 9	Mg 9	Al 9	Si 9	P 9	S 9	Cl 9	Ar 9
Ne 10	Na 10	Mg 10	Al 10	Si 10	P 10	S 10	Cl 10	Ar 10	K 10
Na 11	Mg 11	Al 11	Si 11	P 11	S 11	Cl 11	Ar 11	K 11	Ca 11
Mg 12	Al 12	Si 12	P 12	S 12	Cl 12	Ar 12	K 12	Ca 12	Sc 12
Al 13	Si 13	P 13	S 13	Cl 13	Ar 13	K 13	Ca 13	Sc 13	Ti 13
Si 14	P 14	S 14	Cl 14	Ar 14	K 14	Ca 14	Sc 14	Ti 14	V 14
P 15	S 15	Cl 15	Ar 15	K 15	Ca 15	Sc 15	Ti 15	V 15	Cr 15
S 16	Cl 16	Ar 16	K 16	Ca 16	Sc 16	Ti 16	V 16	Cr 16	Mm 16
Cl 17	Ar 17	K 17	Ca 17	Sc 17	Ti 17	V 17	Cr 17	Mm 17	Fe 17
Ar 18	K 18	Ca 18	Sc 18	Ti 18	V 18	Cr 18	Mm 18	Fe 18	Co 18
K 19	Ca 19	Sc 19	Ti 19	V 19	Cr 19	Mm 19	Fe 19	Co 19	Ni 19
Ca 20	Sc 20	Ti 20	V 20	Cr 20	Mm 20	Fe 20	Co 20	Ni 20	Cu 20
Sc 21	Ti 21	V 21	Cr 21	Mm 21	Fe 21	Co 21	Ni 21	Cu 21	Zn 21
Ti 22	V 22	Cr 22	Mm 22	Fe 22	Co 22	Ni 22	Cu 22	Zn 22	
V 23	Cr 23	Mm 23	Fe 23	Co 23	Ni 23	Cu 23	Zn 23		
Cr 24	Mm 24	Fe 24	Co 24	Ni 24	Cu 24	Zn 24			
Mm 25	Fe 25	Co 25	Ni 25	Cu 25	Zn 25				
Fe 26	Co 26	Ni 26	Cu 26	Zn 26					
Co 27	Ni 27	Cu 27	Zn 27						
Ni 28	Cu 28	Zn 28							
Cu 29	Zn 29								
Zn 30									
1	1	2	2	3	3	3	3	3	3

11 Na	12 Mg	13 Al	14 Si	15 P	16 S	17 Cl	18 Ar	19 K	20 Ca
3s ² S	3s ² 1S	3p ² P	3p ² 3P	3p ³ 4S	3p ⁴ 3P	3p ⁵ 2P	3p ⁶ 1S	3d ² D	3d ² 3F
Na 1	Mg 1	Al 1	Si 1	P 1	S 1	Cl 1	Ar 1	K 1 ¹	Ca 1 ¹
Mg 2	Al 2	Si 2	P 2	S 2	Cl 2	Ar 2	K 2	Ca 2 ¹	Sc 2 ¹
Al 3	Si 3	P 3	S 3	Cl 3	Ar 3	K 3	Ca 3	Sc 3	Ti 3
Si 4	P 4	S 4	Cl 4	Ar 4	K 4	Ca 4	Sc 4	Ti 4	V 4
P 5	S 5	Cl 5	Ar 5	K 5	Ca 5	Sc 5	Ti 5	V 5	Cr 5
S 6	Cl 6	Ar 6	K 6	Ca 6	Sc 6	Ti 6	V 6	Cr 6	Mm 6
Cl 7	Ar 7	K 7	Ca 7	Sc 7	Ti 7	V 7	Cr 7	Mm 7	Fe 7
Ar 8	K 8	Ca 8	Sc 8	Ti 8	V 8	Cr 8	Mm 8	Fe 8	Co 8
K 9	Ca 9	Sc 9	Ti 9	V 9	Cr 9	Mm 9	Fe 9	Co 9	Ni 9
Ca 10	Sc 10	Ti 10	V 10	Cr 10	Mm 10	Fe 10	Co 10	Ni 10	Cu 10
Sc 11	Ti 11	V 11	Cr 11	Mm 11	Fe 11	Co 11	Ni 11	Cu 11	Zn 11
Ti 12	V 12	Cr 12	Mm 12	Fe 12	Co 12	Ni 12	Cu 12	Zn 12	
V 13	Cr 13	Mm 13	Fe 13	Co 13	Ni 13	Cu 13	Zn 13		
Cr 14	Mm 14	Fe 14	Co 14	Ni 14	Cu 14	Zn 14			
Mm 15	Fe 15	Co 15	Ni 15	Cu 15	Zn 15				
Fe 16	Co 16	Ni 16	Cu 16	Zn 16					
Co 17	Ni 17	Cu 17	Zn 17						
Ni 18	Cu 18	Zn 18							
Cu 19	Zn 19								
Zn 20									
4	4	5	5	5	5	5	5	6	6

21 Sc	22 Ti	23 V	24 Cr	25 Mm	26 Fe	27 Co	28 Ni	29 Cu	30 Zn
3d ³ 4F	3d ⁴ 5D	3d ⁵ 6S	3d ⁶ 5D	3d ⁷ 4F	3d ⁸ 3F	3d ⁹ 2D	3d ¹⁰ 1S	4s ² S	4s ² 1S
Sc 1	Ti 1	V 1	Cr 1	Mm 1	Fe 1	Co 1	Ni 1	Cu 1	Zn 1
Ti 2	V 2	Cr 2	Mm 2	Fe 2	Co 2	Ni 2	Cu 2	Zn 2	
V 3	Cr 3	Mm 3	Fe 3	Co 3	Ni 3	Cu 3	Zn 3		
Cr 4	Mm 4	Fe 4	Co 4	Ni 4	Cu 4	Zn 4			
Mm 5	Fe 5	Co 5	Ni 5	Cu 5	Zn 5				
Fe 6	Co 6	Ni 6	Cu 6	Zn 6					
Co 7	Ni 7	Cu 7	Zn 7						
Ni 8	Cu 8	Zn 8							
Cu 9	Zn 9								
Zn 10									
6	6	6	6	6	6	6	6	7	7

8.9. Nitrogen

Low temperature dielectronic recombination rate coefficients are taken from Nussbaumer and Storey (1983). Photoionization from the excited ²D level of N^o is included, and can be the dominant ionization mechanism in well-shielded regions.

8.10. Oxygen

Low temperature dielectronic recombination rate coefficients are taken from Nussbaumer and Storey (1983).

¹ Neutral and first ion have non-standard filling.

Photoionization from the first two excited states of O^{2+} is included as a general ionization mechanism. This can dominate the ionization of the ion since it occurs behind the $He^+ - He^{++}$ ionization front, which shields the region from 4 Ryd and higher radiation. Similarly, photoionization from the first excited state and all inner shells of O^0 are included.

8.10.1. The O I model atom

A partial Grotrian diagram for the O I atom considered in the Ly β -O I fluorescence problem is shown in Figure 13. Multiplet averaged transition probabilities are taken from unpublished Opacity Project data, and the collision strengths are from the \bar{g} approximation for collisions between electrons and neutrals. Rates for fluorescence between the two transitions are computed as in Netzer et al. (1985).

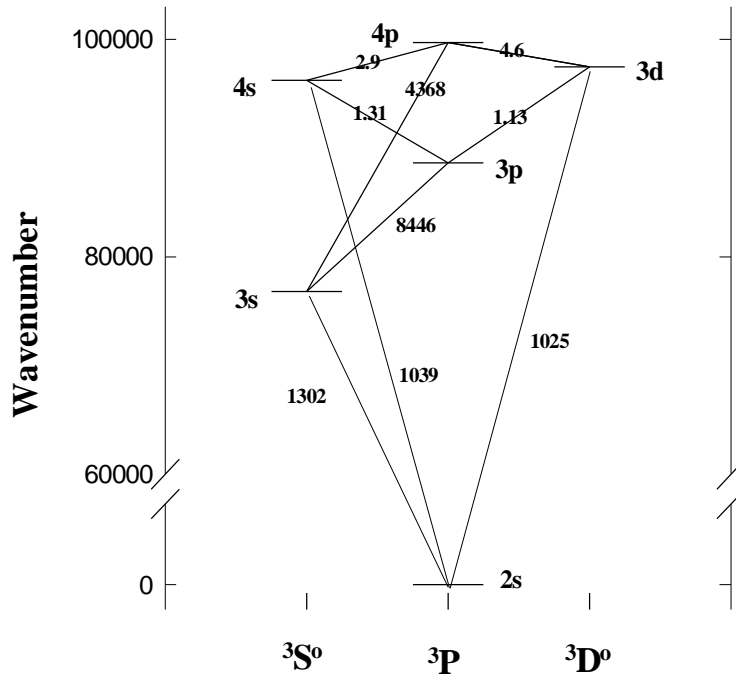


Figure 13 The levels of O^0 included in the calculation of the OI-Ly β pumping problem are shown. oigrot

Level populations including all physical processes are computed in routine **oilevl**. This routine is called by routine **p8446**, which is responsible for the interactions between the hydrogen and oxygen atoms. Routine **p8446** is called by routine **htrans**, and by routine **oxycol**.

8.11. Neon

Low temperature dielectronic recombination rate coefficients are taken from Nussbaumer and Storey (1987).

8.12. Magnesium

Low temperature dielectronic recombination rate coefficients for recombination to the atom are taken from Nussbaumer and Storey (1986). Rate coefficients have not been computed for recombination to the ions. Means of CNO are used.

Photoionization from the excited $^2P^0$ level of Mg^+ is included as a general Mg^+ destruction mechanism using Opacity Project data retrieved from **TopBase**. This can easily be the dominant Mg^+ destruction mechanism in BLR calculations since the excited state has an ionization potential below 1 Ryd. The code will generate a

comment at the end of the calculation if this is a competitive Mg^+ destruction mechanism.

8.13. Aluminum

Low temperature dielectronic recombination rate coefficients for recombination to the atom and first ion are taken from Nussbaumer and Storey (1986). Rate coefficients have not been computed for recombination to other ions. Means of CNO are used.

8.14. Calcium

Low temperature dielectronic recombination rate coefficients have not been computed for this element. Means of CNO are used.

8.14.1. The Ca II model atom

The Ca II ion is treated as a five-level atom plus continuum. The model atom is shown in Figure 14, and is similar to that described by Shine and Linsky (1974).

Collision strengths for j-mixing collisions are from Saraph (1970). Collision and radiative data for the 4s - 4p transition are taken from the compendium of Mendoza (1983), and all other collision data are from Chidichimo (1981) and Saraph (1970). Radiative data for the 3d - 4p and 4s - 3d transitions are from Black, Weisheit, and Laviana (1972); these are in good agreement with the calculations of Osterbrock (1951). The compendium by Shine and Linsky (1974) provides photoionization cross sections for excited levels, which are adopted here. Photoionization of the excited ^2D level by $\text{Ly}\alpha$

(Wyse 1941) and all other line or continuum sources is explicitly included. Recombination contributions to the population of individual levels are included by dividing the excited state recombination coefficient among the excited levels considered, according to their statistical weight and the rules of LS coupling.

All Ca II transitions (including the forbidden lines) can become quite optically thick. Radiative transfer is treated with the escape probability formalism, assuming incomplete redistribution, including destruction by background opacities.

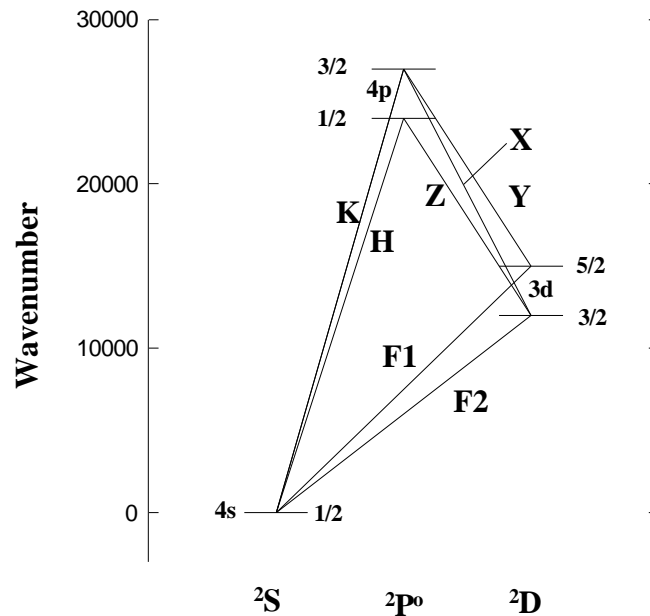


Figure 14 The five levels of Ca^+ included in the calculations are shown. The wavelengths of the predicted lines are K (3934), H (3969), X (8498), Y (8542), Z (8662), F1 (7291), and F2 (7324). ca2grot

8.15. Iron

Low temperature dielectronic recombination rate coefficients have not been computed for this element. Means of CNO are used. Charge transfer rate coefficients are from Neufeld and Dalgarno (1989), Neufeld (1989) and Ferland, Korista, Verner, and Dalgarno (1997).

8.15.1. The FeII model atom

This is an area of extensive activity. The majority of the cooling and emission due to FeII for high-density conditions comes from the simplified model atom proposed by Wills, Netzer, and Wills (1985). The lowest sixteen levels of the first four terms are also included. Figure 15 shows the atom and some of the lines predicted. The lines predicted by this model atom have been checked against the vastly larger and more complex FeII atom Katya Verner is now incorporating into the code, and the two agree very well.

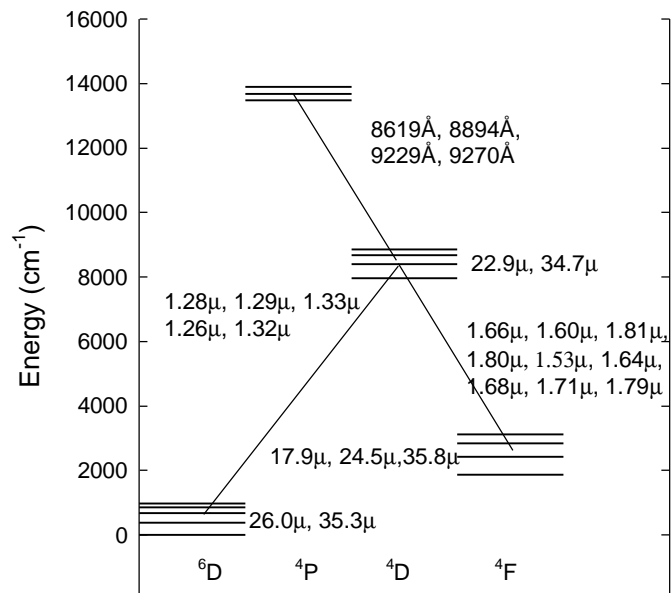


Figure 15 The sixteen level atom used to compute FeII IR emission. Lines predicted are indicated.

8.15.2. The FeIV model atom

FeIV is treated as a twelve-level atom, with energies from Sugar and Corliss (1985), transition probabilities from Garstang (1958), and collision strengths from Berrington and Pelan (1996). Figure 16 shows the model atoms with the lines predicted by the code indicated.

8.15.3. Fe K α emission

The intensity of the Fe K α line is predicted including both recombination and fluorescence. Figure 17 shows the fluorescence yield and K α energy. The line predictions are separated into “cold” iron (i.e., iron with M-shell electrons present) and “hot” iron (those ionization states producing lines with energies greater than ~ 6.4 keV). This includes the recombination and collisional contribution. The “TOTL” K α is the sum of the two.

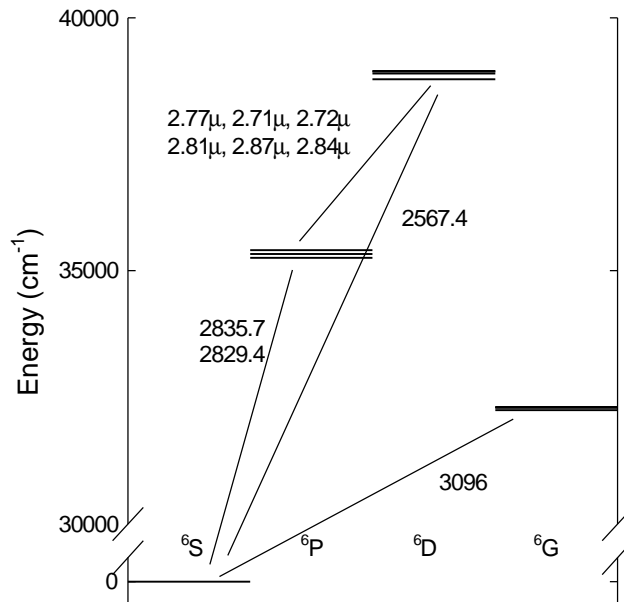


Figure 16 The twelve level atom used to compute FeIV emission. Lines predicted are indicated.

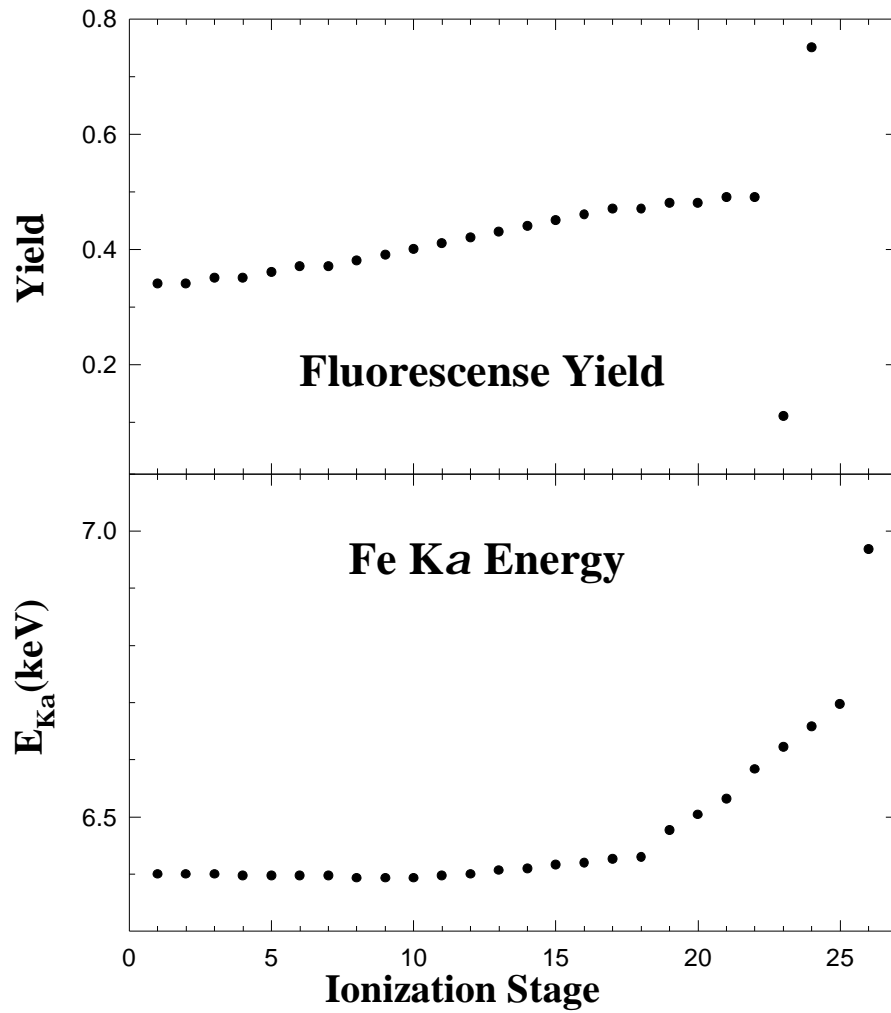


Figure 17 The fluorescence yield and energy of the emitted Fe K α photon are shown as a function of ionization stage. feka

8.16. Heavy Element Opacities

Figure 18 shows a calculation of the opacity of a solar gas with very low ionization.

8.17. Overall Reliability

Table 24
Ionization Balance Reliability

	1 H	2 He	3 Li	4 Be	5 B	6 C	7 N	8 O	9 F	10 Ne
1	A	A	A			A	A	A		
2		A	A	A		A	A	A		A
3			A	A	A	A	A	A		A
4				A	A	A	A	A		A
5					A	A	A	A		A
6						A	A	A		A
7							A	A	A	A
8								A	A	A
9									A	A
10										A

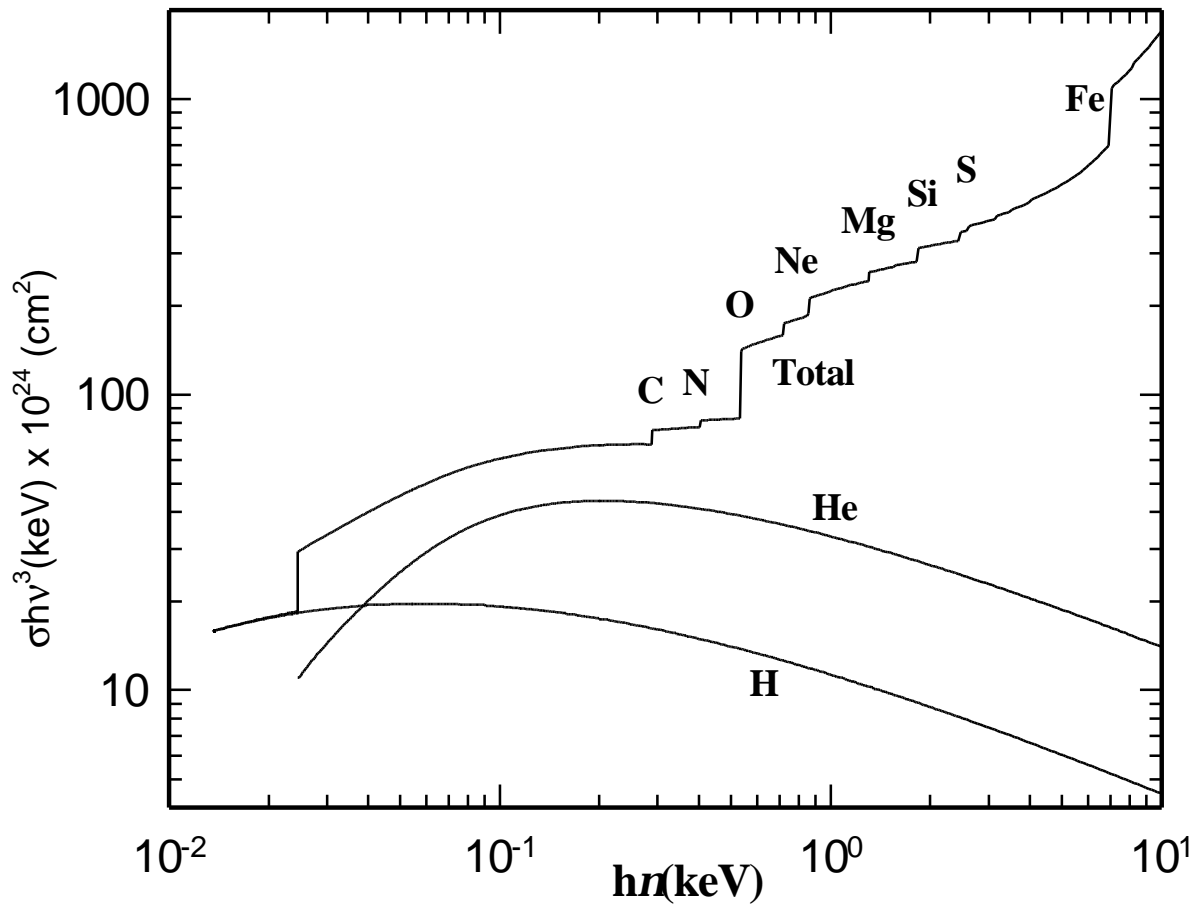


Figure 18 The opacity of a neutral gas with solar abundances is shown as a function of energy. The curve is scaled to allow direct comparison with conventional calculations of opacity at X-Ray energies (i.e., Morrison and McGammon 1983). hevopc

Ionization Balance Reliability Continued

	11 Na	12 Mg	13 Al	14 Si	15 P	16 S	17 Cl	18 Ar	19 K	20 Ca
1	A	A	A							
2		A	A							
3			A							
4				A						
5					A					
6						A				
7							A			
8								A		
9	A								A	
10	A	A								A
11	A	A	A							
12		A	A	A						
13			A	A	A					
14				A	A	A				
15					A	A	A			
16						A	A	A		
17							A	A	A	
18								A	A	A
19									A	A
20										A

Ionization Balance Reliability Continued

	21 Sc	22 Ti	23 V	24 Cr	25 Mn	26 Fe	27 Co	28 Ni	29 Cu	30 Zn
1										
2										
3										
4										
5										
6										
7										
8										
9										
10										
11	A									
12		A								
13			A							
14				A						
15					A					
16						A				
17							A			
18								A		
19	A								A	
20	A	A								A
21	A	A	A							
22		A	A	A						
23			A	A	A					
24				A	A	A				
25					A	A	A			
26						A	A	A		
27							A	A	A	
28								A	A	A
29									A	A
30										A

It is difficult to estimate the overall uncertainty present in an ionization balance calculation. The current photoionization cross section data are based on accurate experiments or the Opacity Project (Verner et al. 1996). These should be accurate to roughly 10% except near resonances. Although resonances are included in the Opacity Project data, the positions of these resonances are uncertain by more than their width because the OP was not intended as a structure calculation.

Recombination coefficients including low temperature dielectronic recombination have yet to be computed for the majority of the stages of ionization of the elements now in CLOUDY, but recombination from parent ions with closed shells is not affected, and good rates exist (Verner and Ferland 1996).

It is possible to make a subjective estimate of the uncertainty in the calculation of the ionization balance for nebular temperatures. Table 24 lists the elements now included in the calculations and gives this estimate of the uncertainty. For recombination from a closed shell autoionization resonances do not occur near threshold, recombination is primarily radiative, and the calculations should be virtually exact. Dielectronic recombination rates are also known for those species treated by Nussbaumer and Storey. These are given a quality weighting of A.

These uncertainties refer to the ionization balance of an optically thin cell of gas at nebular temperatures. The intensities of emission lines will be less uncertain than this for two reasons. First, the thermostat effect of any collisionally excited line prevents its intensity from changing by much. Second is the fact that the integrated

column density in an ion is affected as much by (fairly exact) quantities such as the ionization structure of H or He, as by the atomic data of a particular ion. At coronal temperatures the Burgess mechanism dominates, and the situation should be somewhat better.

8.18. The Bi-Diagonal Matrix

The ionization-recombination balance equations are written as a series of n equations coupling adjacent levels of ionization, i.e.,

$$n_z \Gamma_z^{eff} = n_{z+1} \sum n_x a_{z+1} \quad . \quad (254)$$

where the effective photoionization rate Γ includes all ionization processes (photoionization of valence and inner shells, collisional ionization, charge transfer ionization, etc) and is modified to include the Auger effect. The total recombination rate coefficient $\sum n_x a_{z+1}$ includes all recombination processes (dielectronic, radiative, 3-body, charge transfer). In much of the following this total recombination rate coefficient will be written simply as $n_e \alpha_e$, with the implicit understanding that all recombination processes are actually included.

The vector ***destroy(nelem, ion)*** contains total destruction rates. ***create(nelem, ion)*** is the total creation rates. The resulting ionization balance is solved in routine ***BiDiag***.

9. THERMAL EQUILIBRIUM

9.1. Overview

This section describes the system of equations setting the local thermal balance of a cloud. The electron temperature is the only thermodynamic temperature used to characterize the system. The electron velocity distribution is predominantly Maxwellian (Bohm and Aller 1947) although a trace constituent of non-thermal electrons may contribute under some circumstances. The electron temperature is defined by the balance between heating and cooling.

Heating or cooling can be defined relative to either the ground state or continuum, and this difference has caused some confusion in the literature. CLOUDY defines heating and cooling relative to the continuum, as in Osterbrock (1989). Note that, in this scheme of bookkeeping, photoionization contributes an amount of heat given by $h(\nu - \nu_0)$, where $h\nu_0$ is the ionization potential of the atom or ion, and emission of a recombination line *does not* constitute a cooling process. Heating and cooling rates are computed in cgs units (ergs, not Rydbergs) throughout CLOUDY.

9.2. Thermal Stability

The criterion for thermal stability used by CLOUDY is that the net cooling (i.e., cooling minus heating) has a positive temperature derivative (Field 1965). This can be expressed as

$$\frac{d(\Lambda - G)}{dT} > 0 . \quad (255)$$

The code will print a “u” next to the temperature in the zone results, and make a comment in the end, if possibly thermally unstable solutions were found. The criterion used by the code is that the derivative *at constant density* (isochoric) be positive. The more traditional criterion is that the derivative *at constant pressure* (isobaric) be positive (Field 1965).

The fact that the code identifies a region as possibly thermally unstable does not necessarily show that it is. The derivatives used in equation 255 are those found during the search for the thermal solution. As such, they are evaluated out of equilibrium, as part of the temperature solver. Their primary purpose was not to perform this thermal stability analysis. A section of Part III of this document goes into more detail about the stability check performed by the code, and how to do a better one.

9.3. Compton Energy Exchange

There are two parts to the Compton energy exchange problem. First, photons scatter off an electron at an angle θ , causing a change of photon energy due to Compton recoil given by

$$\frac{\Delta e_-}{e_0} = \left[1 - \frac{1}{1 + (e_0 / m_e c^2)(1 - \cos \theta)} \right] . \quad (256)$$

For isotropic scattering the median scattering angle corresponds to $\cos \theta = 0.5$. Scattering by thermal electrons crates a shift with a distribution centered at

$$\frac{\Delta \mathbf{e}_-}{\mathbf{e}_o} = \frac{4kT}{m_e c^2} \quad (257)$$

and a standard deviation given by

$$\frac{\mathbf{s}}{\mathbf{e}_o} = \sqrt{\frac{2kT}{m_e c^2}} \quad (258)$$

(see, e.g., Zycki et al. 1994).

The net volume heating rate ($\text{erg s}^{-1} \text{cm}^{-3}$) due to Compton energy exchange is given by

$$G_{Comp} - \Lambda_{Comp} = \frac{4p n_e}{m_e c^2} \left\{ \int \mathbf{s}_h J_n h n [1 + \mathbf{h}_n] dn - 4kT \int \mathbf{s}_c J_n dn \right\} \quad (259)$$

(see, for instance, Levich and Sunyaev 1970; and Krolik, McKee, and Tarter 1981). The two terms in braces are the heating and cooling terms respectively, while the factor in brackets in the first term accounts for heating due to both spontaneous and stimulated Compton scattering. Induced Compton heating is important when η_ν is large at frequencies where $h\nu \geq kT$. In fact it is, at most, a few percent effect in most circumstances.

The terms σ_h and σ_c appearing in equation 259 are the effective energy exchange (scattering) cross section for energy exchange, and differ from the Thomson cross section for energies $h\nu \sim m_e c^2$, where the Klein-Nishina cross section must be used. The numerical fits to Winslow's (1975) results, as used by Krolik, McKee, and Tarter (1981) and kindly provided by Dr. C.B. Tarter, were used. Defining

$$\mathbf{a} = \left\{ 1 + \mathbf{n}_{Ryd} \left(1.1792 \times 10^{-4} + 7.084 \times 10^{-10} \mathbf{n}_{Ryd} \right) \right\}^{-1} \quad (260)$$

and

$$\mathbf{b} = \left\{ 1 - \mathbf{a} \mathbf{n}_{Ryd} \left(1.1792 \times 10^{-4} + 2 \times 7.084 \times 10^{-10} \mathbf{n}_{Ryd} \right) / 4 \right\} \quad , \quad (261)$$

where ν_{Ryd} is the photon frequency in Rydbergs, the Compton energy-exchange rate coefficients are then $\sigma_h = \sigma_T \alpha$ and $\sigma_c = \sigma_T \alpha \beta$. Tests show that these are in excellent (much better than 1%) agreement with Guilbert's (1986) calculations for $h\nu < 10$ MeV, the energies where Guilbert's calculations are valid.

The total Compton heating-cooling rates are evaluated zone by zone in routine **highen**. The coefficients for the heating and cooling terms, i.e., α and the product $\alpha\beta$, are calculated in subroutine **SetPoint** at the beginning of the calculation and stored in the vectors **csigh**(ν) and **csigc**(ν). The heating is determined by summing over the continuum;

$$G_{Comp} = \frac{n_e}{mc^2} \mathbf{s}_T \left(h \mathbf{n}_{Ryd} \right)^2 \sum \mathbf{a}_i \mathbf{j}_i n_i^2 (1 + \mathbf{h}_i) \quad (262)$$

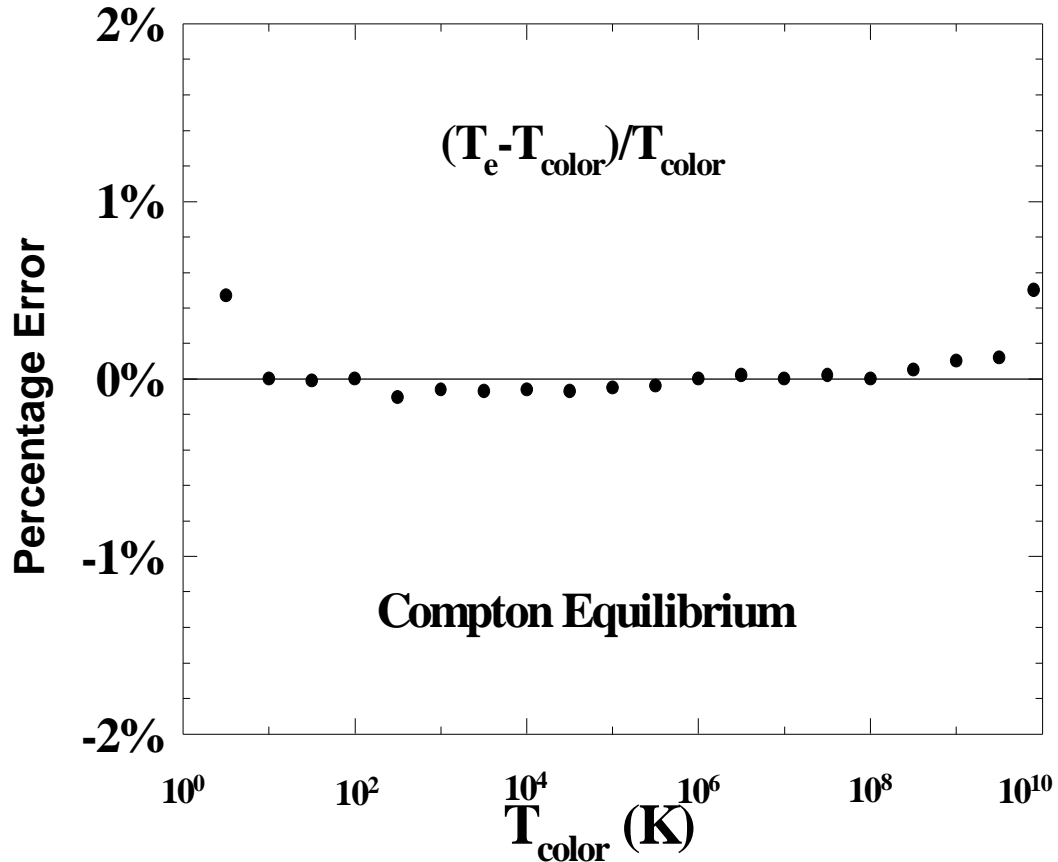


Figure 19 Thermal equilibrium in the Compton Limit. Calculations are for blackbody continua of various temperatures, given as T_{color} along the x-axis. The energy density temperature T_u is set equal to T_{color} . The density is adjusted to maintain ionization parameters $U \sim 10^{10}$, so that the thermal equilibrium equations are dominated by the Compton exchange problem. The deviation of the computed equilibrium temperature T_e from the asymptotic Compton temperature T_{color} is shown. Compton

where ϕ_i is the photon flux, stored in the vector variable **flux**, η_i is the photon occupation number, σ_T is the Thomson cross section, and ν_i is the photon energy in Rydbergs, stored in the vector variable **anu**. The heating and cooling rates are stored as the variables **cmheat** and **cmcool**.

Tests in which Compton energy exchange was the dominant physical process affecting the temperature were made, and the results are shown in Figure 19. A series of models in which the gas was irradiated by black body continua in strict thermodynamic equilibrium (i.e., $T_u = T_{\text{color}}$) and various hydrogen densities, was computed. Over the temperature range $3 \text{ K} \leq T_{\text{color}} \leq 10^{10} \text{ K}$ the computed equilibrium electron temperature equaled the color temperature within much better than 1% ($\langle T_e - T_{\text{color}} \rangle / T_{\text{color}} = -0.00073 \pm 0.0019$).

The input streams for the two limiting cases (for temperatures of $10^{9.5}$ K and 3 K respectively) follow²;

```

title Compton limit; high temperature limit
blackbody 9.5 lte % lte sets blackbody in strict T.E.
hden 10          % low enough for Compton to dominate
stop zone 1
print short
tolerance 0.0001 % set fine tolerance to check temp exactly

```

```

title Compton limit; low temperature limit
black linear 3 lte % set to 3K
lowest temperature linear 2K % allow equil temp below 10K
brems 5           % must have ionizing radiation
ionization parameter -5 % but not too much
hden -10          % set HDEN but does not matter
eden -2           % add some free electrons
stop zone 1
print short
tolerance 0.0001

```

The intended temperature range of validity for CLOUDY is 2.8 K– 10^{10} K. Over the more limited range 10 K – 10^9 K the computed Compton temperature, for conditions in which strict TE is expected, is generally equal to the color temperature within three significant figures (see Figure 19). At temperatures much greater than 10^9 K the electrons become relativistic; CLOUDY is not intended for these conditions. For temperatures much less than 10 K the computed temperature fails high because the energy bandwidth of the continuum array does not extend below $1.001\times$

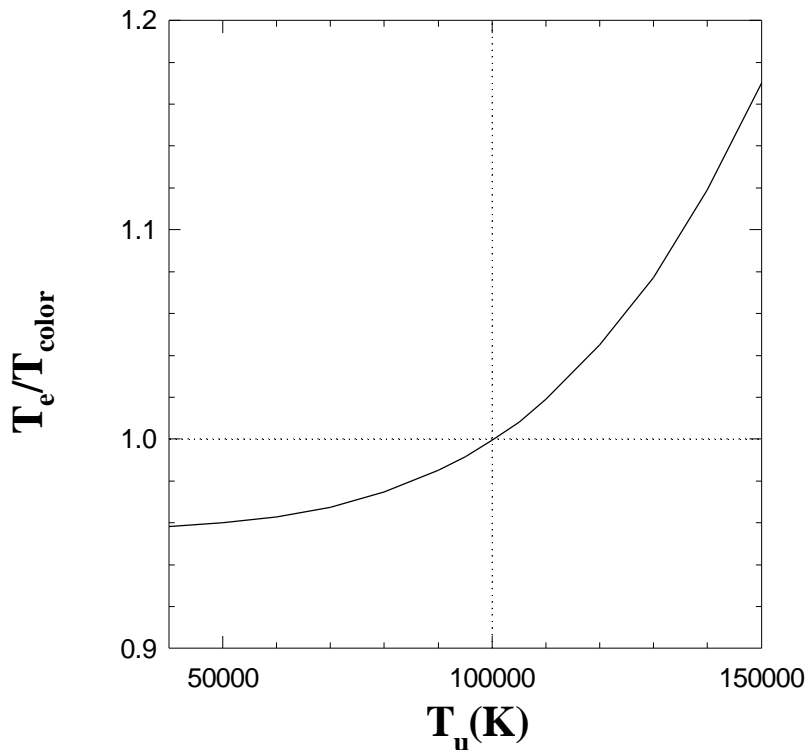


Figure 20 Calculations are for 10^5 K blackbodies and various values of the energy density temperature T_u , indicated along the x-axis. The ratio of the computed equilibrium temperature T_e to the color temperature T_{color} is shown. The two are equal when the energy density and color temperatures are equal. cmpnlte

²The high temperature example will not run on an IEEE 32-bit machine. The continuum overflows because of its extreme energy density. The high temperature tests must be computed on a machine with a longer word, such as a Cray.

10^{-5} Ryd. As a further test, the models presented by Krolik, McKee, and Tarter (1981) were recomputed with excellent agreement (typically within 3%) with their computed Compton temperatures.

For a blackbody radiation field with $T_u \neq T_{\text{color}}$ the Compton temperature will not be equal to T_{color} because induced scattering will not contribute the required amount of heating-cooling. This case is shown in Figure 20, the results of a series of calculations in which the energy density temperature was varied (this is shown as the x-axis), but the color temperature held fixed at 10^5 K.

Note also that when $T_u > T_{\text{color}}$ induced Compton heating drives T_e above T_{color} . Only when the color and energy density temperatures are equal do the equilibrium and color temperatures match.

9.4. Bound Compton Ionization, Heating

Compton scattering can ionize atoms for photons of sufficiently high energy (≈ 2.3 keV for hydrogen). Rates for bound Compton scattering are computed in routine **highen**.

9.5. Expansion Cooling

Adiabatic cooling ($\text{erg cm}^{-3} \text{ s}^{-1}$) due to the hydrodynamic expansion of the gas is given by

$$\Lambda_{\text{exp}} = -\frac{DU}{Dt} = -\frac{p}{r} \frac{Dr}{Dt} - U \nabla \cdot \mathbf{v} \approx kT \frac{dn}{dt} = nkT \left[\frac{a}{v} + \frac{2v}{r} \right] \quad \text{erg s}^{-1} \text{ cm}^{-3} \quad (263)$$

where n , a , v , and r are the total particle density, acceleration, wind velocity, and radius respectively. This cooling term is only included when a wind geometry is computed.

9.6. Free-free Heating-Cooling

The volume free-free heating rate is given by

$$G_{\text{ff}} = 4p \int_{n_l}^{\infty} n_e \mathbf{a}_n(\text{ff}) J_n dn \quad (264)$$

where the free-free cross section is denoted by $\alpha_v(\text{ff})$ and v_l is the low energy limit of the code (1.001×10^{-5} Ryd). The continuum J_v is the sum of the attenuated incident radiation field and the OTS line fields. Diffuse reemission, mainly free-free emission, is *not* included in this integral, as discussed below. The heating rate is called **ffheat**, and is evaluated in routine **freht**.

The cooling by free-free emission, and the subsequent absorption of this radiation, must also be treated. The rate is evaluated in routine **coolr** and is stored as the variable **hbrem**s.

The code works with the difference between cooling and heating, since this is numerically more stable than considering each term as an independent heat source or coolant. The net heating or cooling is calculated in routine **HydroCool**, and is stored directly in the heating array there.

Cooling due to diffuse continua are treated by defining a critical frequency ν_c as follows. Gas at a depth r into the cloud is transparent to photons with energies above a critical frequency ν_c such that

$$t_c = \int_0^r \mathbf{k}(\mathbf{n}_c) f(r) dr = \int_0^r \mathbf{a}_n(ff, \mathbf{n}_c) n_e f(r) dr = 1 \quad (265)$$

and optically thick at lower frequencies. The critical frequency ν_c is evaluated in routine **tauff**. The energy in Rydbergs is stored as **tff**, while the variable **ntff** points to the cell in the continuum array.

The free-free cooling rate is then given by

$$\Lambda_{ff}(t) = \int_{n_c}^{\infty} n_e \mathbf{a}_n(ff) 4\mathbf{p} B_n(T_e) d\mathbf{n} = \Lambda_{ff}(0) \times \exp(-h\mathbf{n}_c / kT) \quad (266)$$

where $\Lambda_{ff}(0)$ is the optically thin cooling rate and $B_n(T_e)$ is Planck's function. This is equivalent to assuming that, for $\nu < \nu_c$, where the cloud is optically thick, free-free heating and cooling exactly balance, as suggested by Kirchhoff's law and detailed balance considerations. Energies below ν_c are not included in free-free heating. This critical frequency is not allowed to be less than the plasma frequency for the current conditions.

9.7. Photoelectric Heating, Recombination Cooling

The net heating rate due to photoelectric heating less spontaneous and induced recombination cooling of level n is given by

$$G = G_{n,k} - \Lambda_{ind,n} - \Lambda_{spn,n} \quad (267)$$

where the volume heating rate due to photoionization is

$$G_{n,k} = n_n \int_{n_o}^{\infty} \frac{4\mathbf{p} J_n}{h\mathbf{n}} \mathbf{a}_n h(\mathbf{n} - \mathbf{n}_o) d\mathbf{n} \quad , \quad (268)$$

the volume cooling rate due to induced recombination is

$$\Lambda_{ind,n} = n_e n_p 4\mathbf{p} P_n^* \int_{n_o}^{\infty} \frac{J_n}{h\mathbf{n}} \mathbf{a}_n \exp(-h\mathbf{n} / kT) h(\mathbf{n} - \mathbf{n}_o) d\mathbf{n} \quad , \quad (269)$$

and the cooling rate due to spontaneous radiative recombination is

$$\Lambda_{spn,n} = n_e n_p kT b(T, n) \quad . \quad (270)$$

The cooling rate coefficient $\beta(T, n)$ is evaluated as described on page 233.

9.8. Collisional Ionization - Three-Body Recombination

The net volume heating rate due to collisional ionization less three-body recombination is given by

$$G_{n,k} - \Lambda_{n,k} = \sum_n P_n^* n_e n_p C_{n,k} h\mathbf{n}_o (1 - b_n) \quad (271)$$

where $C_{n,k}$ is the collisional ionization rate. The term $(1 - b_n)$ is only large and positive for very low levels, in which $I_n > kT$. Far from thermodynamic equilibrium

this is usually a net cooling process only for the ground term. This is because departure coefficients for excited states are nearly unity while the ground level usually has $b_n \gg 1$.

9.9. H⁻ Heating and Cooling

9.9.1. H⁻ bound-free

The volume heating rate due to spontaneous absorption (photodissociation) is

$$G_{H^-} = n(H^-) \int_{n_o}^{\infty} \frac{4\mathbf{p}J_n}{h\mathbf{n}} \mathbf{a}_n h(\mathbf{n} - \mathbf{n}_o) d\mathbf{n} \quad (\text{erg s}^{-1} \text{ cm}^{-3}) \quad (272)$$

where symbols have their usual meaning. The volume cooling rate due to induced radiative attachment is

$$\Lambda_{ind, H^-} = n_e n_{H^o} P^*(H^-) \int_{n_o}^{\infty} \mathbf{a}_n \frac{4\mathbf{p}J_n}{h\mathbf{n}} \exp(-h\mathbf{n}/kT) h(\mathbf{n} - \mathbf{n}_o) d\mathbf{n} \quad (\text{erg s}^{-1} \text{ cm}^{-3}) \quad (273)$$

while the volume cooling rate for spontaneous radiative attachment is

$$\Lambda_{spont, H^-} = n_e n_{H^o} 8\mathbf{p} P^*(H^-) \int_{n_o}^{\infty} \mathbf{a}_n \frac{\mathbf{n}^2}{c^2} \exp(-h\mathbf{n}/kT) h(\mathbf{n} - \mathbf{n}_o) d\mathbf{n} \quad (274)$$

9.9.2. H⁻ free-free

Free-free heating and cooling by H⁻ is also significant, although less so than bound-free heating. This is included, making the appropriate correction for stimulated emission, using the cross sections given by Vernazza et al. (1981; see also Bates et al. 1975).

Under most circumstances H⁻ bound-free heating and cooling are much more important than H⁻ free-free processes. This is surprising at first sight, since standard opacity curves comparing bound-free and free-free opacities (Bates et al. 1975; Mihalas 1978) show that the two are comparable. These curves are for strict thermodynamic equilibrium, with H⁻ departure coefficients of unity. Like the ground state of hydrogen, the departure coefficient for H⁻ is often many orders of magnitude larger than unity, so that the H⁻ bound-free opacity and the resulting heating greatly exceed the H⁻ free-free opacity.

9.10. Line Cooling, Hydrogen and Helium

The net heating due to line collisional deexcitation less excitation is given by

$$G_{line} - \Lambda_{line} = \sum_{n=1}^{N-1} \sum_{u=n+1}^N P_n^* n_e n_p C_{u,n} h\mathbf{n}_{u,n} (b_u - b_n) \quad (275)$$

where C_{un} is the downward collision rate. Far from thermodynamic equilibrium collisions involving the ground state tend to cool the gas (since $b_1 \gg 1$) and those between levels with $n \geq 3$ tend to heat the gas (since b_n tends to increase with n).

9.11. Heavy Element Line Heating and Cooling

9.11.1. Overview

All lines of the heavy elements that are transferred are treated in a common vector format. The following sections describe that vector format and the major routines for computing heating and cooling for n -level atoms of the heavy elements. Emission lines are often optically thick. All lines are transferred using escape probabilities, by determining level populations including both collisional and radiative processes (see, for example, Elitzur 1991). Line masing can sometimes occur, and again is treated using escape probabilities.

In all cases the net cooling due to a transition is given as

$$\Lambda_{line} = h n_{u,l} (n_l C_{l,u} - n_u C_{u,l}) \quad (276)$$

where the populations of levels are given by n_i and C_{ij} is the collision rate. This cooling is evaluated in routines **level2**, **level3**, **levelN**, and **beseq**. Each routine is responsible for evaluating the line intensity, cooling, and destruction rate, and entering these into the appropriate stacks. Each routine sets the following attributes.

Lines can act to **heat** rather than cool the gas if an intense continuum is present. This is an important gas heating mechanism for PDRs, for instance (Tielens and Hollenbach 1985). If η is the photon occupation number of the attenuated incident continuum, then the rate atoms are excited from the ground level is given by $\eta \epsilon A_{ul}$ where ϵ is the line escape probability. A fraction $C_{ul} / (C_{ul} + \epsilon A_{ul})$ of these radiative excitations is converted into heat by collisional de-excitation. The net heating due to this process is then

$$G_{FIR} = n_l h_n e_{lu} A_{ul} \left(\frac{C_{ul}}{C_{ul} + e_{lu} A_{ul}} \right) h n \quad \text{erg cm}^{-3} \text{ s}^{-1} \quad (277)$$

where n_l is the density of the ground level. This process is included for all transferred lines.

9.11.2. Array pointers

The elements of the line formation array, and what must be placed there by the cooling routine, are the following:

ipLnPopl The population of lower level.

ipLnPopu The population of upper level.

ipLnPopOpc The population of lower level with correction for stimulated emission.

ipLnInten The line intensity, ergs/s/cm³.

ipLnNPhots The number of photons emitted in the line.

ipLnOTS The part of line destroyed by background opacity.

ipLnAovTOT The ratio $A_{ul} / (A_{ul} + C_{ul})$.

ipLnCool The upward collisional cooling.

Cooling

ipLnHeat, downward collisional heating.

PopLevls(1-n) The level populations.

ipLnCool This is added to the cooling stack by calling **coladd**.

Finally, the routine must evaluate the cooling derivative and add destroyed part of line to local OTS field.

9.11.3. Two level atoms

Cooling due to collisional excitation of two level atoms of the heavy elements is evaluated in routine **level2**. This routine does the following: a) finds the abundance of the two levels by balancing collisional and radiative processes, subject to the sum $n_l + n_u = \text{abundance}$. b) adds the line cooling (or heating) to the total cooling, c) adds the line derivative to dC/dT , d) evaluates the fraction of the escaping line destroyed by background opacity, e) adds this to the local OTS radiation field, f) records the line opacity population $n_l - n_u g_l/g_u$. The populations of the atom are saved in the vector **PopLevls** contained in the common block of the same name. The lowest level is **PopLevls(0)**.

9.11.4. Three level atoms

The level populations, cooling, and line destruction by background opacity sources are computed for three level atoms in routine **level3**.

Routine **level3** is called with three arguments, the three line arrays. Level populations corrected for stimulated emission are returned in the individual line arrays. The true level populations, with no correction for stimulated emission, are returned in the array **PopLevls**, contained in the common block of the same name. The lowest level is **PopLevls(0)**.

Levels are designated by the indices 0, 1, and 2, with 0 the lowest level. The routine is called with three line arrays, indicated by t10, t21, and t20, each representing the downward radiative transition between the indicated levels. Any one of these transitions may be a dummy transition, (using the dummy line **TauDmmy**). The total rates between any two levels $i \rightarrow j$ is indicated by R_{ij} . This includes collisions, radiative decays (both photon escape and destruction by background opacity), and induced transitions. If the total abundance of the parent ion is A, the three balance equations are

$$n_0 + n_1 + n_2 = A \quad (278)$$

$$n_0(R_{01} + R_{02}) = n_1 R_{10} + n_2 R_{20} \quad (279)$$

$$n_1(R_{10} + R_{12}) = n_2 R_{21} + n_0 R_{01} \quad (280)$$

Setting n_0 to $A - n_1 - n_2$ equation 279 becomes

$$(R_{01} + R_{02})(A - n_1 - n_2) = n_1 R_{10} + n_2 R_{20} \quad (281)$$

After gathering terms this equation becomes

$$A(R_{01} + R_{02}) = n_1(R_{10} + R_{01} + R_{02}) + n_2(R_{20} + R_{01} + R_{02}) \quad (282)$$

Substituting for n_0 , equation 280 becomes

$$n_1(R_{10} + R_{12}) = n_2 R_{21} + R_{01}(A - n_1 - n_2). \quad (283)$$

Gathering terms this equation becomes

$$n_1(R_{10} + R_{12} + R_{01}) = AR_{01} + n_2(R_{21} - R_{01}) . \quad (284)$$

Solving 282 for n_1 we obtain

$$n_1 = \frac{A(R_{01} + R_{02})}{R_{10} + R_{01} + R_{02}} - \frac{n_2(R_{20} + R_{01} + R_{02})}{R_{10} + R_{01} + R_{02}} \quad (285)$$

and solving 284 we find

$$n_1 = \frac{AR_{01}}{R_{10} + R_{12} + R_{01}} + \frac{n_2(R_{21} - R_{01})}{R_{10} + R_{12} + R_{01}} \quad (286)$$

Equating the two and gathering terms we obtain

$$n_2 \left(\frac{R_{21} - R_{01}}{R_{10} + R_{12} + R_{01}} + \frac{R_{20} + R_{01} + R_{02}}{R_{10} + R_{01} + R_{02}} \right) = \frac{A(R_{01} + R_{02})}{R_{10} + R_{01} + R_{02}} - \frac{AR_{01}}{R_{10} + R_{12} + R_{01}} \quad (287)$$

with the solution

$$n_2 = A \left(\frac{(R_{01} + R_{02})}{R_{10} + R_{01} + R_{02}} - \frac{R_{01}}{R_{10} + R_{12} + R_{01}} \right) \bigg/ \left(\frac{R_{21} - R_{01}}{R_{10} + R_{12} + R_{01}} + \frac{R_{20} + R_{01} + R_{02}}{R_{10} + R_{01} + R_{02}} \right) . \quad (288)$$

In the code the term in the numerator in the previous equation is called **alpha**, and the denominator **beta**. Replacing n_2 in equation 285 we obtain

$$n_1 = \left[A(R_{01} + R_{02}) - n_2(R_{20} + R_{01} + R_{02}) \right] \bigg/ (R_{10} + R_{01} + R_{02}) . \quad (289)$$

Again the two terms are called **alpha** and **beta**.

9.11.5. N level atoms

The level populations, cooling, and line destruction by background opacity sources are computed for n level atoms in routine **LevelN**. The number of levels n can be as large as the value of **limLevelN** (currently 10) which appears in a parameter statement within the routine.

Routine **LevelN** is called with 12 arguments. These are:

nlev This is the number of levels for the model atom. It is an integer and can be as large as the value of **limLevelN**, currently 20.

abund This is the total abundance of the ion. The total population of the **nlev** levels will add up to this quantity, which is a real variable.

g This is a real vector of dimension **nlev**. It contains the statistical weights of the levels.

Cooling

ex This is a real vector of dimension **nlev**. It contains the excitation temperature (K) of the **nlev** levels *relative to ground*. The excitation temperature of the lowest level should be zero.

p This is a real vector of dimension **nlev** and is the computed population of the **nlev** atom. It will contain all zeros if **abund** is zero, and **p(l)** will equal **abund** if the temperature is so low that the Boltzmann factors are zero for the current cpu.

data This two dimensional real vector is **data(nlev, nlev)**. **data(u,l)** is the effective transition probability (the product of the Einstein A and the escape probability) for the transition. **data(l,u)** is the collision strength for the transition.

dest This two dimensional real vector is **dest(nlev, nlev)**. **dest(u,l)** is the destruction rate (the product of the Einstein A and the destruction probability) for the transition. **dest(l,u)** is not used.

pump This two dimensional real vector is **pump(nlev, nlev)**. **pump(u,l)** is the upward pumping rate (the Einstein B_{lu}) for the transition.

ipdest This two dimensional integer vector is **ipdest(nlev, nlev)**. **ipdest(u,l)** is the pointer to the line in the continuum array. **LevelN** computes the local line destruction rate and includes this in the OTS field if the pointers are non-zero. If this vector contains zeros then no flux is added to the OTS field.

cooltl This real variable is the total cooling in ergs/s produced by the model atom.

chLabel This is a 4 character variable, and is a label for the ion.

negpop This logical variable is true if any of the level populations were negative.

9.11.6. Li Sequence

Table 25 gives the stronger lines of Li-sequence ions. **Level3** is used for this sequence.

Table 25 Lithium Sequence Lines

<i>N</i>	<i>lon</i>	<i>j=3/2-1/2</i>	<i>j=1/2-1/2</i>	<i>j=3/2-1/2</i>	<i>j=1/2-1/2</i>
6	C IV	1548.195	1550.770	312.422	312.453
7	N V	1238.821	1242.804	209.270	209.303
8	O VI	1031.9261	1037.6167	150.088	150.124
10	Ne VIII	770.409	780.324	88.134	
12	Mg X	609.79	624.95	57.88	57.92
13	Al XI	550.03	568.15	48.30	48.34
14	Si XII	499.40	520.67	40.92	
16	S XIV	417.61	445.77	30.43	
18	Ar XVI	353.92	389.14	25.53	
20	Ca XVIII	302.215	344.772	18.69	18.73
26	Fe XXIV	192.017	255.090	10.62	10.66

9.11.7. Boron Sequence

Figure 22 shows levels within the lowest three configurations of the Boron sequence.

9.11.8. Beryllium sequence atoms

The level populations, cooling, and line destruction by background opacity sources are computed for a specialized four level atom in routine **beseq**.

Routine **beseq** is called with five arguments, the collision strengths between the excited triplet levels, the line optical depth array for the fast ($j=1$ to $j=0$) transition, and the transition probability for the slow ($j=2$ to $j=0$) transition. Induced processes are only included for the fast transition. The collision strength stored in the line array is the collision strength for the entire multiplet. Rates to levels within the term are assumed to scale as the ratio of level statistical weight to term statistical weight. The level populations for the ground and excited states, with no correction for stimulated emission, are returned in the array **PopLevls**, contained in the common block of the same name. The lowest level is **PopLevls(0)**.

The total rates between any two levels $i \Rightarrow j$ is indicated by R_{ij} . This includes collisions, radiative decays (for the fast transition, both photon escape and destruction by background opacity, and induced transitions). If the total abundance of the parent ion is A , the three balance equations are

$$n_0 + n_1 + n_2 + n_3 = A \tag{290}$$

$$n_0(R_{01} + R_{02} + R_{03}) = n_1R_{10} + n_2R_{20} + n_3R_{30} \tag{291}$$

$$n_1(R_{10} + R_{12} + R_{13}) = n_3R_{31} + n_2R_{21} + n_0R_{01} . \tag{292}$$

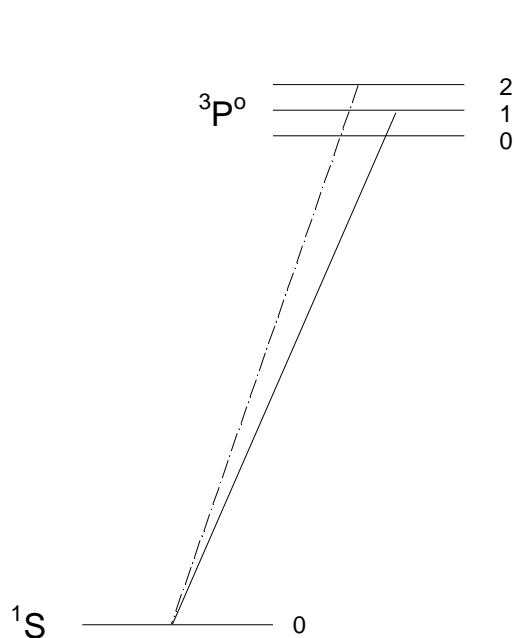


Figure 21 The four levels included in routine beseq. beseq1

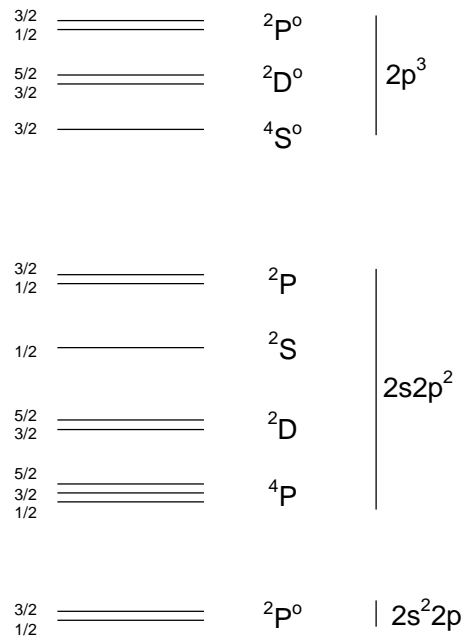


Figure 22 Energy Level Diagram for Boron Sequence. Boron

$$n_2(R_{20} + R_{21} + R_{23}) = n_3R_{32} + n_1R_{12} + n_0R_{02} . \quad (293)$$

Collisions are included in all these terms. R_{32} includes the slow downward line escape, while R_{02} and R_{20} includes escape, destruction by background opacity, and fluorescent excitation - deexcitation. In the code the terms on the LHS of equations 292, 293, and 291 are called α , β , and γ .

9.12. Evaluation of the Cooling Function

9.12.1. Total cooling

The cooling function is evaluated in routine **coolr**. This in turn calls other routines which compute cooling for individual elements. Each individual coolant is entered as a separate quantity in the array **cooling**. Under some extreme circumstances agents which are normally coolants can actually heat the gas. Negative coolants are stored in a parallel array, **heatnt**. Both **cooling** and **heatnt** are part of common block **coolnt**.

The total cooling is the sum of this array, referred to as the variable **ctot**, and evaluated in routine **SumCool**.

9.12.2. The cooling derivative

As the cooling is evaluated, its approximate temperature derivative is computed by making analytic expansions of the cooling for individual agents. For instance, collisionally excited lines of positive ions have collisional excitation rates which depend on the product

$$\Lambda_{line} \approx n_e n_{ion} t^{-1/2} \exp(-T_{exc} / T_e) \quad (294)$$

where T_{ex} is the excitation temperature of the line. In this case the derivative of the cooling function can be expressed as

$$\frac{d\Lambda_{line}}{dT} \approx n_e n_{ion} \frac{d}{dT} T^{-1/2} \exp(-T_{exc} / T) = \Lambda_{line} \left[\frac{T_{exc}}{T^2} - \frac{1}{2T} \right] \quad (295)$$

This derivative is used by the thermal predictor-corrector routine to make the initial guess at a new temperature. This is approximate since both electron and ionic densities also depend on the temperature.

The variable **tsq1** contains the value $1/T^2$, while **halfte** is $1/2T$. Both are part of common block **dcool**.

9.13. Evaluation of the Heating Function

Various contributions to the heating function are evaluated throughout the code. Each heating agent stores its contribution to the total heating within a cell of the two dimensional array **heating**. The total heating is always the sum of the total contents of the **heating** array.

Heating due to photoionization of all stages of ionization of the 30 elements now included in the code are stored as **heating(nelem, ion)**. Heating due to photoionization of ionization stage i ($i=1$ for the atom) of element with atomic

number *nelem* is stored as *heating(nelem,i)*. Other agents are stored in unused portions of this array. The total heating and its temperature derivative are deduced from this array in routine *SumHeat*. The heating is stored as the variable *htot*.

Line heating is treated as a special case. The level population routines are supposed to sort lines into heating and cooling components, and put these into the line vector as *ipLnHeat* and *ipLnCool*. The entries stored as *ipLnHeat* are then added to the heating stack as *heating(1,23)* when the total line cooling is evaluated in routine *SumCool*. The entries stored as *ipLnCool* are added to the cooling stack here too. Normally this will catch all negative coolants early. Attempts to add negative cooling to the cooling stack are trapped and stored in the array *heatnt*. This is added to the total heating in routine *SumCool*.

9.14. Equilibrium Calculations

9.14.1. Hydrogen only

Figure 23 shows the results of a series of calculations in which the full set of statistical and thermal equilibrium equations are solved for thin cells of hydrogen gas with various densities.

The ionizing continuum is, in all cases, a black body with $T_{\text{color}} = 5 \times 10^4$ K, and the energy density of the radiation field is varied, up to the thermodynamic equilibrium limit, $T_u = T_{\text{color}}$.

Although the gas temperature in the thermodynamic equilibrium limit does not depend on the gas density, the physical processes that drive the gas to this temperature do. Thermal equilibrium calculations were performed with three densities chosen to span a fairly wide range. For low densities ($n(\text{H}) = 10^5 \text{ cm}^{-3}$) the gas remains highly ionized for all values of T_u shown and the temperature in thermodynamic equilibrium is set by the balance between Compton and inverse-Compton scattering. The intermediate density case ($n(\text{H}) = 10^{10} \text{ cm}^{-3}$) reaches thermodynamic equilibrium with $\sim 3/4$ of the heating-cooling set by Compton scattering and the remainder due to free-free and free-bound processes. The high-density ($n(\text{H}) = 10^{15} \text{ cm}^{-3}$) case reaches its thermodynamic equilibrium temperature with a balance between free-free ($1/3$ of the total) and free-bound ($2/3$ of the total) processes. In all cases the level populations and electron temperature are within $\sim 1\%$ of their expected thermodynamic equilibrium values when $T_u = T_{\text{color}}$.

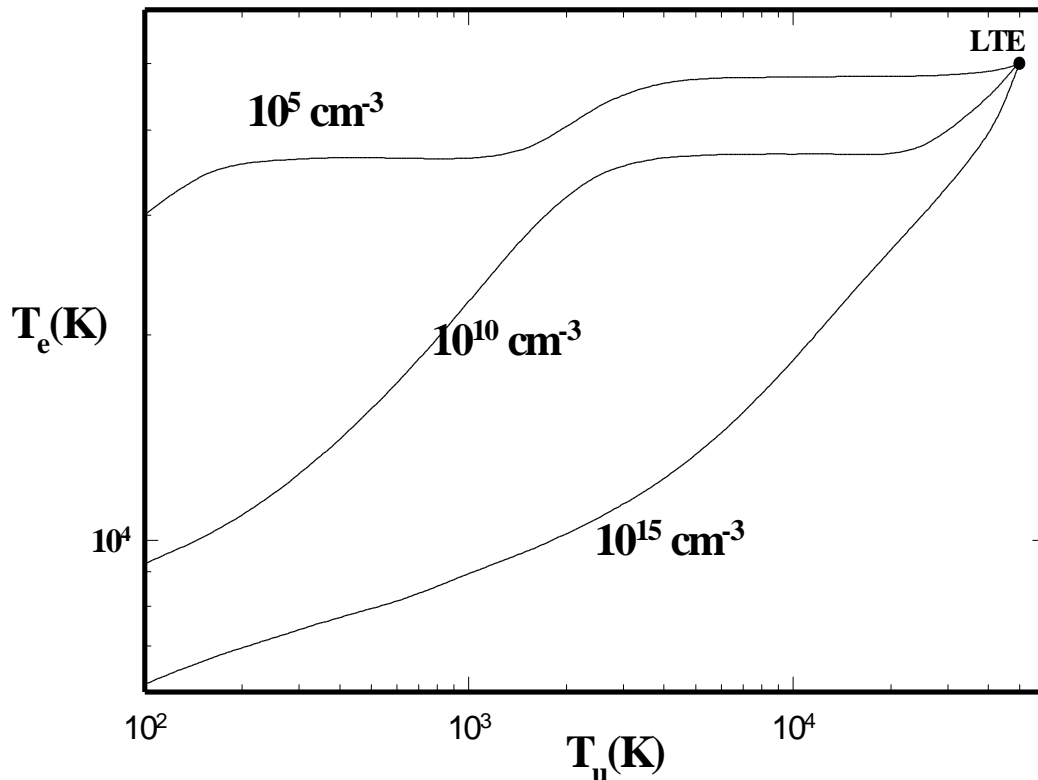


Figure 23 Thermal equilibrium calculations for an optically thin gas with 3 hydrogen densities are shown as a function of the radiation field energy density, parameterized as T_u . Ionization is by a 5×10^4 K black body. Various processes drive the gas to thermodynamic equilibrium when T_u reaches 5×10^4 K. hlte

9.14.2. Metal rich gas

Simulations of very metal rich gas is now a major emphasis of the code (Hamann and Ferland (1993; Ferland et al. 1996). In these cases the thermal and ionization balance is totally dominated by the heavy elements.

Figure 24 shows the results of a series of calculations in which gas with strongly enhanced abundances of the heavy elements is exposed to a series of black body radiation fields with different temperatures and energy densities. Ferland and Rees (1988) and Ferland and Persson (1989) gave analogous calculations for pure hydrogen clouds. The filled circle represents the cases where the energy densities of the radiation field are equal to the color temperature, and strict thermodynamic equilibrium is expected. This is indeed the case. The distribution of ionization for each color temperature is radically different, but the line interactions with this field bring the gas to the expected equilibrium temperature. This tests both the ionization and thermal balance in this extreme environment.

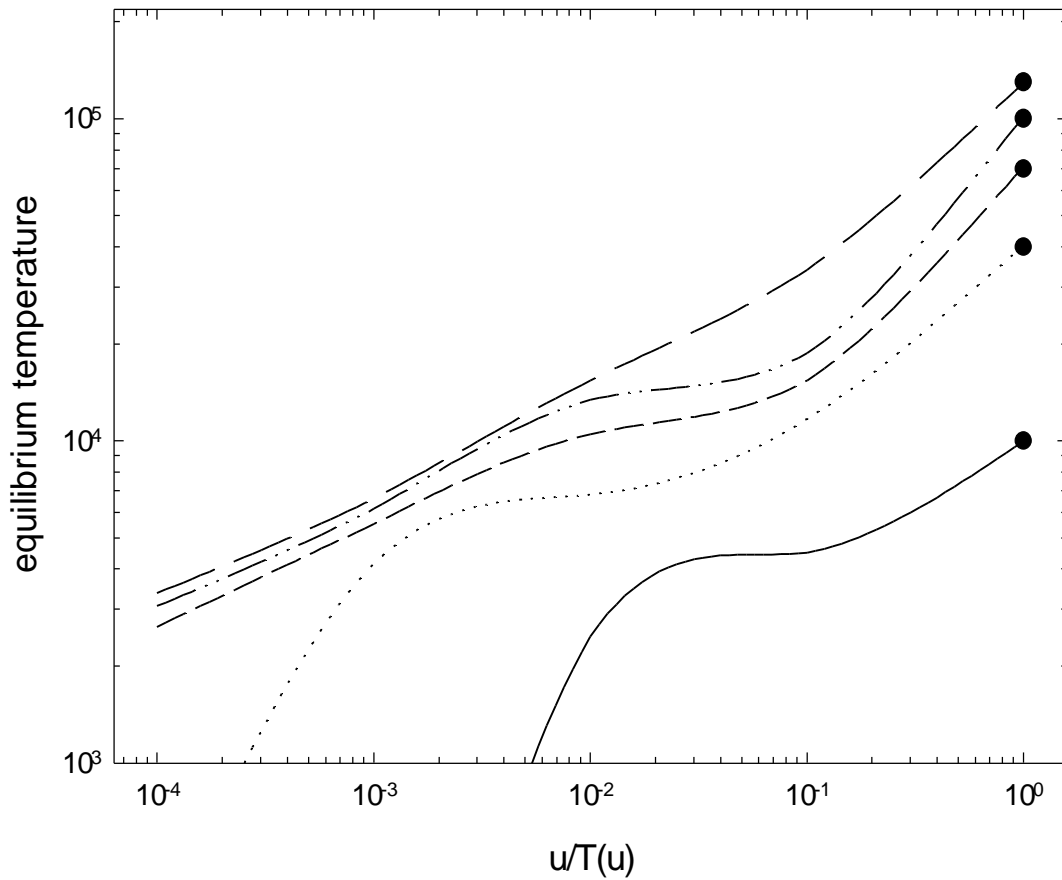


Figure 24 Equilibrium temperature of gas exposed to five black bodies with various energy density temperatures. The color temperatures of the blackbodies are 10,000K, 40,000K, 70,000K, 100,000K and 130,000K. The metallicity was 10 times solar (Hamann and Ferland 1993) so that heating cooling of thousands of heavy element emission lines dominates the thermal equilibrium. The simulation is of an optically thin cell of gas with density 10^{10} cm^{-3} (results do not depend on this density). The x-axis is the local energy density relative to the energy density in thermodynamic equilibrium at that temperature. The gas goes to thermodynamic equilibrium when the radiation field does (the color and energy density temperatures are equal). highzlte

10. GRAIN PHYSICS

10.1. Overview

The following discussion outlines some physical processes relating to grains, as incorporated in CLOUDY. It is adopted from Baldwin et al. (1991), and was written in close collaboration with P.G. Martin.

Several grain populations, types of graphite and “astronomical silicates”, are available. Usually one of each type, for a total of two, is selected, although there is no limit to the number of grain populations. Optical properties like opacity of the species are based on a realistic power-law size distribution. Other properties (like potential and temperature) are computed for a mean grain size rather than calculated for each individual size.

10.2. Grain Opacity

Grains are not included in the calculation by default. When enabled with the `grain` command the default mixture has interstellar medium (ISM) properties. Grains more similar to those seen in Orion or planetary nebulae are also available.

10.2.1. ISM grains

The optical constants for the default (ISM) grain species are from the calculations of Martin and Rouleau (1990). These extend the work of Draine and Lee (1984) to ionizing energies where the grains are strongly absorbing. These opacity calculations were based on the Mathis, Rumpl, and Nordsieck (1977) power-law size distribution to simulate interstellar extinction in diffuse clouds.

10.2.2. Orion grains

Grains within the Orion Nebula have a relatively large ratio of total to selective extinction R and an exceptionally gray opacity in the ultraviolet. These are both indicative of a deficiency in small grains and a larger mean grain size. To account for this, a second set of opacity functions is included, the Orion group. For this the value of the smallest size (a_0) in the Mathis et al. (1977) size distribution was increased from $0.0025\mu\text{m}$ to $0.03\mu\text{m}$. While this simple adjustment of the size distribution is not entirely adequate for explaining the details of the visible and near ultraviolet Orion extinction curve (Mathis and Wallenhorst 1981), it should be an improvement for the ionizing ultraviolet portion, which is most important.

The Orion extinction curve is designed to simulate the large R grains observed in this HII region. Relative to ISM standard grains the total amount of grain material was preserved, so that α_{abs} in the infrared and in the EUV and X-Ray regions remains unchanged. The main differential effect is to lower the cross section through a broad peak at 1 Ryd.

10.2.3. PN grains

Infrared opacities for the silicate component are taken from unpublished work by K. Volk. Ultraviolet silicate cross sections, and the graphite constituent, are standard ISM.

10.2.4. Extinction

The ISM extinction properties, both effective scattering (subscript *scat*) and absorption (subscript *abs*), are shown in Figure 25.

The quantities plotted are cross sections (cm^2) per H nucleon: $\sigma = \kappa/n(\text{H})$, where κ (cm^{-1}) is the opacity due to grains and $n(\text{H})$ (cm^{-3}) is the local density of H in any form. Rather than the total scattering cross section σ_s , an effective scattering cross section $\sigma_{\text{scat}} = \sigma_s (1-g)$ is plotted. This discounts the radiation scattered near the forward direction. The asymmetry parameter g approaches unity at high and low energies, particularly for larger grains, so that σ_{scat} becomes much less than α_{abs} .

The optical depth τ is σ times the hydrogen column density (or κ integrated over the path). Absorption attenuates the incident radiation field as $\exp(-\tau_{\text{abs}})$. The effects of scattering are more difficult to model. In an open geometry, scattering attenuates approximately as $(1+0.5 \tau_{\text{scat}})^{-1}$. However, in a closed geometry, to within factors of order unity, the scattered light is not lost from the beam, and the scattering opacity can be ignored. In either case, effective grain scattering optical depth is generally fairly small through the ionized nebula at ionizing energies.

10.3. Photoelectric Emission

As discussed below, photoelectric emission from grains contributes directly to heating the gas and, through the grain potential U_g established, affects radiative and collisional heating of the grains and the grain drift velocity.

The photoionization rate of a grain, per unit projected area, is

$$\Gamma_g = \int_{n_o}^{\infty} Q_{\text{abs}} \frac{4\pi J}{hn} \hat{Y} dn \quad (296)$$

where \hat{Y} is the effective photoelectric yield per absorbed photon, Q_{abs} is the absorption efficiency factor, and $4\pi J/h\nu$ symbolizes the photon flux of direct, diffuse, and OTS radiation fields. For the OTS line component, the integral is of course just a sum over the line photons that are sufficiently energetic. The threshold for photoemission, to be determined self-consistently, is given by $h\nu_o = \max\{V_n + V_g, V_n\}$, where V_n is the photoelectric threshold for a neutral grain and $V_g = eU_g$.

V_g will depend on grain size through Q_{abs} and \hat{Y} . In the present implementation, a typical V_g is defined for each species by using Q_{abs} averaged over the size distribution: $Q_{\text{abs}} = \alpha_{\text{abs}}/\Sigma = \kappa_{\text{abs}}/n(\text{H})\Sigma$. The projected grain area per H, Σ , is similar for each species: $2.1 \times 10^{-22} \text{ cm}^2$ for graphite and $2.4 \times 10^{-22} \text{ cm}^2$ for silicates.

\hat{Y} is constructed as follows. The basic laboratory data measure the yield (per absorbed photon) for a neutral surface, Y_n . For each incident photon energy $h\nu$, the photoelectrons emerging from the neutral surface have varying energies E , with a probability distribution $p_n(E)$. To account for electron escape from finite sized

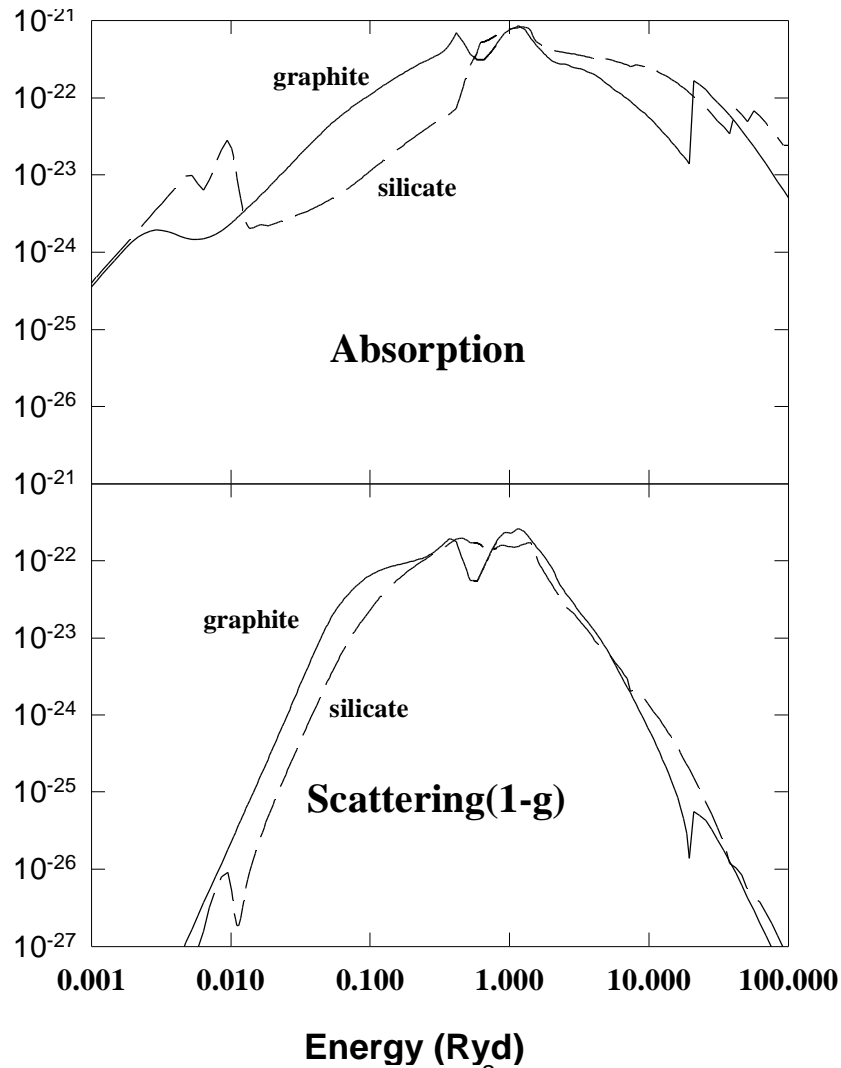


Figure 25 The absorption and scattering cross sections (cm^2 per hydrogen nucleus) for the two ISM grain populations, graphite and silicate, are shown. The effective scattering cross section is the scattering cross section multiplied by $1-g$, where g is the asymmetry parameter. grnopc

grains, yields measured for semi-infinite sheets in the laboratory have to be corrected by a factor $f(E)$ (which introduces a size dependence). Such a correction would change the shape of the probability distribution as well as increase the integrated emission from a neutral surface (Draine 1978 gives an approximate expression for the overall increase). Then, formally

$$\hat{Y} = Y_n \int_{E_0}^{(hn-V_n)} f p_n dE \quad (297)$$

where $E_0 = \max\{0, V_g\}$ introduces the fact that the lowest energy photoelectrons do not escape from positively charged grains.

The form adopted is

$$Y_n = \min\{Y_0(1 - V_n / hn), Y_1\} \quad (298)$$

for $h\nu \geq V_n$, and $V_n = 8 \text{ eV}$ and $Y_0 = 0.5$ is assumed for both grain populations; according to Draine (1978) this combination gives about the right amount of

photoelectric emission to heat neutral H I clouds in interstellar space ($h\nu \leq 13.6$ eV). For the higher energies a cap at $Y_1 = 0.2$ is introduced, which is suggested by experimental data. For p_n a simple form that is independent of E (Draine 1978) is adopted:

$$p_n = (h\nu - V_n)^{-1} . \quad (299)$$

While only approximate, this induces the physically correct response (decrease) in \hat{Y} (and the photoelectric heating) when the grain is positively charged. Because the form of $f(E)$ is highly uncertain $f = 1$ is assumed (this again avoids a size dependency). Extension of the flat cap in Y_n to high energies also addresses this issue to some degree. With these assumptions, \hat{Y} is known in analytic form:

$$\hat{Y} = Y_n \min\left\{1, 1 - V_g / (h\nu - V_n)\right\} . \quad (300)$$

10.4. Collisional Charging of a Grain

Per unit projected area of a grain, collisions with particles of space density n , mass m , and charge Z ($Z = -1$ for electrons) give an effective recombination rate

$$a(gr) = -n \bar{v} SZ h , \quad (301)$$

where

$$\bar{v} = \sqrt{8kT / \pi m_e} \quad (302)$$

is the mean particle speed. In this expression, and for other collisional rates involving n below, it is implicit that there is a sum of similar terms over all species in the gas. For electrons S is the sticking probability which we take to be 1 (Spitzer 1948; Watson 1972; Draine 1978). For positively charged nuclei, SZ is the charge transfer efficiency, taken to be Z here. The last factor η , the correction for Coulomb interactions between the grain and the recombining particles of charge Z , is given in terms of

$$y = ZV_g / kT_e \quad (303)$$

by

$$h = \begin{cases} 1 - y & \text{if } y \leq 0 \\ \exp(-y) & \text{if } y > 0 \end{cases} \quad (304)$$

Terms for positively charged nuclei are included, but are usually small relative to the contribution from free electrons.

10.5. Grain Potential

The steady state grain potential is determined for each grain species independently by requiring charge balance. Expressed as a balance per unit area this is $\alpha_{gr} = \Gamma_{gr}$. Because of the many dependencies on V_g , this is carried out numerically.

10.6. Grain Drift Velocity

The grain drift velocity is determined by balancing the radiative acceleration due to the direct attenuated radiation field with the drag forces given by equations 1–6 of Draine and Salpeter (1979). The equations are solved numerically for the drift velocity, including interactions with electrons and all ions present in the gas.

10.7. Radiative Heating and Cooling of a Grain

Once the grain potential is known, the rate of radiative heating of the grain per unit projected area is

$$G_{\text{grain}}(\text{rad}) = \int_0^{n_o} Q_{\text{abs}} 4\mathbf{p} J d\mathbf{n} + \int_{n_o}^{\infty} Q_{\text{abs}} \frac{4\mathbf{p}J}{h\mathbf{n}} (h\mathbf{n} - EY) d\mathbf{n}. \quad (305)$$

The last term represents the portion of the photon energy that does not heat the grain, but rather passes to the escaping electrons:

$$EY = Y_n \int_{E_o}^{(h\mathbf{n} - V_n)} E f p_n dE. \quad (306)$$

With the above approximations for f and p_n this is given analytically by

$$EY = 0.5 Y_n \min \left\{ (h\mathbf{n} - V_n), \left[(h\mathbf{n} - V_n)^2 - V_g^2 \right] / (h\mathbf{n} - V_n) \right\}. \quad (307)$$

The cooling of a grain by radiative losses, per unit projected area, is given by

$$\Lambda_{\text{grain}}(\text{rad}) = \int_0^{\infty} Q_{\text{abs}} 4\mathbf{p} B_n(T_g) d\mathbf{n} \quad (308)$$

where $B_n(T_g)$ is the Planck function for the grain temperature.

10.8. Collisional Heating of a Grain

Collisions with electrons, ions, and neutral particles also heat the grains. Per unit projected area of the grain, this heating rate may be written as

$$G_{\text{grain}}(\text{col}) = n \bar{v} S \left(2kT_e \mathbf{x} - ZV_g \mathbf{h} + I\mathbf{h} - 2kT_g \mathbf{h} \right). \quad (309)$$

The first term corresponds to kinetic energy extracted from the gas. The factor ξ makes adjustment for Coulomb interactions and is given by

$$\mathbf{x} = \begin{cases} 1 - y / 2 & \text{if } y \leq 0 \\ (1 + y / 2) \exp(-y) & \text{if } y > 0 \end{cases}. \quad (310)$$

The second term in $G_{\text{grain}}(\text{col})$ allows for the change of the particle's energy in the grain potential. In the third term, the product $I\eta$ is the average chemical energy released per impact. Here it is assumed that when impinging ions recombine the ionization energy released is deposited as heat in the grain (there is then no corresponding term for heating the gas in Λ_g below). The last term describes the effect of thermal evaporation of neutralized ions and thermally accommodated neutral particles (there is no corresponding term for electrons).

In implementing the above processes, S for electrons is again the sticking probability. For positively charged nuclei, S is the energy transfer efficiency, taken here to be unity (this process should be evaluated consistently with that for charge transfer). For neutral particles of mass m striking a grain whose typical atom has mass M , the accommodation coefficient $S \approx 2 m M / (m + M)^2$ (Draine 1978).

10.9. Grain Temperature

The equilibrium grain temperature is determined by the balance between cooling (Λ) and heating (G) by radiative and collisional processes. For the radiative terms, Q_{abs} averaged over the size distribution is used to obtain a typical temperature for each species.

As a test of the bandwidth of the code, and its behavior in a well-defined limit, tests were computed in which the grains were irradiated by black body radiation in strict thermodynamic equilibrium (i.e., the color and energy density temperatures were equal). Radiation temperatures between 10 K and 10^9 K, the temperature limits to the code, were used. These tests showed that the deduced grain equilibrium temperature was within much better than 1 percent of the blackbody temperature.

10.10. Photoelectric Heating of the Gas

Heating of the gas by photoemission from grains can be an important process in ionized regions (Spitzer 1948; Oliveira and Maciel 1986). For charged grains this heating rate ($\text{erg cm}^{-3} \text{ s}^{-1}$) is given by

$$G_{\text{gas}} = \int_{n_0}^{\infty} k_{\text{abs}} \frac{4\pi J}{h\nu} (EY - V_g \hat{Y}) d\nu. \quad (311)$$

The first term describes the energy of the photoelectrons as they leave the surface, balancing the similar term in $G_{\text{grain}}(\text{rad})$. The second term compensates for the grain potential, and can be seen to balance the related term in $G_{\text{g}}(\text{col})$ when charge balance holds.

10.11. Collisional Cooling of the Gas

The gas is cooled as the gas particles hit the cooler grain surface. Per unit volume, this cooling rate may be written as

$$\Lambda_{\text{gas}} = n n(H) \Sigma \bar{v} S (2kT_e \mathbf{x} - 2kT_{\text{grain}} \mathbf{h}) \cdot \mathbf{h}, \quad (312)$$

the individual terms consistently balancing the corresponding ones in $G_{\text{g}}(\text{col})$ (see equation 310).

10.12. Grain Sublimation

The code checks that grain survival is likely by comparing the highest grain temperature with the sublimation temperatures. These are taken to be 1400 K for silicates and 1750 K for graphite and are based on the paper by Laor and Draine (1993). These values are stored in the vector **sublimat** and initialized in block data **martin**. A warning will be printed at the end of the calculation if the grain

temperature rises above the sublimation point. A caution will be printed if the temperature rises above 90% of the sublimation point.

10.13. Ionic Recombination on Grain Surfaces

Positive ion recombination on grain surfaces proceeds at a rate $n_{\text{ion}}n_{\text{H}}\alpha_{\text{gr}}$ where the recombination coefficient is taken from Draine and Sutin (1987; their equation 5.15). For a standard grain size distribution this rate coefficient is $\sim 5.8 \times 10^{-13} T_e^{-0.5} \text{ cm}^3 \text{ s}^{-1}$. This process is included for all ions included in the calculation when grains are present, but is not generally important. The rate coefficient is evaluated in routine *hmole* and stored as the variable *gionrc*.

10.14. Grain Variables

ndust The number of grain species. This variable appears in parameter statements throughout the code. Currently *ndust* is 20.

IgDustOn This logical variable is true if grains are enabled, and false otherwise. This is the variable to check to determine whether grains exist in the current model.

dqabs(energy, ndust) Absorption Q for this grain species as a function of energy.

dqscat(energy, ndust) Scattering Q for this grain species as a function of energy.

dston1(ndust) A logical variable that indicates whether this grain species is enabled.

dstab1(energy, ndust) Absorption cross section for this grain species

dstsc1(energy, ndust) Scattering cross section for this grain species.

dstab(energy) Total absorption cross section for all grain species.

dstsc(energy) Total scattering cross section for all grain species.

dstq(ndust) The grain charge, in units of number of electrons.

dstpot(ndust) The grain potential, in Rydbergs.

dstdft(ndust) The grain species' drift velocity.

avdft(ndust) Variable used to derive average drift velocity of a grain species.

dustp(4, ndust) These are parameters describing the grain species, and are set in block data *martin*. They are defined in Peter Martin's program that computes grain optical parameters. The four elements of the array are the grain density, molecular weight, normalizing abundance, and depletion.

eev(limcrs, ndust) is an *limcrs* long array of energies (in Rydbergs, despite the variable name). ***ndpts*** of these are energies where the grain optical parameters are defined.

sab(limcrs, ndust) is an *limcrs* long array of absorption cross sections for the grain species, at the ***ndpts*** energy points. These are defined as the effective absorption cross section per hydrogen nucleon.

sse(limcrs, ndust) is an ***limcrs*** long array of scattering cross sections for the grain species, at the ***ndpts*** energy points. These are defined as the effective scattering cross section per hydrogen nucleon, multiplied by $(1-g)$ where g is the grain asymmetry factor.

ndpts(ndust) is the number of energies where the grain optical properties are defined, for each species.

darea(ndust) is the grain surface area (cm^2) per hydrogen nucleon.

dsize(ndust) is the grain radius (cm) per hydrogen nucleon.

dwork(ndust) Grain species neutral surface work function in Rydbergs.

dstfac(ndust) This is the log of the depletion scale factor for each grain species. It is equal to 0 for “normal” abundances, -1 for 1/10th of “normal”, etc. This is the first optional number that appears on the ***grains*** command. The number remains the log of the depletion throughout the calculation.

tedust(ndust) The equilibrium temperature for a grain species.

11. OTHER PHYSICAL PROCESSES

11.1. Overview

This section describes other physics processes that have been incorporated into CLOUDY. Some of these are taken from published papers that have described the formalism used by CLOUDY in detail. The original papers are cited in the beginning of each section.

11.2. Cosmic Ray Interactions

The implementation of cosmic rays was done in collaboration with Richard Mushotzky. This section is taken from Ferland and Mushotzky (1984).

Synchrotron radio sources are usually modeled in terms of an interaction between a magnetic field and a relativistic gas with a typical energy per electron of a few hundred MeV (see Pacholczyk 1970; Longair 1981). The spectral index of the radio emission for radio-loud active galaxies is usually ~ -0.7 , and this suggests that the electrons, which make the dominant contribution to synchrotron emission, have a density (per unit energy interval) given by $n(\text{cr}, E) \sim E^{-2.4}$ (Kellerman 1966). The total relativistic electron density is sensitive to the lower bound of the energy distribution, which is typically of order 10–100 MeV, corresponding to relativistic factor of $\gamma \sim 10$ –100 (Lee and Holman 1978).

The cosmic ray density used by CLOUDY is defined as

$$n(\text{cr}) = \int_{E_{\min}}^{E_{\max}} n(\text{cr}, E) dE \quad (313)$$

with the lower bound set to $E_{\min} = 5$ MeV, corresponding to $\gamma \sim 10$. The density is only weakly sensitive to the upper limit $E_{\max} \approx 10$ GeV because of the strong convergence of the electron density function, although uncertainties in the lower energy bound introduce a fundamental uncertainty. Cosmic ray protons should have much smaller effects than the electrons, so the total cosmic ray electron density $n(\text{cr})$ is the only parameter.

The code assumes that the gas is “optically thin” to the energetic electrons. Serious and fundamental uncertainties afflict detailed treatments of the penetration of energetic particles into gas, particularly if magnetic fields are present. In the simplest case penetration is impeded only by ionization and heating losses resulting from two-body collisions. In this case the ability to heat an entire cloud is determined by the range of a particle, or the column density of gas required to stop it (see Rossi 1952). Relativistic electrons have a range that is given to within 15% by (Berger and Seltzer 1965)

$$R_e = 10^{25} \left(\frac{E}{100 \text{ MeV}} \right)^{0.8} \text{ cm}^{-2} \quad (314)$$

for a gas composed of neutral hydrogen. The range of a 100 MeV electron in a fully ionized gas, in which bremsstrahlung and Coulomb losses are more important than ionization, would be some 10 times smaller.

The relativistic particles both heat and ionize the gas. The main concern is for the rate with which energy is transferred to the cold gas (Lea and Holman 1978; Ginzberg and Syrovatskii 1964). In the H^+ zone the main interaction will be with free electrons. Kinetic energy is passed to the cold electrons at a rate

$$G_{cr} = 8.5 \times 10^{-19} n_e n(cr) \quad (\text{erg cm}^{-3} \text{ s}^{-1}) \quad (315)$$

by direct Coulomb interactions (Jackson 1975; Spitzer 1962; Ginzburg and Syrovatskii 1964; Pacholczyk 1970). Here n_e is the thermal electron density, and the integration is over the electron distribution given above.

In regions where hydrogen is neutral the main interaction between thermal and relativistic gases is through ionization of the cold gas. For large neutral fractions very little of the energy of secondary electrons goes into actually heating the gas (Rossi 1952; Spitzer and Tomasko 1968). Calculations show that secondary electrons have typical energies of ~ 40 eV, and that there is roughly one ionization per 15 eV deposited. Using the Bethe-Bloch approximation (Ginzburg and Syrovatskii 1964) the neutral heating rate is

$$G_{cr} = 3.7 \times 10^{-20} n(H^o) n(cr) \quad (\text{erg cm}^{-3} \text{ s}^{-1}) \quad (316)$$

and the H^o ionization rate is

$$\Gamma = 1.5 \times 10^{-8} n(cr) n(H^o) \quad (\text{cm}^{-3} \text{ s}^{-1}) \quad (317)$$

This ionization rate was scaled through Lotz's (1967) curves to include collisional ionization of heavy elements in the calculation of heavy element ionization equilibria.

If cosmic rays are not included, and the hydrogen ground state photoionization rate falls below the galactic background cosmic ray ionization rate, then a comment will be generated warning that the cosmic ray background should perhaps be included. According to Spitzer (1978), the background cosmic ray ionization rate is very uncertain, but of the order of $2 \times 10^{-17} \text{ s}^{-1}$ for neutral hydrogen. According to the equations above, this rate corresponds to a cosmic ray density of $\sim 2 \times 10^{-9} \text{ cm}^{-3}$, the value used as the “background” cosmic ray density option for the `cosmic ray` command.

The discussion above, as well as the code, includes only two-body Coulomb interactions, and *does not* include collective effects, such as those discussed by Scott et al. (1980). Rephaeli (1987) notes that collective effects may not be important in most circumstances.

11.3. Line Radiation Pressure

Line radiation pressure was implemented in CLOUDY in collaboration with Moshe Elitzur. The following was written in collaboration with Moshe, and is adopted from Elitzur and Ferland (1986).

11.3.1. Formalism

For radiation intensity I_ν , the standard expression for the radiation pressure per unit frequency, P_ν , is (e.g. Schwarzschild 1965)

$$P_n = \frac{1}{c} \int I_n \mu^2 d\Omega \quad , \quad (318)$$

where $\mu = \cos(\theta)$ and θ is the direction of propagation of the radiation. When the radiation field is isotropic, its pressure and energy density,

$$u_n = \frac{1}{c} \int I_n d\Omega \quad , \quad (319)$$

are related by the familiar expression

$$P_n = \frac{1}{3} u_n \quad . \quad (320)$$

This relation holds for a rather wide range of circumstances. If the angular distribution of I_ν is expanded in a power series in μ , then only powers higher than the second will lead to violations of equation 320. However, the successive coefficients of this expansion are decreasing approximately like the optical depth (e.g. Schwarzschild 1965, p 40), so deviations from equation 320 will only be proportional to $1/\tau^2$. Hence, when the medium is optically thick at the frequency ν equation 320 is an excellent approximation for the radiation pressure.

The only radiative quantity we need to know in order to calculate the radiation pressure is the angle-averaged flux, J_ν , since

$$u_n = \frac{1}{c} 4\pi J_n \quad . \quad (321)$$

The integrated radiation pressure is then

$$P(n) = \frac{4\pi}{3c} \int J_n d\mathbf{n} \quad . \quad (322)$$

Introducing the line-width, defined by

$$\Delta n = \frac{1}{\bar{J}_{u,l}} \int J_n d\mathbf{n} \quad , \quad (323)$$

where

$$\bar{J}_{u,l} = \int J_n \Phi(n) d\mathbf{n} \quad (324)$$

is the integrated mean intensity in the line and $\Phi(\nu)$ is the normalized line profile $[\int \Phi(n) d\mathbf{n} = 1]$. The quantity \bar{J} is readily available in the escape probability approximation because it is related directly to the source function S by

$$\bar{J}_{u,l} = S(1 - P_{u,l}) \quad (325)$$

where $P_{u,l}$ is the photon escape probability. The line source function S is simply $B_\nu(T_{exc})$, the Planck function of the line excitation temperature. The final expression for the pressure due to a line at frequency ν is therefore

$$P(\mathbf{n}) = \frac{4p}{3c} B_n(T_{exc}) \Delta n (1 - P_{u,l}) \quad (326)$$

Combining equation 326 with equation 144 on page 216 we obtain the final form of the line radiation pressure,

$$P(\mathbf{n}) = \frac{8phn^3}{3c^3} \frac{n_u / g_u}{(n_l / g_l - n_u / g_u)} \Delta n (1 - P_{u,l}) \quad (327)$$

In these expressions the line width is given in frequency units. Within the code the line width is given in velocity units, and the line pressure is given as

$$\begin{aligned} P(\mathbf{n}) &= \frac{8phn^4}{3c^4} \frac{n_u / g_u}{(n_l / g_l - n_u / g_u)} \Delta \nu (1 - P_{u,l}) = \frac{8ph}{3I^4} \frac{n_u / g_u}{(n_l / g_l - n_u / g_u)} \Delta \nu (1 - P_{u,l}) \\ &= 6.872 \times 10^{-68} \mathbf{n}^4 \frac{n_u / g_u}{(n_l / g_l - n_u / g_u)} \Delta \nu (1 - P_{u,l}) \quad (328) \\ &= 5.551 \times 10^{-26} I^{-4} \frac{n_u / g_u}{(n_l / g_l - n_u / g_u)} \Delta \nu (1 - P_{u,l}) \end{aligned}$$

11.3.2. Line width

The line width is a crucial parameter in the calculations since the line radiation pressure is directly proportional to it. For lines with a moderate optical depth (i.e., $\tau \leq 10^4$) the damping wings are optically thin, and the line emission profile is essentially identical to the absorption profile. Then $\Phi(\nu)$ is simply described by the Doppler profile $\pi^{1/2} \exp(-x^2)$, where $x = (\nu - \nu_0) / \Delta \nu_{Dop}$ is the dimensionless frequency shift from line center and $\Delta \nu_{Dop} = (2kT/m)^{1/2} \nu_0 / c$ is the Doppler width. The line full width is then

$$\Delta n = \Delta n_{Dop} \times 2(\ln \tau)^{1/2} \quad (329)$$

for $\tau \gg 1$.

The situation when the line optical depth exceeds $\sim 10^4$ is much more complicated. This is because scattering in the damping wings becomes significant, and the frequency dependence of the emission profile is not known before the entire radiative transfer problem is solved. In general, it is known that, for Ly α (generally the most important source of line radiation pressure) and large optical depths, the line width (in dimensionless units) is

$$x = k(a\tau)^{1/3} \quad (330)$$

(Adams 1972; Harrington 1973; Bonilha et al. 1979). In this expression a is the damping constant ($a \approx 4.72 \times 10^{-4} t_4^{-1/2}$ for Ly α), τ is the line center optical depth, t_4 is the temperature in units of 10^4 K, and k is a number of order unity.

The frequency width required here is the value that will provide a rectangular profile with the same area as the proper integral of the source function. The results of Adams (1972) are adopted, and the resulting expression for the full line width in the case of large optical depths ($\tau \gg 1$) is

$$\Delta n = \Delta n_{Dop} 2.3 (a t)^{1/3} \quad (331)$$

An important point, evident from the plots provided by Adams for the source function as a function of frequency (his Fig 3), is that the width of the frequency distribution varies very little with position in the slab. This is also evident from the mean intensity plots of Harrington, as mentioned above, and is a result of the strong coupling between distant regions caused by scattering in the line wings. The expression provided in equation 331 for all locations in the slab, with τ being half the total slab thickness.

11.3.3. Background opacity and thermalization

Background opacity is included in the determination of the level populations using the formalism outlined in the section on line radiative transfer. Its main effect is to lower the line excitation temperature by providing a second “escape” (actually destruction) route for trapped photons. This is assumed to be the only effect background opacity has on radiation pressure. Balmer continuous absorption typically has an optical depth only of order unity, while the line optical depths are many orders of magnitude larger. Absorption in the Balmer continuum can only compete with line scattering in the extreme wings, at frequency shifts exceeding $\sim (a \tau)^{1/2}$, which are much larger than the line width predicted by equation 331.

Collisional de-excitation can also break the assumption of pure scattering because a photon will be lost to the thermal pool before the radiative process can take place. This will happen when the density is high enough that the rate for collisional de-excitation, C_{ul} , exceeds the probability for the effective rate for the transition, $P_{ul} A_{ul}$, where P_{ul} is the line escape probability and A_{ul} is the Einstein coefficient. Because at large optical depths P_{ul} is essentially equal to τ^{-1} , the “effectively thin” assumption breaks down when

$$t \approx A_{u,l} / C_{u,l} \quad (332)$$

Once the line optical depth exceeds $\sim A/C$, a “thermalization limit” is encountered, and the assumption of a purely scattering nebula does not apply anymore. Therefore, in evaluating the optical depth for the line width expression (equation 331) the minimum of the actual line optical depth and the one prescribed by A/C is used. This is a conservative estimate of the effect of collisions on photon scattering. This is probably the most poorly understood part of the calculation of the line radiation pressure.

11.4. Radiative Acceleration

The radiative acceleration (cm s^{-2}) due to the direct attenuated continuum flux F_ν , for density ρ , is given by

$$a_{rad} = \frac{1}{rc} \int F_n \bar{\kappa}_n d\mathbf{n} + \frac{1}{rc} \sum_l F_n(l) \kappa_l \mathbf{g} B_{l,u} . \quad (333)$$

Here $\bar{\kappa}_n$ is the effective continuous opacity. The radiative acceleration is computed in routine **radinc** and includes the usual photoelectric and free-free absorption in the gas, and Compton and Rayleigh scattering. In addition it includes the term $\kappa_{abs} + (1-g)\kappa_s$ for the grain contributions if grains are present. The integral is over all energies considered by the code (from $\lambda \approx 1$ cm to $h\nu \approx 100$ MeV).

The second term is a sum is over all transferred lines (typically 10^4 to 10^5 transitions). Here κ_l is the line opacity, B_l is the Einstein coefficient, and γ_l is the escape probability in the direction towards the source of ionizing radiation (Ferland and Rees 1988).

11.5. Pressure Laws

11.5.1. Units

Pressure is force per unit area. The unit of force in the cgs system is the dyn, which is 10^{-5} N. The fundamental units of the dyn are g cm s^{-2} . For pressure these are dyn cm^{-2} or $\text{gm cm}^{-1} \text{s}^{-2}$.

11.5.2. Ideal gas laws

For a non-relativistic non-degenerate gas the energy density is

$$u = \frac{3}{2} n_{tot} kT_e \quad (334)$$

and the pressure is

$$P_{gas} = n_{tot} kT_e = \frac{2}{3} u \text{ dynes cm}^{-2}. \quad (335)$$

n_{tot} is the total particle density (cm^{-3}). For a relativistic non-degenerate gas the energy density is

$$u = 3 n_{tot} kT_e \quad (336)$$

and the pressure is

$$P_{gas} = n_{tot} kT_e = \frac{1}{3} u \text{ dynes cm}^{-2}. \quad (337)$$

11.5.3. Equation of state

When the pressure is held constant (with the **constant pressure** command) the pressure law is given by

$$P(r) = P_{gas}(r_o) + \int_{r_o}^r a_{rad} r dr = P_{gas}(r) + P_{line}(r) \quad (338)$$

where

$$P_{gas}(r_o) = n_{tot} kT \quad (339)$$

is the gas pressure at the illuminated face of the cloud stored as the variable **PresInit**. The total particle density n_{tot} is (referred to by the variable **pden**), and r is the radius of the current position.

11.5.4. Turbulent pressure?

Turbulence can be included as a line broadening mechanism. Its only affect is in modifying the line opacities and resulting optical depths. Turbulence should add a component to the total pressure of

$$P_{\text{turb}}(r_o) = \frac{1}{2} r v_{\text{turb}}^2 = 5.8 \times 10^6 \left(\frac{n}{10^5 \text{ cm}^{-3}} \right) \left(\frac{v_{\text{turb}}}{1 \text{ km s}^{-1}} \right)^2 \text{ cm}^{-3} \text{ }^\circ \text{K} \quad (340)$$

where n is the density and v_{turb} is the turbulent velocity. Turbulent pressure is not included in the pressure law since it would be either negligible, or so large that it would not be possible to determine the gas pressure.

11.5.5. Ram or dynamic pressure

Pressure associated with energy of bulk motion can be referred to as ram or dynamic pressure. It is given by ρv^2 .

11.5.6. Pressure variables and routines

TotalPressure This routine evaluates the sum of the gas and line radiation pressures. This routine *does not* evaluate the force term due to the attenuation and reflection of the incident continuum. The function has a single dummy argument, and returns the total pressure in dynes/cm².

PresInit This is the gas pressure at the illuminated face of the cloud.

pgas This is the gas pressure, nkT , with units dynes/cm²., and is evaluated in routine **TotalPressure**.

prad This is the line radiation pressure, evaluated as described on page 298. It is also evaluated in **TotalPressure**.

pinteg The integrated radiative force on the gas is evaluated in routine **radinc** and is stored as the variable **pinteg**. This is kept separate from the local gas pressure since it is really a global quantity, unaffected by changes at the current position.

pnow This is the current sum of gas and local line radiation pressure.

presur This routine obtains the current total pressure, and ratios that with the desired total pressure. This scale factor is then applied to various physical quantities.

perror This is the fractional error allowed in the pressure convergence. It currently is set in a data statement within **presur**.

presok **presur** will set the variable **presok** to false if the change in the local conditions was too large, and so capped, and to true if a good final pressure was achieved. The pressure is declared converged by **presur** when **pnow** (the local pressure) is within **perror** of being equal to the sum of **PresInit** and **pinteg**.

Plonte This routine calls **presur**.

11.6. Wind Geometry

CLOUDY will do a simple wind geometry if the `wind` command is specified. The effective acceleration is written as $a_{\text{eff}} = a_{\text{rad}} - g_{\text{grav}}$, where a_{rad} is computed in equation 333 above, and g_{grav} is the inward gravitational acceleration due to the central object. The default is one solar mass. The velocity is computed assuming that the acceleration is constant across the zone. In this case the change in the wind velocity v between the inner and outer edges of a zone of thickness dr will be

$$v^2 - v_o^2 = 2a_{\text{eff}} dr \quad (341)$$

where v_o is the velocity at the inner edge. The calculation will stop if the velocity ever falls below zero.

All calculations involving the velocity and density associated with this wind are performed in routine `presur`. The density at the illuminated face of the cloud is entered with the `hden` command. The density is varied across the model to conserve mass flux (i.e., the product $\rho(r) r^2 v(r)$ is kept constant). Because of this, a filling factor would not make physical sense, and should not be used. Note also that it is usually necessary to set an outer radius when a wind model is computed to stop the calculation from extending to infinity.

A simple Sobolev approximation is used for line transfer when a wind is computed. The effective optical depth is given by;

$$\tau_{l,u}(r) = a_{l,u} \left(n_l - n_u \frac{g_l}{g_u} \right) r \frac{v_{\text{th}}}{\max(v_{\text{th}}, v_{\text{exp}})} \quad (342)$$

where r is the smaller of the radius or depth and v_{th} and v_{exp} are the thermal and expansion velocities respectively. The choice of the smaller of the radius or depth is not in strict keeping with the Sobolev approximation, but is necessary since calculations often begin at very large radii from the central object. The optical depths would have unphysically large values were this choice not made.

Figure 26 shows a test case in which a wind is driven in the plane parallel electron scattering limit. As can be seen the numerical solution is in

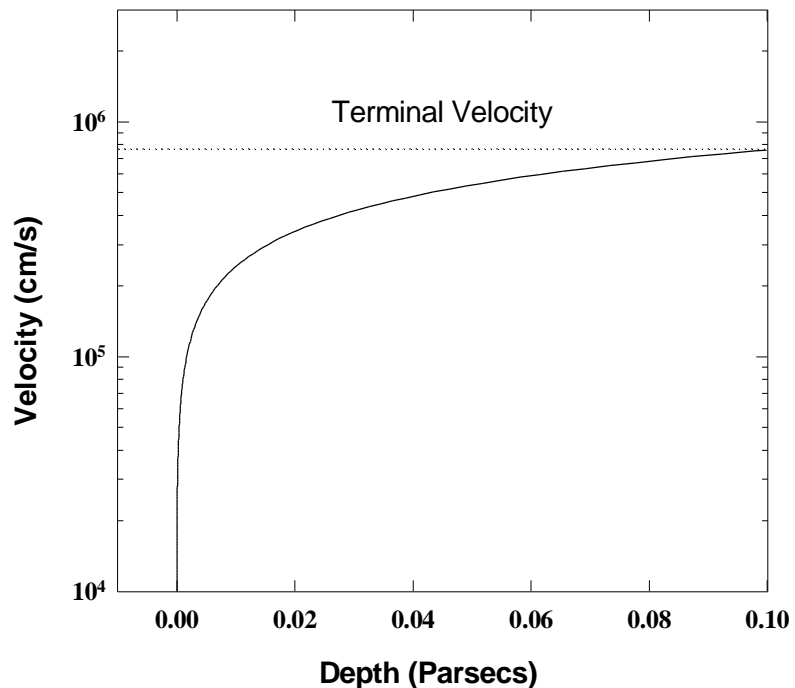


Figure 26 The wind velocity is computed using the input stream shown in one of the test cases in the last section. Parameters were chosen to have a readily computed final velocity. The velocity at the outer edge of the slab is within 1 percent of its expected value. wind

excellent agreement with the analytically predicted result.

11.7. Secondary Ionization

11.7.1. Ionization, heating, and cooling

Although the electron velocity distribution is predominantly Maxwellian (Bohm and Aller 1947), a small constituent of non-thermal secondary electrons may be present when high-energy radiation is present. Secondary ionizations by supra-thermal electrons are treated following Xu and McCray (1991). All sources of energetic electrons, including both Auger and primary electrons, are considered in the initial input of high-energy electrons into the gas. The resulting coefficient giving the rate of non-thermal electrons is stored as the variable **csupra**, which has units s^{-1} . A typical energy of an electron in the non-thermal shower is ~ 20 eV; this energy is used to evaluate collisional ionization and excitation cross sections. Secondary ionization is included among the general ionization processes considered for all species. The coefficient giving the rate for excitations of Ly α is given as **x12**.

11.7.2. Evaluation of rate of hot electron energy input

The variable **ipSecIon** points to the lowest photon energy (100 eV) where a photoelectron can produce secondary ionization. Below this energy photoelectrons are assumed to produce 100% heat with no secondary ionization.

Each of the routines that evaluate photoionization or Comptonization rates records the total energy input by photons with energy greater than this. These are saved with units Rydbergs per photoionization per atom, e_{Ryd}^* .

11.7.3. Secondary rates per atom

The secondary ionization energy redistribution coefficients are evaluated in routine **nockon**. Three variables, the heating efficiency **heatef**, the ionization efficiency **efionz**, and the efficiency for exciting Ly α **exctef**, are defined. In the following equations e_{Ryd}^* is the initial energy of the hot photoelectron.

heatef This is a fraction (between 0 and 1) of the energy of the photoelectron that goes into heating the Maxwellian electron bath. The heat actually deposited in the free electrons ($\text{Ryd cm}^3 \text{s}^{-1}$) is given by

$$\Lambda_{\text{sec}} = e_{\text{Ryd}}^* \times \text{HEATEF}. \quad (343)$$

efionz This is the number of hydrogen ionizations produced per Rydberg of heat input by suprathreshold electrons. The number (s^{-1}) of knock-on secondary ionizations is given by

$$r_{\text{ion}} = \text{CSUPRA} = e_{\text{Ryd}}^* \times \text{EFIONZ}, \quad (344)$$

exctef This is the energy in Rydbergs that goes into Ly α excitations. The number (s^{-1}) of excitations of Ly α is given by

$$r_{\text{Ly}\alpha} = \text{SECLA} = e_{\text{Ryd}}^* \times \text{EXCTEF} \times 4 / 3, \quad (345)$$

Table 27 Secondary Ionization Efficiencies

Electron fraction	Secondary Ionization	Heating Efficiency	Ly α Excitations	sum
1.00E-04	3.75E-01	1.11E-01	4.19E-01	9.06E-01
3.16E-04	3.66E-01	1.51E-01	3.99E-01	9.15E-01
1.00E-03	3.51E-01	2.03E-01	3.71E-01	9.25E-01
3.16E-03	3.28E-01	2.73E-01	3.35E-01	9.36E-01
1.00E-02	2.92E-01	3.66E-01	2.87E-01	9.45E-01
3.16E-02	2.39E-01	4.87E-01	2.25E-01	9.51E-01
1.00E-01	1.64E-01	6.40E-01	1.50E-01	9.54E-01
3.16E-01	6.98E-02	8.24E-01	6.50E-02	9.59E-01
1.00E+00	0.00E+00	9.97E-01	0.00E+00	9.97E-01

Table 26 Secondary Ionization Variables

Agent	Ionization	Lya
Hydrogen	sechi	hlax
Helium	seche	helax
Compton	seccmp	scmpla
Heavies	secmet	smetla

11.7.4. Total interaction rates

The interaction rates per unit volume are given by the rates per atom (given by the variables in Table 26) and the density of the atom. This results in the total number of secondary interactions per unit volume. This total rate is converted into a rate per target atom by dividing the volume rate by the number of *atoms* per unit volume, given by the variable **collid** (evaluated by routine **TotalPressure**). The results are the rates (with units s^{-1}) referred to by the variable **csupra** (secondary ionization rate) and **x12** (secondary rate of excitation of Lyman lines).

11.7.5. Rates during the hydrogen balance solution

The hydrogen ionization balance is performed in routine **hlevel**. In deep regions of X-Ray ionized clouds the dominant source of secondaries is often inner shell ionization of the heavy elements, especially oxygen. Often secondary ionization is the dominant ionization source of hydrogen, and in this case the secondary ionization rate changes as the electron density changes, during searches for the ionization balance. It would not be computationally expedient to reevaluate all heavy element ionization rates during the search for the hydrogen ionization balance, so, during this search an effective secondary ionization rate, given by a simple scaling law using the current electron fraction, and the secondary rate and electron fraction where it was last evaluated. The effective suprathemal rate is referred to as **csupeff**.

11.7.6. Molecules and Suprathemal Electrons

The collisional and heating effects of the suprathemal secondary electrons following inner-shell photoionization are treated using standard assumptions (Bergeron and Souffrin 1971; Shull and van Steenberg 1985; Voit 1991).

8 eV of heat is deposited for each H_2 ionization by a cosmic ray (Tielens and Hollenbach 1985). Relative rates are taken from HM89.

The result of this is a secondary ionization rate that must then be multiplied by scale factors that account for the relative collision cross section for each species relative to hydrogen. These are taken from HM89 and TH85.

Secondary electrons also produce a diffuse background of electronic H₂ lines that can photodissociate most molecules. This is treated using the scaling rule of Gredel, Lepp, and Dalgarno (1987) and Gredel et al. (1989).

11.8. Jeans Length and Mass

The Jeans length and mass are computed for each zone in the calculation. The smallest computed Jeans length and mass are saved, and a note is printed at the end of the calculation if the computed structure is Jeans unstable.

The expression for the Jeans length is

$$l_J = \left(\frac{\rho k T}{\mu m_p G r} \right)^{1/2} = 6.257 \times 10^7 \left(\frac{T}{\mu r} \right)^{1/2} \quad (\text{cm}) \quad (346)$$

where μ is the mean mass per particle

$$\mu = \frac{\sum n_i m_i}{\sum n_i} \quad (\text{gm}) \quad (347)$$

of the gas (referred to as the variable **wmole**) and ρ is the density of the gas (gm, referred to as the variable **densty**). Both are computed in routine **TotalPressure**.

The Jeans mass is then given by

$$M_J = \frac{4\rho}{3} r \left(\frac{l_J}{2} \right)^3 \quad (\text{gm}) \quad (348)$$

where the mass is that of a sphere with radius $\lambda_J / 2$.

The minimum Jeans mass is evaluated in routine tauinc as the calculation progresses. The code will generate a comment if the computed structure is Jeans unstable.

11.9. Luminosity Distance

The luminosity distance D_L is given by equation 349.

$$D_L = \begin{cases} \frac{cz}{H_o} (1 + z/2) & q_o = 0 \\ \frac{c}{H_o q_o^2} \left\{ q_o z + (q_o - 1) \left[(2q_o z + 1)^{1/2} - 1 \right] \right\} & q_o > 0 \\ \frac{2c}{H_o} \left[1 + z - (1 + z)^{1/2} \right] & q_o = 1/2 \end{cases} \quad (349)$$

For $q_o = 1/2$ and $H_o = 70 \text{ km/s/Mpc}$ the luminosity distance is

$$D_L = 2.643 \times 10^{26} \left[1 + z - (1 + z)^{1/2} \right] \quad \text{cm} \quad (350)$$

The proper distance D is given by $D_L = D(1 + z)$.

12. GLOSSARY OF SYMBOLS

As far as possible, the notation used by HAZY follows standard texts (Osterbrock 1989; Mihalas 1978). This is a summary of some of the symbols used. Page references to Part II of HAZY or the numerical quantity are listed in the third column of this glossary.

The fundamental constants now used by the code are from a variety of revisions of the basic data, some dating back to the 1970's. An effort is now underway to convert the constants to the 1986 CODATA recommended values (see <http://physics.nist.gov/PhysRefData/codata86/codata86.html>).

Symbol	Description	Units	Notes
a	Stefan radiation density	erg cm ⁻³ K ⁻⁴	7.56464×10 ⁻¹⁵
a	damping constant	-	page 217
a ₀	Bohr radius	cm	0.5291775×10 ⁻⁸
a _{rad}	radiative acceleration	cm s ⁻²	page 298
A _{ul}	radiative rate from level <i>u</i> to <i>l</i>	s ⁻¹	
b _n	departure coefficient	-	page 231
B	magnetic field	esu	
B _v	Planck function	erg cm ⁻² s ⁻¹ Hz ⁻¹ sr ⁻¹	
c	speed of light	cm s ⁻¹	2.997925×10 ¹⁰
C	collisional rate	s ⁻¹	
C _{ul}	line collision rate	s ⁻¹	
D _{ul}	line destruction probability	-	page 218
f	oscillator strength		
f(r)	filling factor	-	
f _v F _v	flux density	erg cm ⁻² s ⁻¹ Hz ⁻¹	
g	grain asymmetry factor	-	page 290
g _i	statistical weight	-	
g _{III}	T aver free-free gaunt factor	-	
G	energy gains	heating	erg cm ⁻³ s ⁻¹
I	integrated intensity	erg s ⁻¹ sr ⁻¹ Hz ⁻¹	
I _n	ionization potential of level <i>n</i>	erg; Ryd	
I _v	intensity	erg s ⁻¹ sr ⁻¹ Hz ⁻¹	
h	Planck's constant	erg s	6.62620×10 ⁻²⁷
J	integrated mean intensity	erg s ⁻¹ sr ⁻¹	
J _v	mean intensity	erg s ⁻¹ sr ⁻¹ Hz ⁻¹	
k	Boltzmann constant	eV deg ⁻¹	8.6171×10 ⁻⁵
k	Boltzmann constant	erg deg ⁻¹	1.38062×10 ⁻¹⁶
L _☉	luminosity of sun	erg s ⁻¹	3.826×10 ³³
m _A	mass of atom A	gm	
m _{AMU}	atomic mass unit	gm	1.6605402×10 ⁻²⁴
m _e	electron mass	gm	9.10956×10 ⁻²⁸
m _e c ²	electron energy	Ryd	3.75584×10 ⁴
m _p	proton mass	gm	1.6726231×10 ⁻²⁴
M _J	Jeans' mass	gm	page 307

M_{\odot}	mass of the sun	gm	1.989×10^{33}
M_{\oplus}	mass of the Earth	gm	5.977×10^{27}
n_e	electron density	cm^{-3}	
n_j	population of level j	cm^{-3}	
n_p	proton density	cm^{-3}	
$n(\text{H})$	total H density, all forms	cm^{-3}	
$n(x)$	density of species x	cm^{-3}	
$n(\text{cr})$	cosmic ray density	cm^{-3}	page 297
n	atom's level		
$N(x)$	column density of species x	cm^{-2}	
$N(\text{H})$	total H col den, all forms	cm^{-2}	
N_{eff}	effective H column density	cm^{-2}	
$P^*(x)$	LTE relative population	cm^3	page 231
P_{gas}	gas pressure	dyn cm^{-2}	page 303
P_{lines}	line radiation pressure	dyn cm^{-2}	page 303
P_{tot}	total pressure	dyn cm^{-2}	page 303
P_{ul}	line escape probability	-	page 218
$P_{\tau x}(n)$	continuum escape prob	-	
pc	parsec	cm	3.085678×10^{18}
q_{ij}	line collisional rate coefficient	$\text{cm}^3 \text{s}^{-1}$	
q_n	collisional rate coefficient	$\text{cm}^3 \text{s}^{-1}$	
q_e	electron charge	esu	4.80325×10^{-10}
Q_{abs}	grain absorption efficiency	-	page 290
$Q(\text{H})$	hydrogen ionizing photons	s^{-1}	
r	radius	cm	
$r_{l,u}$	rate	s^{-1}	
r_o	inner radius	cm	
R	total to selective extinction	-	
R_{H}	Rydberg unit for H	-	page 206
R_{∞}	Rydberg unit for inf mass	-	page 206
R_{\odot}	radius of the sun	cm	6.9599×10^{10}
T_e	electron temperature	cm^{-3}	
T_{exc}	excitation temperature	K	page 228
T_{color}	color temperature	K	
T_{low}	lowest temp allowed	K	2.8 K
T_u	energy density temperature	K	page 239
u	energy density	erg cm^{-3}	
U_g	grain potential	volt	page 292
v	velocity (mean or projected)	cm s^{-1}	
\bar{v}	mean particle speed	cm s^{-1}	page 292
v_{Dop}	Doppler velocity	cm s^{-1}	page 214
v_{exp}	expansion velocity	cm s^{-1}	
v_{th}	thermal velocity	cm s^{-1}	page 214
v_{turb}	turbulent velocity	cm s^{-1}	page 214
V_g	grain potential	eV	page 292
V_n	grain work function	eV	page 292
W	geometric dilution factor	-	

x	relative shift from line center	-	page 213
X_c	continuous to total opacity	-	page 217
\hat{Y}	grain photoelectric yield	-	page 290
z	redshift	-	
Z	nuclear charge	-	
$\alpha(n, T)$	recombination coefficient	$\text{cm}^3 \text{s}^{-1}$	page 233
$\bar{\alpha}(n, T)$	effec recomb coefficient	$\text{cm}^3 \text{s}^{-1}$	page 208
α_v	continuous abs cross section	cm^2	
α_{lu}	line absorption cross section	cm^2	page 213
β	recombination cooling coef	$\text{cm}^3 \text{s}^{-1}$	page 235
η_v	photon occupation number	-	page 239
δr	zone thickness	cm	
Δr	depth into cloud	cm	
$\gamma_{u, l}$	cont pumping probability		page 219
Γ_n	photoionization rate	s^{-1}	page 238
Γ	reciprocal lifetime of up level	s^{-1}	page 217
Γ_{OTS}	OTS photoionization rate	s^{-1}	page 209
κ	absorption opacity	cm^{-1}	
κ_{lu}	line absorption opacity	cm^{-1}	
κ_s	continuous scattering opacity	cm^{-1}	
κ_v	continuous absorption opacity	cm^{-1}	
λ_J	Jeans' length	cm	page 307
Λ	energy loss, cooling	$\text{erg cm}^{-3} \text{s}^{-1}$	
μ	mean molecular weight	-	page 307
Ω	energy specific collision strength		page 221
Ω	shell coverage	sr	
$\Omega/4\pi$	covering factor	-	
$\Phi(H)$	flux of ionizing photons	$\text{cm}^{-2} \text{s}^{-1}$	
φ_v	photon flux density	$\text{cm}^{-2} \text{s}^{-1} \text{Ryd}^{-1}$	
φ_{OTS}	flux of OTS photons	$\text{cm}^{-2} \text{s}^{-1}$	page 209
ρ	mass density	gm cm^{-3}	
πa_0^2	area of first Bohr orbit	cm^2	87.9737×10^{-18}
σ_T	Thomson cross section	cm^2	6.6524×10^{-25}
σ_v	scattering cross section	cm^2	
σ_{Ray}	Rayleigh scat cross section	cm^2	page 211
Σ	projected grain area	cm^2	page 290
τ	optical depth	-	
τ_{abs}	absorption optical depth	-	
τ_{scat}	scattering optical depth	-	
$\tau_{u, l}$	line optical depth	-	
Y	thermal averaged collision strength		page 221
ν	frequency	Hz	
ν_{Ryd}	frequency	Ryd	
$\delta\nu$	line width	Hz	
$\delta\nu_{\text{Dop}}$	Doppler width	Hz	

χ_n	$h\nu/kT$	-
----------	-----------	---

13. REFERENCES

- Abbott, D. C., 1982, ApJ 259, 282
Adams, T., 1972, ApJ 174, 439
Aldrovandi, S., & Pequignot, D., 1972, A&A 17, 88
Aldrovandi, S., & Pequignot, D., 1974, Revista Brasileira de Fisica, 4, 491
Ali, B., Blum, R.D., Bumgardner, T.E., Cranmer, S.R., Ferland, G.J., Haefner, R.I., & Tiede, G.P., 1991, Publ. A.S.P. 103, 1182
Allen, C.W., 1976, *Astrophysical Quantities*, Third Edition (London: Athlone Press).
Aller, L.H., 1984, in *Physics of Thermal Gaseous Nebulae*, (Reidel: Dordrecht).
Aller, L.H., & Czyzak, S.J. 1983, ApJ Sup. 51, 211.
Arimoto, N., & Yoshii, Y., 1987, A&A 173, 23
Arnaud, M., & Raymond, J., 1992, ApJ 398, 394
Arnaud, M., & Rothenflug, R., 1985, A&AS 60, 425
Avni, Y., & Tananbaum, H., 1986, ApJ 305, 83
Avni, Y., Worrall, D. M., & Morgan, W. A., ApJ 1995, 454, 673
Avrett, E.H., & Loeser, R., 1988, ApJ 331, 211
Bajtlik, S., Duncan, R.C., & Ostriker, J.P. 1988, ApJ 327, 570
Balbus, S.A., & McKee, C.F., 1982, ApJ 252, 529
Baldwin, J., Ferland, G.J., Martin, P.G., Corbin, M., Cota, S., Peterson, B.M., & Slettebak, A., 1991, ApJ 374, 580
Baldwin J.A., Ferland, G.J., Korista, K.T., Carswell, R., Hamann, F., Phillips, M., Verner, D., Wilkes, B., & Williams, R.E., 1996, ApJ 461, 683
Baldwin, J. A., Ferland, G.J., Korista K. T., and Verner, D., 1995ApJ 455, L119
Baldwin, J., Wampler, J., and Gaskell, C.M., 1989, ApJ 338, 630
Bässgen, G., Bässgen, M., & Grewing, M., 1988, Ast.Ap. 200, 51
Bates, D.R., Kingston, A. E., & McWhirter, R.W.P., 1962, Proc. R. Soc., A267, 297
Bechtold, J., Weymann, R.J., Lin, Z., & Malkan, M. A., 1987, ApJ 315, 180
Bell, K.L., Kingston, A. E., & McIlveen, W. A., 1975, J. Phys. B 8, 358
Berger, M.J., & Seltzer, S.M., 1965, NASA SP-3012
Bergeron, J., & Collin-Souffrin, S., 1971, A&A 14, 167
Berrington, K., and Pelan, A., 1995, A&AS 114, 367
Bethe, H., 1930, Ann. Phys. 5, 325
Bica, E., 1988, A&A 195, 76
Bieniek, R.J., & Dalgarno, A., 1979, ApJ 228, 635
Binette, L., Prieto, A., Szuszkiewicz, E., & Zheng, W., 1989, ApJ 343, 135
Black, J.H., 1978, ApJ 222, 125
Black, J.H., 1987, in *Interstellar Processes*, Hollenbach & Thronson, editors
Bohm, D., & Aller, L.H., 1947, ApJ 105, 131
Bonihala, J. R. M., Ferch, R., Salpeter, E. E., Slater, G., & Noerdlinger, P., 1979, ApJ 233, 649
Borkowski, K.J., & Harrington, J.P., 1991, ApJ 379, 168
Boyd, R., & Ferland, G.J., 1987, ApJ 318, L21
Bowen, I. S., 1960, ApJ 132, 1
Bregman, J.D., Allamandola, L.J., Tielens, A.G.G.M., Geballe, T.R., and Witteborn, F.C., 1989, ApJ 344, 791
Broad, J.T., & Reinhardt, W. P., 1976, Phys Rev A 14, 2159
Brown, R.L., & Mathews, W.G., 1970, ApJ 160, 939
Burgess, A., 1965, ApJ 141, 1588
Burgess, A., & Summers, H.P., 1969, ApJ 157, 1007
Burgess, A., & Summers, H.P., 1976, MNRAS 174, 345
Butler, S. E., Bender, C.F., & Dalgarno, A., 1979, ApJ 230, L59
Butler, S. E., & Dalgarno, A., 1979, ApJ 234, 765
Butler, S. E., Heil, T. G., & Dalgarno, A., 1980, ApJ 241, 442
Butler, S. E., & Dalgarno, A., 1980, ApJ 241, 838
Callaway, J. 1994, At Dat Nuc Dat Tab 57, 9

- Cameron, A.G.W., 1982, in *Essays in Nuclear Astrophysics*, ed CA Barnes, DD Clayton, & DN Schramm, (Cambridge Univ Press; London)
- Canfield, R.C., & Puetter, R.C., 1980, ApJ 236, L7
- Cardelli, J. A., 1994, Science 264, 209
- Cardelli, J. A., et al. 1991, ApJ 377, L57
- Carswell R.F. and Ferland, G.J. 1988, MNRAS 235, 1121
- Castor, J.I., 1970, MNRAS 149, 111
- Chaffee, F. H., & White, R. E., 1982, ApJ Sup. 50, 169
- Chan, E.S., Avrett, E.H., & Loeser, R., 1991, A&A 247, 580
- Chapman, R. D., & Henry, R.J.W., 1971, ApJ 168, 169
- Chidichimo, M.C., 1981, J. Phys. B. 14, 4149
- Clavel, J., & Santos-Lleo, M., 1990, A&A 230, 3
- Clegg, R.E.S., 1987, MNRAS 229, 31p
- Clegg, R.E.S., & Harrington, J.P., 1989, MNRAS 239, 869
- Cohen, E.R., and Taylor, B.N., 1987, Rev Mod Phys 57, 1121
- Cota, S.A., 1987, Ph.D. Thesis, OSU
- Cota, S.A., & Ferland, G.J., 1988, ApJ, 326, 889
- Cowie, L.L., & Songaila, A., 1986, ARAA 24, 499
- CrinkLaw, G., Federman, S. R., & Joseph, C. L., 1994, Ap J 424, 748
- Crosas, M., & Weisheit, J.C., 1993, MNRAS 262, 359
- Cruddace, R., Paresce, F., Bowyer, S., & Lampton, M., 1974, ApJ 187, 497
- Dalgarno, A., & Kingston, A. E., 1963, Observatory 83, 39
- Dalgarno, A., & McCray, R.A., 1973, ApJ 181, 95
- Dalgarno, A., & Roberge, W.G., 1979, ApJ 233, L25
- Davidson, K., 1972, ApJ 171, 213
- Davidson, K., 1975, ApJ 195, 285
- Davidson, K., 1977, ApJ 218, 20
- Davidson, K., & Netzer, H., 1979, Rep. Prog. in Physics 51, 715
- Davidson, K., & Fesen, R.A., 1985, Ann. Rev. A&A 23, 119
- Desert, F.-X., Boulanger, F., and Puget, J.L., 1990, A&A 237, 215
- Dove, J.E., Rush, A., Cribb, P., & Martin, P.G., 1987, ApJ 318, 379
- Dove, J.E., & Mandy, M.E., 1986, ApJ, 311, L93
- Draine, B.T., 1978, ApJS 36, 595
- Draine, B.T., & Lee, H.M., 1984, ApJ 285, 89
- Draine, B.T., & Salpeter, E. E., 1979, ApJ 231, 77
- Draine, B.T., & Sultin, B., 1987, ApJ 320, 803
- Drake, S.A., & Ulrich, R.K., 1980, ApJS 42, 351
- Elitzur, M., 1982, Rev. Mod. Phys 54, 1125
- Elitzur, M., 1984, ApJ 280, 653
- Elitzur, M, 1992, *Astronomical Masers*, Kluwer, Dordrecht
- Elitzur, M., Ferland, G.J., Mathews, W.G., & Shields, G., 1983, ApJ 272, L55
- Elitzur, M., & Ferland, G.J., 1986, ApJ 305, 35
- Elvis, M. et al. 1994, ApJS 95, 1
- Fabian, A. C., Pringle, J.E., & Rees M.J., 1976, MNRAS 175, 43
- Federman, S. R., et al. 1993, ApJ 413, L51
- Ferguson, J., Ferland, G.J., & A. K. Pradhan, 1995, ApJ 438, L55
- Ferguson, J., & Ferland, G.J., 1997, ApJ 479 363
- Ferguson, J.W., Korista, K.T., Baldwin, J.A., & Ferland, G.J., 1997, ApJ 487, 122
- Ferland, G.J., 1977, ApJ 212, L21
- Ferland, G.J., 1979, MNRAS 188, 669
- Ferland, G.J., 1980a, MNRAS 191, 243
- Ferland, G.J., 1980b, BAAS 12, 853
- Ferland, G.J., 1980c, PASP 92, 596
- Ferland, G.J., 1986, PASP 98, 549
- Ferland, G.J., 1986, ApJ, 310, L67
- Ferland, G.J., 1992, ApJ 389, L63
- Ferland, G.J., 1993, ApJS 88, 49

13 REFERENCES

- Ferland, G.J., Baldwin J. A., Korista, K.T., Hamann, F., Carswell, R., Phillips, M., Wilkes, B., & Williams, R. E., 1996, ApJ 461, 683
- Ferland, G., Binette, L., Contini, M., Harrington, J., Kallman, T., Netzer, H., Pequignot, D., Raymond, J., Rubin, R., Shields, G., Sutherland, R., & Viegas, S., 1995, in *The Analysis of Emission Lines*, Space Telescope Science Institute Symposium Series, R. Williams & M. Livio, editors (Cambridge University Press)
- Ferland, G.J., & Elitzur, M., 1984, ApJ 285, L11
- Ferland, G.J., Fabian, A. C., & Johnstone, R.M., 1994, MNRAS 266, 399
- Ferland, G.J. Korista, K.T. and Peterson, B.M., 1990, ApJ 363, L21
- Ferland, G.J., Korista, K.T., Verner, D. A., and Dalgarno, A., 1997, ApJ 481, L115
- Ferland, G.J., Lambert, D.L., Netzer, H., Hall, D. N. B., & Ridgway, S.T., 1979a, ApJ 227, 489
- Ferland, G.J., Lambert, D.L., Slovak, M., Shields, G. A., & McCall, M., 1982, ApJ 260, 794
- Ferland, G.J., & Mushotzky, R.F., 1982, ApJ 262, 564
- Ferland, G.J., & Mushotzky, R.F., 1984, ApJ 286, 42
- Ferland, G.J., & Netzer, H., 1979, ApJ 229, 274
- Ferland, G.J., & Netzer, H., 1983, ApJ 264, 105
- Ferland, G.J., Netzer, H., & Shields, G. A., 1979, ApJ 232, 382
- Ferland, G.J., Peterson, B.M., Horne, K., Welsh, W.F., & Nahar, S.N., 1992, ApJ 387, 95
- Ferland, G.J. & Persson, S. E., 1989, ApJ 347, 656
- Ferland, G.J. & Rees, M.J., 1988, ApJ 332, 141
- Ferland, G.J., & Shields, G. A., 1978, ApJ 226, 172
- Ferland, G.J., & Shields, G. A., 1985, in *Astrophysics of Active Galaxies & Quasi-stellar Objects*, J.S. Miller, Ed.
- Ferland, G.J., & Truran, J.W., 1981, ApJ 244, 1022
- Ferland, G.J., Williams, R. E., Lambert, D. L., Shields, G. A., Slovak, M., Gondhalekar, P.M., & Truran, J.W., 1984, ApJ 281, 194
- Field, G. B., 1965, ApJ 142, 431
- Francis, P.J. 1993, ApJ 407, 519
- Gaetz, T.J., & Salpeter, E. E., 1983, ApJS 52, 155
- Garstang, R.H., 1958, MNRAS, 118, 57
- Gavril, M., 1967, Phys Rev 163, 147, also JILA Report #86, Sept 19, 1966
- Ginzburg, V. I., & Syrovatskii, S.I., 1964, *The Origin of Cosmic Rays*, (Oxford: Pergamon)
- Gould, R. S., 1978, ApJ 219, 250
- Gredel, R., Lepp, S., & Dalgarno, A., 1987, ApJ 323, L137
- Gredel, R., Lepp, S., Dalgarno, A., & Herbst, E., 1989, ApJ 347, 289
- Greenhouse, M., et al. 1993, ApJS 88, 23
- Grevesse, N., & Anders, E., 1989, *Cosmic Abundances of Matter*, AIP Conference Proceedings 183, p. 1, Ed. C. J. Waddington, (New York: AIP)
- Grevesse, N. & Noels, A. 1993 in *Origin & Evolution of the Elements*, ed. N. Prantzos, E. Vangioni-Flam, & M. Casse (Cambridge Univ. Press, p. 15)
- Guhathakurta, P., and Draine, B.T., 1989, ApJ 345, 230
- Guilbert, P.W., 1986, MNRAS 218, 171
- Guilbert, P., & Rees, M.J., 1988, MNRAS 233, 475
- Habing, H.J., 1968, Bull. Astr. Inst. Netherlands 19, 421
- Halpern, J. P., & Grindlay, J.E., 1980, ApJ 242, 1041
- Hamann, F., & Ferland, G., 1992, ApJ 391, L53
- Hamann, F., & Ferland, G.J., 1993, ApJ 418, 11
- Harrington, J. P., 1969, Ap J 156, 903
- Harrington, J. P., 1973, MNRAS 162, 43
- Heitler, W., 1954, *The Quantum Theory of Radiation* (Oxford: Oxford University Press)
- Hjellming, R.M., 1966, ApJ 143, 420
- Hollenbach, D., & McKee, C.F., 1979, ApJS 41, 555
- Hollenbach, D., & McKee, C.F., 1989, ApJ 342, 306
- Hubbard, E.N., & Puetter, R.C., 1985, ApJ 290, 394
- Hummer, D.G., 1962, MNRAS 125, 21
- Hummer, D.G., 1968, MNRAS 138, 73
- Hummer, D.G., 1988, ApJ 327, 477

- Hummer, D. G., Berrington, K. A., Eissner, W., Pradhan, A. K., Saraph H. E., Tully, J. A., 1993, A&A, 279, 298
- Hummer, D.G., & Kunasz, 1980, ApJ 236, 609
- Hummer, D.G., & Seaton, M.J., 1963, MNRAS 125, 437
- Hummer, D.G., & Storey, P., 1987, MNRAS 224, 801
- Hutchings, J.B., 1976, ApJ 205, 103
- Ikeuchi, S., & Ostriker, J.P., 1986, ApJ 301, 522
- Jackson, J. D., 1975, *Classical Electrodynamics* (New York: Wiley)
- Janev, R.K., Langer, W. D., Post, D. E., & Evans, K., 1987, *Elementary Processes in Hydrogen–Helium Plasmas* (Springer--Verlag; Berlin)
- Jenkins, E.B., 1987, in *Interstellar Processes*, D. Hollenbach & H. Thronson, Eds, (Dordrecht: Reidel), p.533
- Johnson, L.C., 1972, ApJ 174, 227
- Johnstone, R.M., Fabian, A. C., Edge, A. C., & Thomas, P.A., 1992, MNRAS 255, 431
- Kallman, T.R., & McCray, R., 1982, ApJS 50, 263
- Karzas, W.J., & Latter, R., 1961, ApJS 6, 167
- Kaastra, J.S., & Mewe, R., 1993, A&AS 97, 443
- Kato, T., 1976, ApJS 30, 397
- Kellerman, K.I., 1966, ApJ 146, 621
- Khromov, G.S., 1989, Space Science Reviews 51, 339
- Kingdon, J.B., & Ferland, G.J., 1991, PASP 103, 752
- Kingdon, J.B., & Ferland, G. J., 1993, ApJ, 403, 211
- Kingdon, J.B., Ferland, G. J., & Feibelman, W.A., 1995, ApJ, 439, 793
- Kingdon, J.B., & Ferland, G.J., 1995, ApJ 450, 691
- Kingdon, J.B., & Ferland, G.J., 1996, ApJS 106, 205
- Korista, K.T., & Ferland, G.J., 1989, ApJ 343, 678
- Korista, K.T., Baldwin, J., and Ferland, G.J., 1997, ApJ in press
- Krolik, J., McKee, C.M., & Tarter, C.B., 1981, ApJ 249, 422
- Kurucz, R.L., 1970, SAO Special Reports 309
- Kurucz, R.L., 1979, ApJS 40, 1
- Kurucz, R.L., 1991, in *Proceedings of the Workshop on Precision Photometry: Astrophysics of the Galaxy*, A.C. Davis Philip, A.R. Upgren, & K.A. James (Davis, Schenectady), p 27
- Kwan, J., & Krolik, J., 1981, ApJ 250, 478
- Lambert, D.L., & Pagel, B.E.J., 1968, MNRAS 141, 299
- La Franca, Franceshini, A., Cristiani, S., & Vio, R., 1995, A&A 299, 19
- Lame N.J., and Ferland, G.J., 1991 ApJ 367, 208
- Landini, M., & Monsignori Fossi, B., 1990, A&AS 82, 229
- Landini, M., & Monsignori Fossi, B., 1991, A&AS 91, 183
- Lanzafame, A. ., Tully, J. A., Berrington, K. A., Dufton, P. L., Byrne, P. B., & Burgess, A., 1993, MNRAS 264, 402
- Laor, A., & Draine, B.T., 1993, ApJ 402, 441
- Latter, W.B., & Black, J.H., 1991, ApJ 372, 161
- Lea, S., & Holman, G., 1978, ApJ 222, 29
- Lennon, D. J., & Burke, V.M., 1991, MNRAS 251, 628
- Lenzuni, P., Chernoff, D.F., & Salpeter, E.E., 1991, ApJS 76, 759
- Levich, E.V., & Sunyaev, R.A., 1970, Astrophys Let 7, 69
- Lepp, S., & Shull, J.M., 1983, ApJ 270, 578
- Lightman, A. P., & White, T.R., 1988, ApJ 335, 57
- Lites, B.W., & Mihalas, D., 1984, Solar Physics 93, 23
- Liu, X.-W., Storey, P.J., Barlow, M.J., & Clegg, R.E.S., 1995, MNRAS, 272, 369
- Longair, M. S., 1981, *High Energy Astrophysics*, (Cambridge, Cambridge University Press)
- Lotz, W., 1967, ApJS 14, 207
- MacAlpine, G. M., 1971, ApJ 175, 11
- Maguire, S., 1993, *Writing Solid Code*, Microsoft Press
- Mallik, D.C.V., & Peimbert, M., 1988, Rev Mexicana 16, 111
- Martin, P.G., 1979, *Cosmic Dust* (Oxford, Clarendon Press)
- Martin, P.G., 1988, ApJS 66, 125

- Martin, P.G., & Ferland, G.J., 1980, ApJ 235, L125
Martin, P.G., & Whittet, D.C.B., 1990, ApJ 357, 113
Masters, A. R., Pringle, J. E., Fabian, A. C., & Rees, M. J., 1977, MNRAS 178, 501
Mathews, W.G., Blumenthal, G. R., & Grandi, S.A., 1980, ApJ 235, 971
Mathews, W.G., & Ferland, G.J., 1987, ApJ 323, 456
Mathis, J. S., 1982, ApJ 261, 195
Mathis, J. S., 1985, ApJ 291, 247
Mathis, J. S. Rimpl, W., & Nordsieck, K.H., 1977, ApJ 217, 425
Mathis, J. S., & Wallenhorst, S.G., 1981 ApJ 244, 483
Matteucci, F., & Tornambe, A., 1987, A&A 185, 51
Matteucci, F., & Greggio, A., 1986, A&A 154, 279
Mendoza, C., 1983, in *Planetary Nebulae*, IAU Sym 103, D. R. Flower, Ed., p 143, (Dordrecht: Reidel)
Mihalas, D., 1972, *Non-LTE Model Atmospheres for B & O Stars*, NCAR-TN/STR-76
Mihalas, D., 1978, *Stellar Atmospheres*, 2nd Edition (W.H. Freeman: San Francisco)
Mihalszki, J. S., & Ferland, G. J., 1983, PASP 95, 284
Morrison, R., & McCammon, D., 1983, ApJ 270, 119
Morton, D. C., York, D. G., & Jenkins, E.B., 1988, ApJS 68, 449
Nahar, S.N., & Pradhan, A. K., 1992, ApJ 397, 729
Netzer, H., 1990, in *Active Galactic Nuclei, Saas-Fee Advanced Course 20*, Courvorsier, T.J.-L., & Mayor, M., (Springer-Verlag; Berlin)
Netzer, H., Elitzur, M., & Ferland, G.J., 1985, ApJ 299, 752
Netzer, H., & Ferland, G.J., 1984, PASP 96, 593
Neufeld, D. A., 1989, Harvard Research Exam
Neufeld, D. A., & Dalgarno, A., 1989, Phys Rev A, 35, 3142
Nussbaumer, H., & Storey, P.J. 1983, A&A 126, 75
Nussbaumer, H., & Storey, P.J. 1984, A&AS 56, 293
Nussbaumer, H., & Storey, P.J. 1986, A&AS 64, 545
Nussbaumer, H., & Storey, P.J. 1987, A&AS 69, 123
Oliveira, S., & Maciel, W.J., 1986, Ap&SS 126, 211
Oliva, E., Pasquali, A., and Reconditi, M., 1996, A&A 305, 210
Osterbrock, D. E., 1951, ApJ 114, 469
Osterbrock, D. E., 1989, *Astrophysics of Gaseous Nebulae & Active Galactic Nuclei*, University Science Press
Osterbrock, D. E., & Flather, E., 1959, ApJ 129, 26
Osterbrock, D. E., Tran, H.D., & Veilleux, S., 1992, ApJ 389, 305
Ostriker, J. P., & Ikeuchi, S., 1983, ApJ 268, L63
Pacholczyk, A.G., 1970, *Radio Astrophysics* (San Francisco: Freeman)
Palla, F., Salpeter, E. E., & Stahler, S. W., 1983, ApJ 271, 632
Peebles, P.J.E., 1971, *Physical Cosmology*, (Princeton U. Press; Princeton)
Peimbert, M., ApJ 150, 825
Pengelly, R.M., 1964, MNRAS 127, 145
Pequignot, D., 1986, *Wordshop on Model Nebulae*, (Paris: l'Observatoire de Paris) p363
Pequignot, D., & Aldrovandi, S.M.V., 1986, A&A 161, 169
Pequignot, D., Petitjean, P., and Boisson, C., 1991, A&A 251, 680
Peterson, J.R., Aberth, W., Moseley, J., & Sheridan, J., 1971, Phys Rev A, 3, 1651
Press W.H., Teukolsky, S.A., Vetterling, W.T., & Flannery, B.P., 1992, *Numerical Recipes*, (Cambridge University Press; Cambridge)
Puetter, R.C., 1981, ApJ 251, 446
Puy, D., Alecian, G., Le Bourlot, J., Leorat, J., Pineau des Forets, G., 1993, A&A 267, 337
Raymond, J.C., Cox, D. P., & Smith, B.W., 1976, ApJ 204, 290
Rees, M.J., Netzer, H., & Ferland, G.J., 1989, ApJ 347, 640
van Regemorter, H., 1962, ApJ 136, 906
Rauch, T., 1997 A&A 320, 237
Rephaeli, Y., 1987, MNRAS 225, 851
Reilman, R.F., & Manson, S.T., 1979, ApJS 40, 815, errata 46, 115; 62, 939
Roberge, W.G., Jones, D., Lepp, S., & Dalgarno, A., 1991, ApJS 77, 287
Rossi, B., 1952, *High-Energy Particles* (New York; Prentice-Hall)

- Rowan, T., 1990, *Functional Stability Analysis of Numerical Algorithms*, Ph.D. Thesis, Department of Computer Sciences, University of Texas at Austin
- Rubin, R.H., 1968, ApJ 153, 671
- Rubin, R.H., 1983, ApJ 274, 671
- Rubin, R.H., Simpson, J.R., Haas, M.R., & Erickson, E.F., 1991, ApJ 374, 564
- Rybicki, G. B., & Hummer, D. G. 1991, A&A, 245, 171
- Rybicki, G. B., & Hummer, D. G. 1992, A&A, 262, 209
- Rybicki, G. B., & Hummer, D. G. 1994, A&A, 290, 553
- Rybicki, G. B., & Lightman, A.P., 1979, *Radiative Processes in Astrophysics* (Wiley, New York)
- Sanders, D. B., et al. 1989, ApJ 347, 29
- Saraph, H. E., 1970, J.Phys.B. 3, 952
- Savage, B. D., and Sembach, K. R., 1996, ARAA 34, 279
- Sciortino, S., et al., 1990, ApJ 361, 621
- Scott, J.S., Holman, G.D., Ionson, J. A., & Papadopoulos, K., 1980, ApJ 239, 769
- Schuster, A., 1905, ApJ 21, 1
- Schutte, W.A., Tielens, A.G.G.M., and Allamandola, L.J., 1993 ApJ 415, 397
- Schwarzschild, M., 1965, *Structure & Evolution of the Stars*, (New York: Dover)
- Seaton, M.J., 1959, MNRAS 119, 90
- Seaton, M.J., 1987, J.Phys. B 20, 6363
- Sellmaier, F.H., Yamamoto, T., Pauldrach, A.W.A., & Rubin, R.H. 1996, A&A, 305, L37
- Shine, R.A., & Linsky, J.L., 1974, Solar Physics 39, 49
- Shull, J.M., 1979, ApJ 234, 761
- Shull, J.M., & Van Steenberg, M. E., 1982, ApJS 48, 95
- Shull, J.M., & Van Steenberg, M. E., 1985, ApJ 298, 268
- Sellgren, K., Tokunaga, A.T., and Nakada, Y., 1990, ApJ 349, 120
- Sikora, M., Begelman, M.C., & Rudak, B., 1989, ApJ, 341, L33
- Simonyi, C., 1977, *Meta-Programming: A Software Production Method*, Thesis, Stanford University
- Snow, T. P., & Dodger, S. L., 1980, ApJ 237, 708
- Snow, T. P., & York, D. G., 1981, ApJ 247, L39
- Snow, T.P., & Witt, A., 1996, ApJ 468, L65
- Spitzer, L., 1948, ApJ 107, 6
- Spitzer, L., 1962, *Physics of Fully Ionized Gasses*, (Interscience: New York)
- Spitzer, L., 1978, *Physical Processes in the Interstellar Medium*, (Wiley: New York)
- Spitzer, L., 1985, ApJ 290, L21
- Spitzer, L., & Tomasko, M.G., 1968, ApJ 152, 971
- Stecher, T.P., & Williams, D.A., 1967, ApJ 149, 29
- Stoy, R.H., 1933, MNRAS 93, 588
- Storey, P.J., 1994, A&A 282, 999
- Storey, P.J., & Hummer, D. G., 1991, Comput. Phys. Commun. 66, 129
- Storey, P.J., & Hummer, D. G., 1995, MNRAS 272, 41
- Swings, P., & Struve, O., 1940, ApJ 91, 546
- Tarter, C.B., & McKee, C.F., 1973, ApJ 186, L63
- Tielens, A.G.G.M., & Hollenbach, D., 1985a, ApJ 291, 722
- Tielens, A.G.G.M., & Hollenbach, D., 1985b, ApJ 291, 746
- Tout, C.A., Pols, O.R., Eggleton, P.P. and Han, Z., 1996, MNRAS 281, 257
- Turner, J., & Pounds, K., 1989, MNRAS 240, 833
- Van Blerkom, D., & Hummer, D. G., 1967, MNRAS 137, 353
- van Regemorter, H., 1962, ApJ 136, 906
- Vedel, H., Hellsten, U., and Sommer-Larsen, J., 1994, MNRAS 271, 743
- Vernazza, J.E., Avrett, E.H., & Loeser, C.B., 1981, ApJS 45, 635
- Verner, D.A., Yakovlev, D.G., Band, I.M., & Trzhaskovshaya, M.B., 1993, Atomic Data Nuc Data Tables 55, 233
- Verner, D.A., & Yakovlev, 1995, A&AS 109, 125
- Verner, D.A., & Ferland, G.J., 1996, ApJS 103, 467
- Verner, D. A., Ferland, G., Korista, K., & Yakovlev D. G., 1996, ApJ, 465, 487
- Verner, D.A., Verner, K., & Ferland, G.J., 1996, Atomic Data Nuc Data Tables, 64, 1
- Voronov, G.S., 1997, ADNDT 65, 1

13 REFERENCES

- Voit, G. M., 1991, ApJ 377, 1158
Vriens, L., & Smeets, A.H.M., 1980, Phys Rev A 22, 940
Watson, W. D., 1972, ApJ 176, 103
Weisheit, J.C., 1974, ApJ 190, 735
Weisheit, J.C., and Collins, L.A., 1976, ApJ 210, 299
Weisheit, J.C., & Dalgarno, A., 1972, Ap. Letters, 12, 103
Weisheit, J., Shields, G. A., & Tarter, C.B., 1981, ApJ 245, 406
Werner, K., & Heber, U., 1991, in *Stellar Atmospheres: Beyond Classical Models*, p 341, NATO ASI Series C, eds. L. Crivellari, I. Hubney, & D.G. Hummer, (Kluwer; Dordrecht)
White, R. E., 1986, ApJ 307, 777
Wiese, W.L., Smith, M.W., and Glennon, B.M., 1966, NSRDS-NBS 4
Wilkes, B.J., Ferland, G.J., Truran, J., & Hanes, D., 1981, MNRAS 197, 1
Wilkes, et al 1994, ApJS 92, 53
Wilkinson, D.T., 1987, in *13th Texas Symposium on Relativistic Astrophysics*, M.P. Ulmer, ed., (World Scientific; Singapore), p209
Williams, R.E., 1967, ApJ 147, 556
Williams, R.E., 1992, ApJ 392, 99
Wills, B., Netzer, H., & Wills D., 1985, ApJ 288, 94
Winslow, A.M., 1975, Lawrence Livermore Lab. report UCID-16854
Wishart, A.W., 1979, MNRAS 187, 59p
Wolfire, M. G., Tielens, A., & Hollenbach, D., 1990, ApJ 358, 116
Worral et al 1987, ApJ 313, 596
Wyse, A. B., 1941, PASP 53, 184
York, D. G., Meneguzzi, M., & Snow, T. 1982, ApJ 255, 524
Xu, Y., & McCray, R., 1991, ApJ 375, 190
Zamorani, G., et al. 1981, ApJ 245, 357
Zycki, P.T., Krolik, J.H., Zdziarski, A.A., and Kallman, T.R., 1994, 437, 597
Zygelman, B., & Dalgarno, A., 1990, ApJ 365, 239

14. INDEX

- A –
- absolute magnitude, 26
 absolute magnitude command, 26
 abundances
 absolute defined, 50
 changing input order, 55
 command, 51
 default, 50
 depletion, 57
 fluctuations, 56
 ionic, 262
 overview, 50
 printed, 601
 reading from table, 56
 scale defined, 50
 set, 51
 starburst, 54
 variables used, 423
 abundances command, 51
 abundances starburst command, 54
 acceleration. *see* radiative acceleration
 adding lines, 229
 adding models together, 411, 412
 adiabatic cooling. *see* expansion cooling
 age
 checking, 65
 printing, 98
 age command, 11, 65
 agn command, 32
 albedo
 punch
 cloud, 107
 gas, 112
 Alfvén velocity, 86
 alpha code, 402
 alpha ox
 printed, 602
 setting, 31
 aluminum, 267
 apparent helium abundance, 616
 arbitrary density law, 60
 assign statement in VMS, 43
 Atlas 1991 atmospheres, 45
 atlas.in
 input script, 457
 atomic data references, 418
 atomic mass, 214
 atomic weight, 214, 262
 Auger effect, 258, 263
 averaging over terms, 224
- B –
- background
 cosmic, 34, 36, 37
 cosmic ray, 84, 298
 background command, 34
 bangot, 410
 Be-sequence cooling, 284
 beta code, 402
 Bethe-Block approximation, 298
 blackbody
 definition, 206
 evaluated, 206
 blackbody command, 35
 vary, 124
 blister.in
 input script, 458
 predictions, 444
 blr.in
 input script, 459
 Bohr radius, 222, 308
 Boltzmann factor
 continuum, 204
 line, 213
 Born approximation, 222
 bound-free
 opacity, 212
 Bowen OI, 266
 brems.in
 input script, 459
 bremsstrahlung
 continuum, 36
 cooling, 277
 heating, 277
 opacity, 212
 bremsstrahlung command, 36
 brightness temperature, 604
 broken code, 419
- C –
- calcium, 267
 Cameron abundances, 52
 carbon, 263
 carbon fully molecular,
 stopped because of, 609
 casea.in
 input script, 460
 casebn2.in
 input script, 461
 casebn8.in
 input script, 461
 casec.in
 input script, 462
 caunot, 410
 cautions
 checks, 4
 printed, 611
 routine to print, 410
 cdColm, 408
 cdDriv, 407
 cdEms, 408
 cdGett, 412
 cdInit, 406
 cdIonf, 408
 cdLine, 407
 cdNoex, 407
 cdNwcns, 409
 cdOutp, 406
 cdRead, 406
 cdTalk, 407
 cextra command, 82
 changes to code, 418
 charge transfer
 heavy element, 135, 260
 punching rates, 114
 statistical, 135
 turning off, 133
 chemical composition
 printed, 601
 set, 51
 Cloudy
 84 vs 80, 436
 90 vs 84, 434
 adding lines, 229
 changes to code, 418
 date, 419
 flowchart, 414
 future improvements, 437
 history, 431
 known modes, 437
 mailing list, 401
 making a revision, 437
 revision history, 431
 running 1 model, 402
 running a grid, 405
 search phase, 423
 setting up, 1
 size, 431
 source versions, 402
 version numbers, 419
 cloudy.ini file, 21, 132
 co-adding many models, 411, 412
 coding conventions, 416
 broken code, 419
 changes to code, 418
 characters, 418
 integers, 417
 logical variables, 418
 real numbers, 417
 routine descriptions, 419
 sanity checks, 418
 strong typing, 417
 test code, 419
 collion.for
 input script, 464
 collision rate, 222
 detailed balance, 236
 ionization, 259
 collision strengths
 averaging, 224
 defined, 221
 g-bar, 222
 column density, 420
 effective
 defined, 90
 printout, 616
 ionized, 90
 neutral, 90
 total, 90
 printed, 605
 command
 comments, 20
 continue option, 20
 example, 21
 format, 18
 line length, 19
 numerical input, 20
 reading in, 414
 temperature conventions, 21
 comments
 input stream, 20
 comparison calculations, 440
 comphi.in
 input script, 465
 compiling command, 128
 compiling stellar
 atmospheres, 128
 complo.in
 input script, 465
 composition. *see* abundance
 Compton
 bound heating, 277
 bound ionization, 238, 277
 cooling
 calculated, 274
 output, 606
 energy exchange
 accuracy, 275
 methods, 274
 turning off, 133
 heating
 calculated, 274
 output, 606
 ionization, 134
 temperature, 275
 output, 603
 timescale
 output, 617
 compton.in
 test input, 466
 computer
 Cray, 401
 Exemplar, 136
 Sparcstation, 401
 conserv.in
 input script, 466
 constant density command, 59
 constant gas pressure
 command, 59
 constant pressure command,
 59
 constant temperature
 command, 82
 continue command, 20
 continuous heavy element
 opacity, 269
 continuum
 agn, 32
 arrays, 203
 binning, 202, 260
 changing, 129
 Boltzmann factor, 204
 cell width, 204
 changing resolution, 203
 described, 202
 diffuse, 6, 204
 printed, 98
 punched, 105
 diffuse printed, 621
 emission, 240
 energy bounds, 202

- energy pointer, 203
 fluorescence, 218
 frequencies saved, 203
 frequency array, 203
 generation, 205
 high energy limit, 136, 202
 incident
 defined, 6
 punched, 106
 incident printed, 621
 intensity
 specifying, 25
 ionization edge pointers, 203
 low energy limit, 202
 luminosity
 specifying, 25
 mesh defined, 202
 normalization, 206
 occupation number, 204, 232, 239, 603
 opacity, 209
 optical depth, 205
 OTS, 204, 208
 outward, 204
 outward only, 209
 outward punched, 107
 PDR, 27
 photon flux, 204
 plasma frequency, 212
 pointers, 203
 printing, 98
 range, 33, 202
 reflected, 204
 defined, 7
 printed, 98
 resolution, 129
 shape commands, 33
 specify, 2
 summed, 205
 surface brightness, 623
 transmitted
 defined, 6
 convergence
 tracing, 117
 conversion factors, 207
 coolcurve.for, 427
 input script, 467
 coolhii.in
 input script, 470
 predictions, 441
 cooling
 adiabatic, 277
 balance, 84, 87
 Be-sequence atoms, 284
 bremsstrahlung, 277
 collisional, 279
 Compton, 116, 133, 134, 274, 277, 606
 cyclotron, 85
 definition, 273
 derivative, 285
 error, 616
 evaluation, 285
 expansion, 277
 extra, 82
 free-free, 277, 278
 grain, 73, 293, 294, 606
 H-, 279
 heavy elements, 280
 history, 115
 hydrodynamic, 277
 hydrogen lines, 279
 hydrogen recombination, 233
 induced, 278
 low energy continuum, 33, 34, 39
 map, 84, 86, 97
 n level atoms, 282
 numerical derivatives, 138
 plot, 97
 printout, 98, 615
 punch, 108
 recombination, 233, 278
 tests, 286
 three level atoms, 281
 two level atoms, 281
 cooling flow continuum, 41
 corners4.for
 input script, 469
 coronal equilibrium
 command, 83
 coronal.in
 input script, 468
 cosmic ray, 82, 83, 86
 background, 84, 298
 command, 83
 physics, 297
 range, 297
 cosmic ray command, 83, 298
 cosmology
 distance, 307
 covering factor
 command, 65
 computational details, 424
 defined, 8
 geometric, 424
 radiative transfer, 425
 sphere option, 68
 covering factor command, 65
 Cray, 401
 critical density, 223
 cyclotron cooling, 85
 cylinder command, 66
- D—
- damping constant
 defined, 217
 stored, 217, 226
 density
 arbitrary law, 60
 commands, 59
 constant, 59
 constant gas pressure, 59
 constant total pressure, 59
 cosmic ray, 83, 297
 electron
 evaluated, 421
 limiting, 91
 output, 604
 energy, 35
 fluctuations, 61
 globule law, 62
 H-, 246
 LTE, 245
 H2
 LTE, 245
 hydrogen, 28, 59
 LTE, 231
 molecules, 245
 output, 604
 mass, 421
 molecules, 245
 particle, 421
 power-law, 63, 64
 range, 13
 structure
 output, 613
 structure saved, 422
 table entered, 61
 total particle, 303
 wind law, 304
 density per particle, 421
 departure coefficients
 hydrogen, 231
 printing, 98
 depletion factors, 57
 depth
 defined, 7
 derivative
 cooling, 285
 heating, 286
 numerical heating, cooling, 138
 destruction probability, 217
 hydrogen, 232
 line
 complete, 218
 dielectronic recombination
 3rd and 4th row elements, 130
 Burgess, 130
 Nussbaumer and Storey, 130
 dielectronic recombination
 command, 130
 diffuse fields
 defined, 6
 evaluated, 204
 punching source function, 115
 test case, 474
 transfer, 71
 diffuse fields command, 71
 diffuse OTS command, 71, 208
 diffuse outward command, 71, 209
 dilution factor, 36
 dissociation energy
 H-, 245
 H2, 245
 H2+, 245
 distance
 from redshift, 307
 dlaw command, 60
 Doppler width
 computed, 214
 double optical depths
 command, 71
 dqher.in
 input script, 470
 predictions, 453
 drive command, 131
 drive escape probabilities, 131
 drive fread, 131
 drive gaunt factor command, 131
 drive hyas command, 131
 drive molecules command, 131
 drive pointers command, 131
 drive starburst command, 132
 drive.for
 input script, 471
 dumping
 line, 228
 dust. see grain
 dyn, 302
- E—
- eden command, 132
 eden.in
 input script, 472
 Einstein coefficients, 215
 electron
 adding extra, 132
 density
 evaluated, 421
 saved, 421
 mean speed, 85
 non-thermal secondaries, 305
 secondary ionization, 305
 supra-thermal, 305
 temperature. see temperature
 element
 abundances stored, 262
 chemical symbols, 262
 ionization stage symbols, 262
 names, 263
 periodic table, 258
 element table command, 56
 elements command, 54
 vary, 124
 elements read command, 55
 emission line list, 626
 emission measure, 616
 end of input stream, 19
 end of line characters, 19
 energy density
 gas, 302
 energy density command, 72
 equivalent width
 computing, 621
 escape probability
 heavy element, 225
 helium, 256
 hydrogen, 232
 line, 216
 complete, 217
 incomplete, 217
 maser, 218
 routines, 216
 escape probability command, 71
 excitation energy, 213
 excitation temperature, 228
 Exemplar, 136
 expansion cooling, 277
 extinguish command, 36
- F—
- f(nu) command, 27
 fabden, 60
 Fe II atom
 command, 72
 punching intensities, 112
 Fe II command, 72

- filling factor, 66, 69, 304, 606, 616
 defined, 8, 67
 filling factor command, 66
 vary, 124
 fine structure lines, 225
 fireball command, 37
 floating point errors, 401, 429
 flowcharts, 414
 Cloudy, 414
 ionte, 415
 MainCl, 414
 Plonte, 414
 TauInc, 415
 fluc.in
 input script, 472
 fluctuations command, 56, 61
 fluorescence
 continuum, 218
 yields, 263
 flux
 converting to luminosity, 623
 force temperature command, 84
 free-free
 cooling, 277
 H-, 279
 emission, 240
 gaunt factor, 114, 212
 heating, 277
 H-, 279
 opacity, 212
 free-free cooling
 plasma frequency, 278
 fudge factors command, 132
- G —
- gas
 albedo
 punched, 107, 112
 energy density, 302
 equation of state, 302
 heat content, 302
 mass density, 421
 opacity
 punching, 111
 particle density, 421
 pressure, 59, 303
 gaunt factor
 drive command, 131
 free-free, 114, 212
 g-bar approximation, 222
 geometry
 closed, 9, 68, 613
 closed expanding, 221
 closed static, 221
 cylindrical, 7
 definition, 7
 details, 419
 disk, 65
 ionized from both sides, 71
 matter-bounded, 9, 89, 91
 open, 3, 8, 68, 76, 80, 221, 613
 plane parallel, 7, 67, 611
 plane parallel vs spherical, 34, 65
 printed, 611
 radiation-bounded, 10, 89
 specify, 2, 3
 spherical, 4, 7, 68, 80, 611
 thick shell, 7, 611
 wind, 7, 69, 221, 617
 globule command, 62
 globule.in
 input script, 473
 glossary
 routines, 692
 symbols, 308
 Go continuum, 28
 gold code, 402
 grain, 289
 absorption efficiency factor, 290
 agb, 74
 area, 290
 collisional charging, 292
 drift velocity, 293
 dust to gas ratio, 74
 exist?, 295
 extra species, 74
 gas cooling, 294
 gas heating, 294
 gray, 74
 heating and cooling, 293
 HII Hegion, 74
 ionic recombination, 134, 295
 ISM, 73
 opacity, 289
 punching, 112
 Orion, 74
 PAH, 74
 photoelectric emission, 290
 planetary nebula, 74
 potential, 292
 quantum heating, 80
 specifying, 72
 temperature, 294
 variables, 295
 grains command, 72
 grey1.opac, 74
 grid0.for
 input script, 474
- H —
- H II region abundances, 52
 Habing radiation field, 27
 Hartree, 207
 Hazy
 printing, 438
 hden command, 62
 vary, 124
 heating
 balance, 84, 87
 bound Compton, 277
 bremsstrahlung, 277
 collisional ionization, 278
 Compton, 116, 133, 134, 274, 277, 603, 606
 continuum, 202
 cosmic ray, 84, 297, 298
 definition, 273
 derivative, 286
 evaluated, 285
 extra, 82, 85, 607
 fine structure lines, 225, 280
 free-free, 134, 277, 278, 616
 grain, 73, 290, 292, 293, 294, 606
 H-, 279
 heating array, 285
 history, 115
 hydrogen lines, 279
 line, 286
 low energy continuum, 33, 39
 map, 84, 86, 97
 neutron, 87
 numerical derivatives, 138
 photoelectric, 278, 613
 plot, 97
 print, 99, 116
 printout, 615
 punch, 108
 quantum grain, 80
 secondaries, 135
 structure saved, 421
 tests, 286
 total, 605, 616
 evaluated, 286
 heavy element
 abundances stored, 262
 adding lines, 229
 atomic weights, 262
 Auger ejection, 258, 263
 charge transfer, 260
 chemical symbols, 262
 collisional ionization, 259
 depletion, 57
 FeII atom, 72
 fluorescence yields, 263
 ionization pointers, 260, 263
 ionization potentials, 260
 ionization stored, 262
 labels for lines, 228
 limits, 16
 line pointers, 226
 line transfer, 225
 molecules, 253
 names, 263
 number of subshells, 261
 opacity offsets, 260
 overview, 257
 photoionization cross section, 258
 photoionization rates
 stored, 263
 punching opacity, 112
 punching pointers, 113
 recombination
 dielectronic, 259
 grain surface, 295
 radiative, 259
 reliability, 271
 shell number, 263
 TauLines subdirectory, 229
 helium
 continuum pointers, 256
 escape probability, 256
 ion, 255
 line pointer, 256
 printout
 ionization, 606
 lines, 614
 punching, 108
 radiative transfer, 256
 recombination coefficients, 256
 recombination efficiency
 punching, 114
 singlets, 255
 statistical weight, 240
 triplets, 255
 helium collisions command, 76
 hemis.in
 input script, 474
 hextra command, 85
 high temperature approach
 command, 85
 highn.in
 input script, 475
 HII region abundances, 52
 hiiregions.for
 input script, 476
 hizlte.for
 input script, 477
 hizqso.in
 input script, 478
 Hungarian naming
 convention, 416
 hydrodynamic cooling, 277
 hydrogen
 2s 2p collisions turned off, 133
 balance equations, 236
 Boltzmann factors, 231
 collisional ionization, 236
 collisional rate equations, 236
 collisions turned off, 77
 column density, 90
 continuum pointer, 232
 density, 28, 59, 62
 LTE, 231
 saved, 421
 departure coefficient, 231
 destruction probability, 232
 emission, 240
 escape probability, 232
 H-, 246
 H2, 250
 HeH+, 250
 induced recombination, 237
 ionization energies, 231
 ionization processes, 108
 ionization solution, 236
 level energies, 231
 level populations punched, 108
 levels command, 77
 line intensities, 623
 line pointer, 232
 lowest temp command, 77
 matrix inversion routines, 77
 molecules, 245
 negative ion, 246
 number of levels, 77
 oscillator strengths, 232
 overview, 14
 populations punched, 108
 radiative rate equations, 237
 recombination coefficients, 233, 238
 elements defined, 236

- recombination cooling, 233
 - recombination efficiency
 - punching, 114
 - statistical weight, 231, 240
 - three body recombination, 236
 - top off, 78
 - transition probabilities, 232
 - driving, 131
 - turning off 2s 2p collisions, 133
 - turning off collisions, 77
 - hydrogen command, 76
- I—
- illuminate command, 67
 - illuminated face, 7
 - induc.in
 - input script, 478
 - induced emission probability, 215
 - induced recombination, 237
 - infinite loop. see unending loop
 - init command, 21, 132
 - initialization command, 21, 132
 - initialization file, 21, 132
 - inner radius, 8
 - input line. see command
 - intensity command, 25, 27
 - vary, 124
 - interpolate command, 38
 - interstellar radiation field, 41
 - ionic abundances, 262
 - ionization parameter
 - command, 28
 - ionization potential
 - density, 260
 - elements, 260
 - pointers, 260
 - ionte
 - flowchart, 415
 - iron, 268
 - Fe II atom, 72
 - ISM abundances, 52
 - ism.in
 - input script, 479
 - isobaric, 59
 - isochoric, 59
 - isoelectronic sequence, 263
 - iterate command, 78
 - iteration
 - last, 423
 - variables, 422
- J—
- Jeans length, 307, 617
 - Jeans mass, 307, 617
- K—
- kk.in
 - input script, 480
 - predictions, 454
 - kmt.for, 427
 - kmt.in
 - input script, 481
 - K-shell energy limit, 137
 - Kurucz 1991 atmospheres, 45
- L—
- l(nu) command, 28
 - labels for lines, 228
 - lalpha.in
 - input script, 482
 - laser command, 39
 - laser1.in
 - input script, 482
 - laser2.in
 - input script, 483
 - laser3.in
 - input script, 484
 - ldl.in
 - input script, 484
 - level 1 line, 225, 227
 - level 2 line, 225, 227
 - levels
 - averaging, 224
 - line
 - adding to line arrays, 229
 - array
 - printing, 228
 - array punched, 109
 - asymmetries, 622
 - beaming, 622
 - Boltzmann factor, 213
 - closed expanding geometry, 221
 - closed static geometry, 221
 - continuum contrast, 622
 - continuum pumping
 - contribution, 625
 - correction for stimulated emission, 213
 - data punched, 110
 - dumping, 228
 - energy pointer, 203
 - equivalent width, 621
 - escape probability, 216
 - excitation temperature, 228
 - fine structure heating, 225, 280
 - heating, 286
 - hydrogen escape
 - probability, 232
 - infrared defined, 225
 - intensities
 - with grains, 624
 - label
 - generating, 228
 - punching, 110
 - level 1, 225, 227
 - level 2, 225, 227
 - list, 626
 - masing, 280
 - open geometry, 221
 - optical depth, 213
 - optical depth arrays, 221, 229
 - optical depth printing, 101
 - output, 634
 - outward, 204
 - pointer, 203
 - radiation pressure, 298
 - maximum printed, 616
 - printed, 605
 - stop, 608
 - redistribution function, 227
 - reflected, 204
 - source function, 216
 - spectroscopic designation, 228
 - surface brightness, 623
 - thermalization length, 223
 - trace, 116
 - transfer flowchart, 415
 - wavelength convention, 626
 - width, 214
 - wind geometry, 221
 - line cooling. see cooling
 - liner.in
 - input script, 485
 - linpack routines, 77
 - loop. see infinite loop
 - LTE
 - H- density, 245
 - H departure coefficient, 231
 - H level population, 231
 - H2 density, 245
 - lte.in
 - input script, 485
 - ltemetl.in
 - input script, 486
 - luminosity
 - converting to flux, 623
 - distance, 307
 - sun, 308
 - luminosity command, 25, 29
 - vary, 124
- M—
- machine environment, 401
 - magnesium, 266
 - magnetic field
 - cyclotron cooling, 85
 - pressure, 86
 - magnetic field command, 85
 - magnitude
 - absolute, 26
 - visual, 26
 - MainCl
 - flowchart, 414
 - map
 - number of steps, 138
 - output, 428
 - plot map command, 97
 - punch output, 111
 - map command, 86
 - map.in, 426
 - input script, 486
 - Martin, P.G.
 - added lines, 97
 - print sort, 102
 - maser
 - correction for stimulated emission, 213
 - escape probability, 218
 - mass
 - AMU, 308
 - electron, 308
 - Jeans', 308
 - proton, 308
 - sun, 309
 - mass density, 421
 - matchn2.in
 - input script, 487
 - matrix inversion routines, 77
 - matter-bounded geometry, 9
 - mean speed
 - electron, 85
 - metals command, 56
 - vary, 124
 - Milne relation, 233, 240
 - molecular weight, 421
 - molecules, 16, 243
 - drive command, 131
 - heavy element, 253
 - hydrogen, 245
 - printed, 607
 - Moore's Law, 431
- N—
- naming convention, 416
 - negative line intensities, 615
 - negative mole abundance,
 - stopped because of, 609
 - neon, 266
 - neutron
 - heating, 87
 - neutrons command, 87
 - ngc5548.in
 - input script, 487
 - nitrogen, 265
 - nlr.in
 - input script, 487
 - predictions, 451
 - no 2p2s command, 133
 - no Auger effect command, 133
 - no charge transfer command, 133
 - no Compton effect command, 133
 - no feii pumping command, 133
 - no fine structure command, 133
 - no free free heating command, 134
 - no grain neutralization
 - command, 134
 - no induced processes
 - command, 134
 - no molecules command, 134
 - no on the spot command, 134
 - no photoionization command, 134
 - no radiation pressure
 - command, 134
 - no recoil ionization command, 134
 - no scattering opacity
 - command, 80
 - no secondary ionization
 - command, 135
 - no Stark broadening
 - command, 135
 - no three body recombination
 - command, 135
 - no vary command, 119, 135
 - normalize command, 4, 95
 - noteot, 410
 - notes
 - checks, 4
 - printed, 611
 - routine to print, 410
 - nova.in
 - input script, 488
 - nuf(nu) command, 29
 - nul(nu) command, 30

- numerical input. see
command
- O—
- observed quantities, 621
occupation number
array, 204
continuum, 220, 239, 603
defined, 204
hydrogen, 232
pumping rate, 216
summed continuum, 205
OI fluorescence, 266
oldblr.in
input script, 488
opacity, 209
absorption array, 205
arrays, 209
background line, 217
bound-free, 212
free-free, 212
heavy element continuous,
269
permitted line, 215
pointers, 209
punching, 111
punching negative, 137
Rayleigh scattering, 211
scattering array, 205
stimulated emission, 213
optical depth
arrays, 221
closed geometry, 221
commands, 70
continuum, 205, 212
convergence, 78
correction for stimulated
emission, 213
double, 71
filling factor, 67
grain, 290
helium, 256
hydrogen, 232
incremented, 205
line, 213
line center, 213
line center vs mean, 214
mean vs line center, 214
open geometry, 221
output, 618
outward
first estimate, 215
later updates, 215
test for definition, 215
printing, 101
sphere, 68
stimulated emission, 213
stopped because of, 609
stopping, 90, 92
updated, 205, 422
wind, 69, 221
optical to X-ray ratio, 31, 602
optim.in
input script, 489
optimize
amoeba method, 120
column density, 120
convergence criteria, 123
example, 119
increment, 120
intensity, 121
iterations, 121
lines, 121
luminosity, 121
no vary command, 119
Powell method, 122
Press et al codes, 119
punch, 122
range of variation, 122
subplex method, 123
tolerance, 123
trace flow, 123
trace starting at xx, 123
variables, 127
optimize column density
command, 120
optimize increment command,
120
optimize intensity command,
121
optimize iterations command,
121
optimize lines command, 121
optimize luminosity
command, 121
optimize Powell, 122
optimize punch command,
122
optimize range command, 122
optimize subplex command,
123
optimize tolerance command,
123
optimize trace flow, 123
optimize trace start command,
123
optimizing the spectrum, 118
Orion abundances, 52
orion.in
input script, 489, 490
orionpdr.in
input script, 491
oscillator strength, 213
absorption, 214
emission, 214
OTS fields
described, 208
punching, 112
output
apparent helium
abundance, 616
cautions, 611
comments, 611
continuum, 620
emission lines, 612
header, 601
line, 634
map, 428
notes, 611
Peimbert, 617
redirection, 406
surprises, 611
warnings, 611
wavelength convention, 626
zone, 604
outward-only approximation,
209
oxygen, 265
- P—
- PAH grains, 74
Paris
H II region, 442, 492
NLR, 493
planetary nebula, 493
parishii.in
input script, 492
predictions, 442
parisnlr.in
input script, 493
predictions, 449
parispr.in
input script, 493
predictions, 446
parsec, 309
particle density, 303, 421
path
setting, 138
PDR continuum, 27
pdr.in
input script, 494
Peimbert temperature
fluctuations, 617
periodic table, 258
phfit command, 138
phi(h) command, 30
vary, 124
photoerosion, 617
photoionization
cross sections, 258
subshell, 112
version, 138
fluorescence yields, 263
rates evaluated, 210
rates punched, 109
rates stored, 263
turning off, 134
physical conditions
punching, 114
Plonte
flowchart, 414
Planck function. see
blackbody
computed, 115
plane parallel geometry, 7
planetary nebula abundances,
52
plasma frequency, 212
free-free cooling, 278
plot
continuum, 96
map, 97
opacity, 96
printed, 612
publication quality, 95
range options, 96
plot command, 95
plot continuum command, 96
plot map command, 97
plot opacity command, 96
pnotes.in
input script, 494
pointers
generating, 203
H continua, 232
H lines, 232
He continua, 256
He lines, 256
heavy element continua, 260
heavy element lines, 227
power law command, 39
vary, 124
power law continuum, 42
pressure
compared, 86
constant, 59, 134
gas, 59
total, 59
convergence, 303
dynamic, 303
gas, 4, 59, 303, 606, 607
getting from code, 409
instability, 60, 70, 608
integrated continuum, 303
magnetic, 60, 86
printed, 607
punching, 114
radiation, 4, 68, 70, 78, 134,
303, 605, 606, 607, 616
ram, 303
total, 59, 302, 607
printed, 607
turbulent, 60, 81, 303
units, 302
variables and routines, 303
primal.in
input script, 495
print ages command, 98
print all command, 97
print arrays command, 98
print continuum command, 98
print coolants command, 98
print departure coefficients
command, 98
print errors command, 99
print every command, 99
print faint command, 99
print heating command, 99
print last command, 99
print line all command, 100
print line collisions command,
100
print line heat command, 100
print line inward command,
100
print line optical depths
command, 100
print line pump command,
100
print line sum command, 101
print off command, 101
print on command, 101
print only command, 101
print optical depths
command, 101
print quiet command, 102
print short command, 102
print sort command, 102
print starting at command,
102
proper distance, 307
punch
dr, 114
_raw continuum, 107
abundances, 104
charge transfer, 114
continuum, 104
continuum bins, 105

- convergence, 107
 - cooling, 108
 - diffuse continuum, 105
 - emitted continuum, 106
 - file name, 103
 - gammas, 109
 - heating, 108
 - helium, 108
 - hydrogen conditions, 108
 - hydrogen ionization, 108
 - hydrogen populations, 108
 - incident continuum, 106
 - initial unit, 137
 - interactive continuum, 106
 - ionization structure, 108
 - ionizing continuum, 106
 - ip, 109
 - line
 - contrast, 622
 - lines
 - array, 109
 - contrast, 104, 138
 - cumulative, 109
 - data, 110
 - intensity, 110
 - labels, 110
 - structure, 110
 - map, 111
 - opacity, 111
 - OTS, 112
 - outward continuum, 107
 - overview, 113
 - PDR, 113
 - physical conditions, 114
 - pointers, 113
 - pressure, 114
 - recombination coefficients, 114
 - reflected continuum, 107
 - reserved, 103
 - results
 - command, 113
 - using, 412
 - source function, 115
 - special, 115
 - tegrid, 115
 - TPredictor command, 115
 - transmitted continuum, 107
 - Verner, 112
 - punch command, 102
 - punch output, 102
- Q —
- Q(H) command, 30
 - vary, 124
 - qheat command, 80
 - quiet mode
 - setting, 102, 407
- R —
- radiation pressure, 303
 - line, 298
 - maximum printed, 616
 - printed, 605
 - stop, 608
 - radiation-bounded
 - geometry, 10
 - radiative acceleration
 - computed, 301
 - printed, 607
 - punched, 114
 - wind, 605
 - radius
 - defined, 7
 - inner, 8
 - saved, 422
 - sun, 309
 - radius command, 67
 - vary, 125
 - range option, 25
 - ratio command, 31
 - rauch.in
 - input script, 495
 - Rayleigh scattering, 13, 68, 77, 211, 302, 619
 - reading commands with fillar, 414
 - reageo, 410
 - recombination
 - arrays, 236
 - coefficients, 236
 - helium, 256
 - punching, 114
 - cooling, 233
 - efficiency, 236
 - punching, 114
 - grain surface, 295
 - hydrogenic, 233, 236
 - induced, 237
 - modifying dielectronic, 130
 - radiative rates, 259
 - three body, 135
 - redirecting output, 406
 - redshift
 - distance, 307
 - reflector.in
 - input script, 495
 - plotted, 7, 622
 - reliability, 16
 - revision history, 431
 - rnfa.in
 - input script, 496
 - predictions, 455
 - rnfb.in
 - input script, 497
 - predictions, 456
 - routine
 - abscf, 213
 - AddOpac, 209
 - bangot, 410
 - beseq, 284
 - BiDiag, 272
 - bnfun, 210
 - boltgn, 204, 414
 - broken, 419
 - caunot, 410
 - cdColm, 408
 - cdDriv, 407, 414
 - cdEms, 408
 - cdErrors, 410
 - cdGetPres, 409
 - cdGett, 113, 412
 - cdGetTe, 409
 - cdInit, 406, 414
 - cdIonf, 408
 - cdLine, 407
 - cdNoex, 407
 - cdNwcns, 409
 - cdOutp, 406
 - cdRead, 406
 - cdTalk, 407
 - cfit, 259
 - chIonLbl, 228
 - chLineLbl, 228
 - Cloudy, 414
 - coladd, 281
 - ColStrGBar, 223
 - conorm, 206
 - conpmp, 131
 - ConvIoniz, 415
 - coolr, 82, 277, 285
 - csphot, 209
 - descriptions, 419
 - dgeco, 77
 - dgesl, 77
 - diffem, 204
 - dmpary, 98
 - DoPunch, 102
 - drvary, 414
 - DumpLine, 228
 - eina, 215
 - EinstA, 131, 232
 - eoovrlp, 217
 - esccom, 216
 - escinc, 216
 - escla, 216
 - escmase, 216, 218
 - esum, 421
 - fabden, 60
 - ffun, 205
 - ffun1, 205
 - fill, 129, 202
 - fillar, 414
 - flcsub, 62
 - fosc, 232
 - freeht, 277
 - fudge, 132
 - gamfun, 210
 - gamk, 210
 - GetPunch, 102
 - gffsub, 212
 - GrnVryDpth, 75
 - hcolst, 231
 - HCTIon, 260
 - HCTRecom, 260
 - HeTran, 256
 - highen, 274, 277
 - hjbar, 232
 - hmole, 245, 295
 - hrfc, 235
 - htrans, 232, 238
 - HydroCool, 277
 - HydroPesc, 232
 - ionte, 414, 415
 - ipConSafe, 203
 - ipLinSafe, 203
 - ipoint, 203
 - ipShells, 263
 - level2, 281
 - level3, 281
 - LevelN, 282
 - LimitSh, 261
 - linpack, 77
 - MainCl, 414
 - MakeCharTran, 260
 - MakeRT, 225
 - MakeStatRT, 225
 - MakeWindRT, 225
 - matin1, 77
 - metdif, 204
 - NextDR, 62, 420
 - nockon, 305
 - noteot, 410
 - oilevl, 266
 - opac0, 209
 - p8446, 266
 - phfit, 258
 - Plonte, 303, 414
 - Plankf, 115, 206
 - presur, 303, 304, 414
 - PrintElem, 424
 - PrtGamma, 210
 - PunCool, 108
 - PunHeat, 108
 - PutCS, 230
 - PutLine, 230
 - radinc, 205, 303
 - rdfile, 74
 - reageo, 410
 - rrfit, 259
 - SetCon, 136
 - SetPoint, 202, 263, 274
 - SumContinuum, 205
 - SumCool, 285, 286
 - SumHeat, 286
 - tauff, 278
 - TauInc, 415, 420
 - tauout, 215
 - TestCode, 419
 - TexcLine, 228
 - tfidle, 421, 422
 - TotalPressure, 303, 307, 421
 - update, 79, 205, 215, 422, 429
 - veclib, 77
 - velset, 214
 - warnot, 410
 - wgadd, 411
 - wginit, 411
 - wgline, 411
 - zonsrt, 419, 422

— S —

 - Saha equation
 - arbitrary species, 243
 - ions, 244
 - molecular hydrogen, 245
 - secondary.in
 - input script, 497
 - secondary ionization
 - physics, 305
 - routines, 305
 - setting rate, 135
 - test case, 497
 - turning off, 135
 - variables, 305
 - set command, 135
 - charge transfer, 135
 - colimt, 135
 - csupra, 135
 - didz, 136
 - dr, 136
 - drmax, 136
 - drmin, 136

- DstWght, 136
 EdenError, 136
 Exemplar, 136
 flxfnt, 136
 iPunDef, 137
 kshell, 137
 negopc, 137
 nend, 137
 nmaps, 138
 numerical derivatives, 138
 path, 138
 phfit, 138
 PunchLWidth, 138
 test, 139
 trace, 139
 trim, 139
 tsqden, 139
 WeakHeatCool, 140
 setting the path, 138
 shell number, 263
 shielded face, 7
 size of code, 431
 Sobolev approximation, 304
 solar luminosity, 308
 solar mass, 309
 solar radius, 309
 sound travel time, 616
 source function
 punching continuum, 115
 Sparcstation, 401
 spectral index
 alpha ox, 31
 incident continuum, 31, 602
 transmitted continuum, 617
 speed
 electron, 85
 sphere
 approximations used, 68
 static vs expanding, 9
 sphere command, 3, 68
 spherical geometry, 7
 sphericity ratio, 420
 sqrden.in
 input script, 498
 stability
 thermal, 273, 604
 starburst abundances, 54, 132
 Stark broadening, 219
 statistical weight
 electron, 231
 H-, 245
 H2, 245
 H2+, 245
 helium, 240
 Ho, 245
 hydrogen, 240
 line, 227
 nuclear ignored, 231
 stellar atmospheres
 Atlas91, 45
 compiling, 128
 Kurucz, 44
 Mihalas, 44
 Werner, 48
 stimulated emission
 optical depths corrected for, 213
 stop
 cabon fully molecular, 609
 code returned busted, 609
 column density reached, 610
 criteria discussed, 89
 dr small rel to thick, 609
 drad small, 609
 highest Te reached, 610
 internal error, 610
 line ratio reached, 610
 low electron fraction, 608
 lowest EDEN reached, 608
 lowest Te reached, 610
 negative mole abundan, 609
 nzone reached, 610
 optical depth reached, 609
 outer radius reached, 610
 radiation pressure, 608
 reason, 608
 temperature out of bounds, 610
 wind velocity < 0, 608
 stop column density
 command, 90
 vary, 125
 stop eden command, 91
 stop efrac command, 91
 stop line command, 91
 stop optical depth command, 92
 stop temperature command, 93
 stop thickness command, 93
 vary, 125
 stop zone command, 94
 Stoy ratio, 101
 strom.in
 input script, 498
 strong typing, 417
 structure variables, 421
 style conventions for coding, 416
 subroutine
 use as a, 404
 sun
 luminosity, 308
 mass, 309
 radius, 309
 supra-thermal ionization. *See*
 secondary ionization
 surface brightness
 computing, 623
 surprises
 checks, 4
 printed, 611
 routine to print, 410
 — T —
 t² analysis, 139
table
 agn, 40
 akn 120, 41
 Atlas, 45
 cooling flow, 41
 crab, 41
 density law, 61
 ISM radiation field, 41
 Kurucz, 44
 Mihalas, 44
 power law, 42
 read, 43
 Rubin, 44
 star
 Atlas, 45
 Kurucz, 44
 Mihalas, 44
 Werner, 48
 table command, 40
 table stars command
 vary, 125
 TauInc
 flowchart, 415
 temperature
 blackbody, 35
 brightness, 604
 Compton, 275
 output, 603
 constant electron, 82
 coronal equilibrium, 83
 cosmic ray, 84
 electron
 output, 604
 energy density, 35
 output, 603, 606
 excitation, 228
 failure, 84, 427
 fireball, 34, 37
 fluctuations, 617
 force, 84
 getting from code, 409
 grain, 73, 294
 output, 606
 high approach, 85
 history, 115
 hydrogen low limit, 77
 input format, 21
 jumps, 428
 last, 422
 line excitation, 228
 LTE limit, 286
 Ly α excitation, 606
 map, 86
 map plot, 97
 mean grain
 output, 618
 multi-phase, 428
 predictor punched, 115
 proposed, 422
 range, 13
 saved, 422
 stability, 428
 stellar atmosphere, 45
 stop command, 93
 t2, 617
 tolerance, 87
 unstable, 604
 variables, 422
 terms
 averaging, 224
 test code, 419
 tests
 atlas.in, 457
 blister.in, 458
 blr.in, 459
 brems.in, 459
 casea.in, 460
 casebn2.in, 461
 casebn8.in, 461
 casec.in, 462
 collion.for, 464
 compfi.in, 465
 complo.in, 465
 compton.in, 466
 conserv.in, 466
 coolcurve.for, 427, 467
 coolhii.in, 470
 corners4.for, 469
 coronal.in, 468
 dqher.in, 470
 drive.for, 471
 eden.in, 472
 fluc.in, 472
 globule.in, 473
 grid0.for, 474
 hemis.in, 474
 highn.in, 475
 hiiregions.in, 476
 hizlte.for, 477
 hizqso.in, 478
 induc.in, 478
 ism.in, 479
 kk.in, 480
 kmt.for, 427
 kmt.in, 481
 lalpha.in, 482
 laser1.in, 482
 laser2.in, 483
 laser3.in, 484
 ldl.in, 484
 liner.in, 485
 lte.in, 485
 ltemetl.in, 486
 map.in, 426, 486
 matchn2.in, 487
 ngc5548.in, 487
 nlr.in, 487
 nova.in, 488
 oldblr.in, 488
 optim.in, 489
 orion.in, 489, 490
 orionpdr.in, 491
 parishii.in, 492
 parisnlr.in, 493
 parispn.in, 493
 pdr.in, 494
 pnotes.in, 494
 primal.in, 495
 rauch.in, 495
 reflector.in, 495, 622
 rnfa.in, 496
 rnfb.in, 497
 secondary.in, 497
 sqrden.in, 498
 strom.in, 498
 varyN.for, 499
 varyNU.for, 500
 vbhum.in, 501
 werner.in, 502
 wind.in, 502
 thermal maps. *see* map
 creating, 97
 thermal stability, 273, 604
 thermalization length, 223
 thick shell geometry, 7
 three body recombination, 135
 three level atoms, 281
 time dependent command, 11,
 87
 timescale
 age command, 65
 Compton, 617
 photoerosion, 617
 sound travel, 616

thermal, 617
 title command, 115
 tolerance command, 87
 trace command, 116
 trace convergence command,
 117
 trace output, 116
 transition probability, 215
 averaging, 224
 driving hydrogenic, 131
 turbulence, 82, 214, 607
 setting, 81
 velocity, 81
 turbulence command, 81
 two level atoms, 281

– U –

unending loop. see loop
 Unix
 path, 138

– V –

V filter, 26
 van Regemorter
 approximation, 222
 variable
 abnset, 424
 alogete, 422
 alogte, 422
 amu, 262
 Anglelllum, 67
 anu, 203, 275
 anuSave, 203
 AtomicWeight, 214, 262
 autocv, 79, 429
 avdft, 295
 bit32, 401
 boltzmann, 207
 called, 414
 cdsqte, 421
 cextpw, 82
 cextra, 82
 ch2pls, 420
 character, 418
 chrgt, 272
 chContLabel, 203
 chDate, 419
 chDffTrns, 71
 chehp, 420
 chElementSym, 262
 chElNames, 263
 chheat, 275
 chi, 420
 chii, 420
 chIonStage, 262
 chLineLabel, 203
 chmin, 420
 chOptRtn, 127
 chVersion, 419
 cmcool, 275
 colden, 420
 colh2, 420
 colimt, 135, 609
 collid, 306
 condif, 204
 cooling, 285
 corind, 204
 covgeo, 65, 424
 covrt, 65, 425
 create, 272

csigc, 274
 csigh, 274
 csupeff, 306
 csupra, 135, 305
 CTHion, 260
 CTHrec, 260
 ctot, 285
 dampln, 217
 darea, 296
 densty, 307, 421
 depabs, 205
 deplon, 424
 depsct, 205
 depset, 423, 424
 depth, 609
 destroy, 272
 didz, 136
 diffus, 105, 204
 dlaw, 61
 dmetal, 57, 424
 doppler, 214
 drad, 419, 609
 dReff, 420, 422
 drnxt, 420
 dsize, 296
 dstab, 295
 dstab1, 295
 dstdft, 295
 dstfac, 296
 dston1, 295
 dstpot, 295
 dstq, 295
 dstsc, 295
 dstsc1, 295
 DstWght, 136
 dustp, 295
 dVeff, 420, 422
 dwork, 296
 e2tau, 205
 eden, 421
 EdenError, 136, 421
 edensqte, 421
 EdenTrue, 421
 ednstr, 421
 eev, 295
 efionz, 305
 efrend, 91
 egamry, 202
 emm, 202
 enRyd, 207
 endedn, 91
 EnergyKshell, 137
 eVdegK, 207
 evRyd, 207
 exctef, 305
 exptau, 205
 facexp, 205
 ffheat, 277
 floating, 417
 flong, 62
 flux, 107, 204, 275
 FluxFaint, 136
 flxfnt, 202
 getpar, 412
 gionrc, 295
 grmetl, 57
 halfte, 285
 hbn, 231
 hbrems, 277
 hbul, 232
 hcbolt, 231
 HCharExcIon, 260
 HCharExcRec, 260
 HCionT, 232
 hcont, 233
 HCTMin, 135
 hdamp, 217
 HdeltaT, 232
 hden, 15
 hdest, 232
 he1dmp, 217
 he1lim, 256
 he1rec, 256
 he1stat, 240
 he1tau, 256
 he2dmp, 217
 he2lim, 256
 he2rec, 256
 he2stat, 240
 he2tau, 256
 he3n, 255
 heatef, 305
 heating, 285
 heatnt, 285
 heatstr, 421
 helax, 306
 hemis, 232
 HEnrRyd, 232
 hesc, 232
 hfrcin, 232
 hgamnc, 237
 hiistr, 421
 HIonPot, 207
 histr, 421
 hlax, 306
 hlbolt, 231
 hlte, 231
 HNIonRyd, 232
 hrec, 236, 238
 hreff, 134
 hstat, 231, 240
 htau, 232
 htlim, 232
 htnext, 232
 htot, 286
 in equations, 418
 integers, 417
 ipElement, 260
 iphe1, 256
 iphe2, 256
 ipHeavy, 261
 iphl, 232
 ipLnAovTOT, 227, 280
 ipLnAul, 227
 ipLnBolt, 227
 ipLnColovTOT, 227
 ipLnCont, 227
 ipLnCool, 227, 280
 ipLnCS, 227
 ipLnCS1, 223, 226, 227
 ipLnCS2, 226, 227
 ipLnDamp, 227
 ipLnDampRel, 226, 227
 ipLnDesP, 226, 227
 ipLnDTau, 227
 ipLnEnrErg, 227
 ipLnEnrWN, 227
 ipLnEscP, 226, 227
 ipLnGF, 227
 ipLnGl, 227

ipLnGu, 227
 ipLnHeat, 227, 281
 ipLnInten, 227, 280
 ipLnInwd, 226, 227
 ipLnIonStg, 227
 ipLnIpCont, 227
 ipLnNelem, 227
 ipLnNPhots, 227, 280
 ipLnOpac, 227
 ipLnOTS, 227, 280
 ipLnPopl, 226, 227, 280
 ipLnPopOpc, 226, 227, 280
 ipLnPopu, 226, 227, 280
 ipLnPump, 226, 227
 ipLnRedis, 227
 ipLnRyd, 227
 ipLnTauCon, 226, 227
 ipLnTauIn, 226, 227
 ipLnTauTot, 226, 227
 ipLnWlAng, 226, 227
 ipLyHeavy, 261
 ipSecIon, 305
 iPunDef, 137
 iter, 79, 414, 422
 itermx, 79, 422
 itoptm, 121
 ItrDim, 93, 94, 422
 KshellLimit, 137
 ldDoPhoto, 415
 LevTrace, 139
 lgAbnSolar, 424
 lgAutoIt, 79
 lgDustOn, 295
 lgElmtOn, 55, 423
 lgFluor, 134
 lgLastIt, 423
 lgOpacOn, 423
 lgOptimFlow, 123
 lgPHFIT, 138
 lgSearch, 423
 lgTauOutOn, 215
 lgTestOn, 139
 lgVarOn, 127
 limfal, 84, 427
 limLevelN, 282
 limpar, 119
 limpun, 102
 limspc, 23, 38
 limTabD, 56, 61
 lmhlvl, 77
 logical, 418
 mxstpl, 92
 naming convention, 416
 nAtlas, 130
 ncell, 202
 ndplot, 95
 ndpts, 296
 ndust, 295
 nend, 137, 423
 nflux, 202
 nh, 232
 nhe1, 256
 nhe2, 256
 nhe3lvl, 255
 nhlvl, 77
 nkrd, 19, 406
 nmaps, 87, 111, 138
 nobslm, 121
 nparm, 127
 npass, 422

- npunlm, 109, 111
 nRauch, 130
 nsShells, 261
 nta, 225
 nterp, 39
 ntff, 278
 nupper, 202
 nvarxt, 127
 nvary, 127
 nvfpnt, 127
 nWerner, 130
 nzdump, 98
 nzlim, 421
 nzone, 414, 422
 occnum, 204
 opac, 205, 209
 ophe1f, 256
 ophe2f, 256
 ophf, 236
 opsv, 209
 otscon, 107, 204, 209
 otslin, 107, 204, 209
 otsmin, 134
 outcon, 107, 204
 outlin, 107, 204
 pden, 303, 421
 pdenstr, 422
 perror, 303
 pestrk, 232
 pgas, 303
 ph2lte, 245
 phmlte, 245
 PhotoRate, 263
 phplte, 245
 pinteg, 303
 pirsq, 420
 pnw, 303
 PopLevls, 281, 284
 prad, 303
 PresInit, 303
 presok, 303, 414
 PunchLWidth, 104, 138, 622
 r1r0sq, 420
 radius, 419
 radstr, 422
 real, 417
 RecomRate, 272
 refcon, 106, 204
 reflin, 204
 rinner, 419
 rmr0, 420
 router, 420
 sab, 295
 scalem, 424
 scatop, 205, 209
 scmpla, 306
 seccmp, 306
 seche, 306
 sechi, 306
 secmet, 306
 smetla, 306
 solar, 423
 SolarSave, 423
 sqabs, 295
 sqscat, 295
 sse, 296
 struc, 421
 sublimat, 294
 SummedCon, 205
 SummedDif, 205
 SummedOcc, 205
 tauabs, 205
 TauDmmy, 281
 TauLines, 225
 taumin, 221
 tausct, 205
 tautot, 205
 te, 422
 te1ryd, 207
 tedust, 296
 tehigh, 93
 telogn, 422
 telow, 93, 139
 tend, 139
 TeProp, 422
 testr, 422
 tfail, 414
 tff, 278
 tlast, 422
 TLineARR, 229
 TLineEXP, 229
 tmn, 210
 tsq1, 285
 tsqden, 139
 varang, 123, 127
 vformt, 127
 vincr, 120, 127
 volstr, 422
 vparm, 127
 vtoler, 123
 WavNKelv, 207
 WavnNRyd, 207
 WeakHeatCool, 140
 widflx, 204
 WindData, 225
 wmole, 307, 421
 x12, 135, 305
 xIonFrac, 262, 424
 yield, 263
 variable naming convention, 416
 varyN.for
 input script, 499
 varyNU.for
 input script, 500
 vbhum.in
 input script, 501
 veclib routines, 77
 velocity
 Alfvén, 86
 Doppler, 81
 electron, 85
 mean speed, 85, 292
 stored, 214
 thermal, 81, 214
 turbulent, 81
 Verner
 Fe II atom, 72
 version numbers, 419
 VMS
 assign statement, 43
 path, 138
 Voigt function, 214
 Volk, Kevin
 grain extra species, 74
 gray grains, 74
 PAH grains, 74
 PN nuclei, 48
 quantum grain heating, 80
 stellar atmospheres, 45, 128
 table density law, 61
 – W–
 warnings
 checks, 4
 printed, 611
 routine to print, 410
 warnot, 410
 wavelength
 output convention, 626
 wavenumber, 222
 Werner atmospheres, 48
 werner.in
 input script, 502
 wgadd, 411
 wginit, 411
 wglne, 411
 wind, 304, 605
 density vs radius, 304
 line transfer, 304
 wind command, 69
 wind.in
 input script, 502
 – X–
 X-ray to optical ratio, 31, 602
 – Z–
 zone
 attenuation, 209
 defined, 4
 limiting number, 18
 output, 604
 stopping, 94
 thickness, 419
 setting, 136
 variables, 422